Ventilated Oscillatory Boundary Layers

Daniel C. Conley
Douglas L. Inman

N00014-89-J-1060

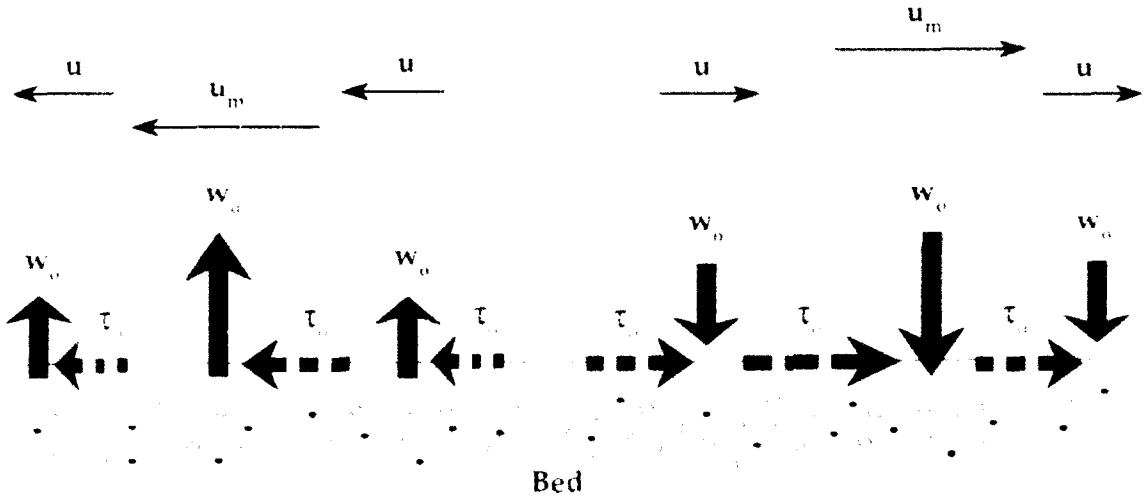

Center For Coastal Studies
Scripps Institution of Oceanography
University of California,
San Diego

February 1993

SIO Reference Series No. 93-9

DISCLAIMER NOTICE

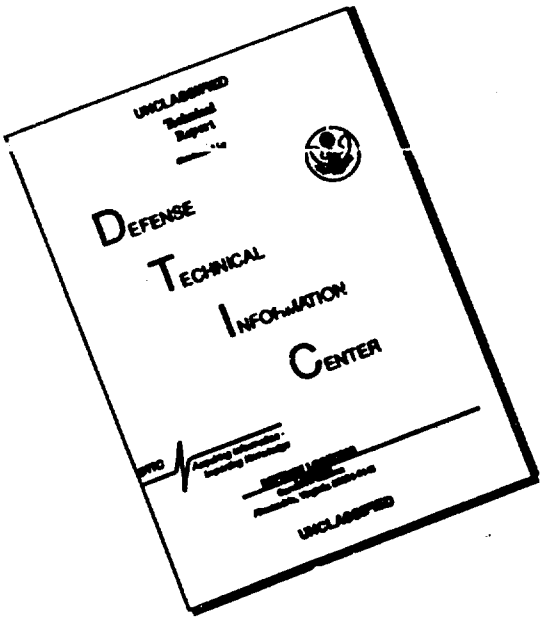

THIS DOCUMENT IS BEST QUALITY AVAILABLE. THE COPY FURNISHED TO DTIC CONTAINED A SIGNIFICANT NUMBER OF PAGES WHICH DO NOT REPRODUCE LEGIBLY.

VENTILATED OSCILLATORY BOUNDARY LAYERS

Daniel C. Conley

Douglas L. Inman

Center for Coastal Studies
Scripps Institution of Oceanography
University of California, San Diego
La Jolla, California 92037-0209

February 1993

SIO Reference Series No. 93-9

TABLE OF CONTENTS

LIST OF FIGURES AND TABLES

Chapter I

Chapter II

Chapter III

ACKNOWLEDGEMENTS

This study was supported by the Office of Naval Research, Coastal Studies, under grant N000 14-89-J-1060. Preliminary aspects of this work were supported by the National Sea Grant program, Department of Commerce, under grant SGC R/C2-77

We are especially indebted to Scott A. Jenkins for ideas and help in the field since the inception of the project. Robert T. Guza, Bradley Werner and Thomas Drake gave generously of their time and provided helpful discussion of data analysis and insights into research direction. The staff of the Scripps Hydraulics Laboratory, Charles Coughran, David Aglietti, John Lyons, Michael Kirk, Domingo Goyena and John Powell, provided ingenuity, resourcefulness and a refreshing sense of accommodation for the laboratory experiments. Aid in instrumentation, field work, and data analysis was provided by William Boyd, Michael Clifton, B. Walton Waldorf, Brian Woodward, Joseph Wasyl and David Skelly. Most figures in this work were drafted by Michael Clark. Chapter 1 was formatted by Cheryl Bastian Alden.

ABSTRACT

A combination of field and laboratory experiments are made in order to expand our knowledge of naturally occurring oscillatory boundary layers. Chapter I describes field observations of the development of wave driven boundary layers at the fluid sediment interface. Under the crest of the wave, this development can be idealized as an identifiable sequence of three parts. The latter parts of this development are never observed to occur under the trough of the wave despite similarities in wave orbital velocity and acceleration. It is proposed that wave induced boundary ventilation, the oscillatory flow through the surface of a permeable bed, may be responsible for this apparent developmental asymmetry.

In chapter II, a laboratory study is presented of ventilated oscillatory boundary layers. These are boundary layers arising from a flow which oscillates parallel to a permeable bed which is subject to oscillating percolation of the same frequency as the bed parallel flow. Measurements of boundary layer velocities, bed stress and turbulent flow properties are presented. It is observed that suction (flow into the bed) enhances the near bed velocities and bed stress while injection (flow out of the bed) leads to a reduction in these quantities. As the ventilated oscillatory boundary layer experiences both these phenomena in one full cycle, the result is a net stress and a net boundary layer velocity in an otherwise symmetric flow. While production of turbulence attributable to injection is enhanced, the finite time required for this to occur leads to greater vertically averaged turbulence in the suction half cycle. Turbulence generated in the suction half cycle is maintained in a compact layer much closer to the bed. These effects appear to hold for $\tilde{R}e$ ranging from 10^5 to 10^6 and for oscillations other than sinusoidal.

Field measurements of wave driven ventilation are presented in chapter III. The measurements are compared against linear theory and ventilation is found to be present and predictable if the local effective thickness of sediment is known. Ventilation is then investigated as a possible mechanism for the maintenance of beach slope. It is shown that when compared against net bed stresses resulting from nonlinear wave forms or bottom wind, the ventilation induced stress asymmetry is an important mechanism for medium to coarse grained sediments.

CHAPTER I

JOURNAL OF GEOPHYSICAL RESEARCH, VOL. 97, NO. C6, PAGES 9631-9643, JUNE 15, 1992

Field Observations of the Fluid-Granular Boundary Layer Under Near-Breaking Waves

DANIEL C. CONLEY AND DOUGLAS L. INMAN

Center for Coastal Studies, Scripps Institution of Oceanography, La Jolla, California

Numerous synchronized time series from video cameras, pressure sensors, current meters, and hot film anemometers on natural beaches show that boundary layer development under the crest of near-breaking waves can be idealized as a process composed of three distinct regimes here referred to as streaking, rolling, and pluming. The rolling and pluming regimes fail to develop under the trough. As a consequence, there is a pronounced asymmetry in instantaneous sand transport and boundary layer phenomena between the wave crest and trough. However, laboratory waves with field scale periods and wave heights over thin sand beds do not exhibit this crest-trough boundary layer asymmetry, indicating that a critical element of similitude is absent in laboratory experiments. We suggest that wave induced boundary ventilation is responsible.

INTRODUCTION

Over the past several decades, considerable effort has been devoted to the study of oscillatory boundary layers in the laboratory under widely varying conditions. However, little work has been done to study these boundary layers under field conditions because of logistical difficulties. In this paper we report on field observations of the development of the fluid-granular oscillatory boundary layer. We present a combination of quantitative and qualitative findings that, although not fully understood, are recurring elements in the development of the fluid-granular boundary layer in the field. We also attempt to identify those aspects of theoretical and laboratory work that can be applied to these field observations.

The Stokes solution for the laminar oscillatory boundary layer over a smooth impermeable bed [*Lamb*, 1945, p. 620] is,

$$u = u_\infty \left[\sin(\theta) - e^{-\frac{z}{\delta_0}} \sin(\theta - \frac{z}{\delta_0}) \right] \qquad (1)$$

where u_∞ is the amplitude of the free stream velocity just above the boundary layer, $\theta = (\sigma t - kx)$ is the phase of the free stream, σ is the radian frequency, k is the wave number, $\delta_0 = \sqrt{2\nu/\sigma}$ is the Stokes parameter, z is the direction normal to the bed, and ν is kinematic viscosity. Using this expression, the laminar shear stress can be derived, giving

$$\frac{\tau}{\rho} = \frac{\sqrt{2}\nu u_\infty}{\delta_0} e^{-\frac{z}{\delta_0}} \sin\left[\theta - \frac{z}{\delta_0} + \frac{\pi}{4}\right] \qquad (2)$$

Notice that the shear stress leads the free stream velocity by $\pi/4$. This solution has been experimentally verified numerous times [e.g., *Sleath*, 1968].

As is true of all turbulent flows, the problem of the turbulent oscillatory boundary layer suffers from the classical closure problem, and no analytic solution exists. On the other hand, many models for these boundary layers have been developed (see *Justesen* [1987] for a review), and they have been the subject of numerous experimental laboratory investigations. The earliest experiments [*Bagnold*, 1946; *Inman and Bowen*, 1962] were designed to measure mean quantities where the mean was taken as the average over a wave cycle. Subsequent experiments for the most part measured phase-averaged quantities in order to identify the mean behavior over a wave cycle and answered questions relating to the range of occurrence of turbulence and the effect of roughness.

Transition to turbulence has been predominantly determined through the use of a wave friction factor, f_w. Using a form similar to that suggested by *Putnam and Johnson* [1949], *Jonsson* [1963] defined one form of the wave friction factor as

$$\frac{\tau_m}{\rho} = \frac{1}{2} f_w u_\infty^2 \qquad (3)$$

where τ_m is the amplitude of the bed stress. It should be noted that this expression only relates the maximum bottom stress to the maximum velocity, regardless of when they occur and provides no information about the temporal behavior of the bottom stress. While this type of formulation may be helpful for calculations regarding threshold values or maximal loading, it is of limited value when information about the boundary layer behavior throughout the wave cycle is desired. The approach used here is to identify a single critical oscillatory Reynolds number $\hat{R}e$, where the friction factors diverge from the laminar relation as implied in relation (2). The idea is that, like steady flow, flows with Reynolds numbers below that value would be considered "laminar" and those with higher values would be considered "turbulent." Because the boundary layer thickness in oscillatory flow is not unambiguously defined and is difficult if not impossible to measure in any situation but the laboratory, we use the oscillatory Reynolds number $\hat{R}e$, based on the orbital diameter d_0.

$$\hat{R}e = \frac{u_\infty d_0}{4\nu} \qquad (4)$$

where d_0 is taken as the value just above the boundary layer.

On the basis of experiments and stability analysis, *Jonsson* [1966] proposed $\hat{R}e = 10^4$ as the value for transition between laminar and turbulent flows in the oscillatory boundary layer over a smooth bed. In a detailed study of wave friction factors, *Kamphuis* [1975] found this value to be the upper limit for the laminar range over a smooth bed. In a reanalysis, *Jonsson* [1980] suggests $\hat{R}e = 10^3$ as the new lower limit for turbulence over smooth beds. *Hino et al.* [1983], using a laser Doppler velocimeter in air to measure velocity profiles through a purely oscillatory boundary layer over a smooth impermeable bed ($\hat{R}e$ =

Paper number 92JC00227.
0148-0227/92/92JC-00227$05.00

3×10^5), partially confirmed this. They reported a turbulent boundary layer where most turbulence production was in the decelerating phase. They also reported that the turbulence is almost entirely dissipated by the start of flow acceleration in the subsequent half-cycle. This raises questions about the idea of an oscillatory boundary layer which is considered to be either purely turbulent or purely laminar throughout the entire cycle.

Jensen et al. [1989] measured the boundary layer development in an oscillatory water tunnel over smooth and rough beds where $\hat{R}e$ ranged from 7.5×10^3 to 6×10^6. They showed that the boundary layer over a smooth bottom could be both laminar and turbulent within one half-cycle. Their results show that the limit for purely laminar boundary layers is approximately $\hat{R}e \le 10^5$ and the limit for purely turbulent boundary layers is approximately $\hat{R}e \ge 10^6$. This indicates that the idea of a single "critical" $\hat{R}e$ is misconceived and explains some of the previously observed variations in the range of the "critical" value of $\hat{R}e$.

Another matter of interest has been the phase lag between the occurrence of maximum bed stress τ_m and maximum free stream velocity u_m. In an oscillating water tunnel study of turbulent flow over two-dimensional concrete ripples, *Jonsson* [1963] found a lag of only 25° as compared with the 45° in laminar flow. $\hat{R}e$ for these experiments was $\approx 6.0\times10^6$. The ratio of wave displacement amplitude, $a_0 = d_0/2$, to Nikuradse roughness parameter, a_0/k_s, was 124, where k_s was determined by fitting measured boundary layer velocity profiles in steady flow to the relation for the turbulent velocity profile over a rough bottom, $(u/u_*) = 5.75\log(30z/k_s)$. Here $u_* = (\tau_0/\rho)^{1/2}$ is the friction velocity and τ_0 is the bed stress.

Sleath [1970] measured the development of the oscillatory boundary layer over beds of loose sand in a wave channel. In these experiments, the bed stress τ_c never exceeded the threshold for grain motion. He found that the measured phase for velocity over beds of fine and medium sand approximately followed the form of relation (1). However, for coarse sand, where a_0/k_s was about 50, he reported a phase lag which approached zero near the bed (rather than the 45° predicted by (1) and the 25° measured by *Jonsson* [1963]). *Jensen et al.* [1989] found that in flow over a smooth bed the phase lag ϕ between τ_m and u_m is $\hat{R}e$ dependent. The phase lag is 45° below a $\hat{R}e$ of 4×10^4; it then falls off, attaining a value of 10° at $\hat{R}e = 10^6$. The phase continues to fall off, though weakly, with $\hat{R}e$ above that value. These results along with those of *Sleath* [1970] suggest that the phase lag is a function of $\hat{R}e$ and a_0/k_s and that for the values of these parameters expected as waves near the shore, the phase will approach zero.

Of the aforementioned laboratory studies [*Hino et al.*, 1983; *Jensen et al.*, 1989; *Jonsson*, 1963; *Kamphuis*, 1975, *Sleath*, 1970] only *Jonsson* mentions asymmetry in the oscillatory boundary layer and, in general, results are only presented for one half-cycle. All the values measured by *Jonsson* [1963], including the free stream velocity, exhibited asymmetry between the two oscillatory half-cycles and he attributed this asymmetry to the mechanism driving the flow.

TRANSITION AND TURBULENCE OVER A FLAT PLATE

Most authors agree that the first instability to occur in the laminar boundary layer consists of two-dimensional Tollmien-Schlichting (T-S) waves. These are small disturbances that satisfy the Orr-Somerfeld linearized disturbance equation. When the amplitude of these waves exceeds a threshold value, they begin to develop three-dimensionality, manifest by periodic fluctuations in the cross-stream direction. At about this same developmental time, secondary short-wavelength instabilities are excited by these background fluctuations, and it is the exponential growth of these secondary instabilities which leads to turbulence [e.g., *Landahl and Mollo-Christensen*, 1986; *Herbert*, 1988]. In steady flow, the development of T-S waves from inception to three-dimensionality occurs over a distance approximately equal to five T-S wavelengths, while the development of secondary instabilities and breakdown is abrupt and occurs over one T-S wavelength.

Conditions for T-S wave stability in steady flow have been calculated by *Jordinson* [1970]. Using the Blasius velocity profile, he calculated the critical Reynolds number Re_{δ^*} as 520 where $Re = u_m\delta^*/\nu$, δ^* is the displacement thickness, and u_m is the free stream velocity. Here critical implies that unstable T-S waves may grow in flows with Reynolds numbers above this value. Jordinson calculated the parameters for the first unstable T-S wave to develop as $\alpha\delta^* = 0.30$, $\sigma\delta^*/u_m = 0.12$, $c/u_m = 0.40$, where α is the wave number, σ is the radian frequency, and c is the phase speed. Using the fact that for the Blasius profile the displacement thickness is approximately one-third the boundary layer thickness δ, this gives as a streamwise wavelength $l_s = 7\delta$. The initial cross-flow wavelength of three-dimensionality l_y is approximately equal to l_s. Relative to the scales of turbulent motion, these are clearly long-wave phenomena.

Considerable study has been invested in recent years to determine the role of turbulent bursting in geophysical flows (see *Kline et al.* [1967] for a description of turbulent bursting). Investigators report observations of turbulent bursting in boundary layers over plowed fields [*Mercerat*, 1972], in tidal currents in the Irish Sea [*Heathershaw*, 1974], and in river flow where its signature is said to be the boils present on the surface of the flow [*Jackson*, 1976].

Additionally, many investigators have found that different characteristics of the bursting cycle have roles in different aspects of sediment transport. In unidirectional flow, *Weedman and Slingerland* [1985] showed that sand streaks formed at low friction velocity ($u_* < 4$ cm/s) in fine to medium sand exhibit the same lateral spacing and statistical distribution as the low speed streaks found in turbulent bursting. The dimensionless spacing s^+ is

$$s^+ \equiv \frac{su_*}{\nu} = 100 \pm 20 \qquad (5)$$

where s is the mean dimensional spacing of the streaks.

Relatively few field studies of the fluid-granular oscillatory boundary layer over permeable beds have been reported in the literature. *Inman* [1957] studied the formation of wave-generated ripples over sand bottoms. Near the surf zone, he observed ripples of low steepness which were "ephemeral" in nature, forming and disappearing in the time scale of individual waves. Sediment motion during the presence of these ripples was described as a "dense layer of suspended particles," fully distinct from the discrete clouds of sediment shed from the crests of vortex ripples of more permanent form. *Madsen* [1974] reports divers' observations that the sediment bed seemingly "explodes" just prior to the passage of the crest of near-breaking waves. No such phenomenon was observed under the trough.

In a field study using a bottom profiler, *Dingler and Inman* [1976] determined the range of occurrence of these ripple types in terms of the wave form of the Shields number θ where

$$\theta = \frac{\rho u_m^2}{(\rho_s - \rho)gD} \qquad (6)$$

and ρ_s is the sediment density. Their results indicate that ripples

of more permanent form, vortex ripples, occur after the onset of motion up to $\theta \approx 40$. Transition ripples, the ephemeral ripples of *Inman* [1957], occur for a range of Shields number of $40 < \theta < 240$. For values of θ greater than 240, the bed becomes flat and no ripples occur. While studies by *Bagnold* [1946], *Inman and Bowen* [1962], *Inman and Tunstall* [1972], and *Tunstall and Inman* [1975] describe quite well the fluid-sediment interactions over vortex ripples at conditions characterized by the lower Shields number ($\theta \leq 40$), no field studies of the fluid-granular oscillatory boundary layer development in conditions of high bottom stress over permeable beds have been reported.

EXPERIMENTS

Experimental Procedure

Beginning in the early 1980s, a series of experiments designed to investigate the fluid-granular oscillatory boundary layer in the region of high bottom stress ($\theta \approx 240$) were conducted adjacent to the ocean pier of Scripps Institution of Oceanography in water depths of 1 ~ 3 m. All the measurements were made just seaward of the breakpoint of the largest waves in a zone where wave heights were 0.5 to 1 m, and the slope of the fine sand beach was approximately 1 in 50. The sand has a median diameter D of about 150 μm and is predominantly quartz with about 10% by weight of heavy minerals, mainly hornblende.

Sensors were mounted on a triangular "surf spider" constructed of welded aluminum tubing with a spacing of 1.85 m between legs (Figure 1). The surf spider was floated into place by divers using air bags and was securely augured into the bed by means of helical plates mounted on rods extending through the hollow legs. The spider was oriented with two legs along a cross-shore line and the sensors were mounted to avoid interference with each other and with the legs [*Inman et al.*, 1985].

The sensors were mounted in a plane perpendicular to the cross-shore direction and included a pressure sensor, a two-component electromagnetic (em) current meter, and two cylindrical hot film probes which were mounted with a 1-cm separation in the longshore and vertical directions. Prior to each run, the probes were adjusted so that the bottom probe was approximately 1 cm above the still bed level (Figure 1). In addition, an 8-mm video camera was aligned and focused so that the hot film probes and the surrounding sand bottom were in the field of view. Numerous still photographs were taken during the experiments.

The pressure sensor was a temperature compensated Statham model PA506-33 absolute pressure transducer. The em current meter was a Marsh-McBirney model 512 OEM with a two-axis, 4-cm-diameter spherical probe with a nearly constant response up to 1.0 Hz. The current meter was placed about 50 cm above the bed and used to measure the instantaneous free stream wave velocity. The current meter was also used in in situ calibrations of the hot films. The anemometry was composed of TSI Incorporated model 1750 constant temperature anemometers (electronics) along with TSI Incorporated model 1210-60 NiCl cylindrical hot film probes. The probes extended from a 3.2-mm-diameter support rod and could be raised to the same level as the current meter for signal comparison or lowered to within 1 cm of

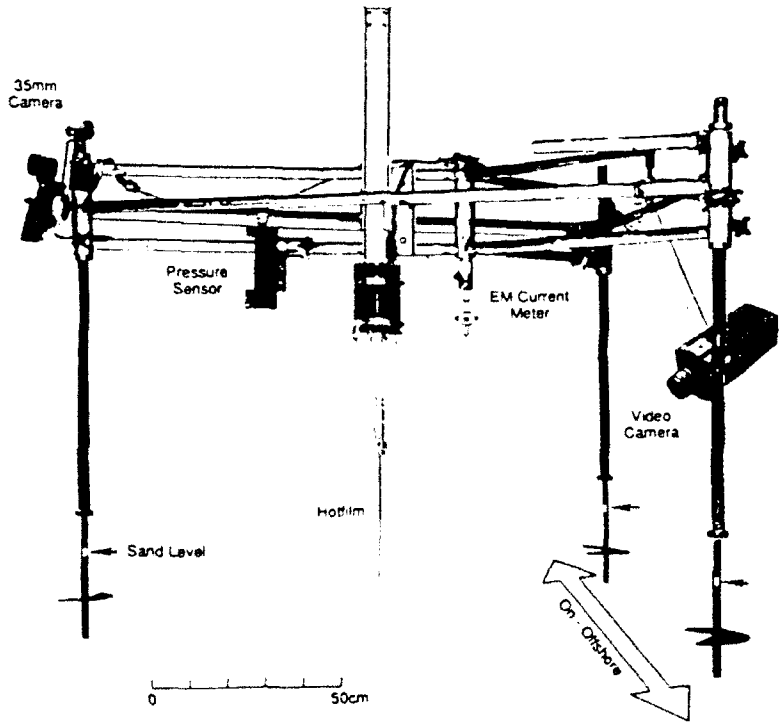

Fig. 1. The surf spider platform used for sensor deployment. The hot film package is mounted on a rack and pinch roller for vertical adjustments in the field.

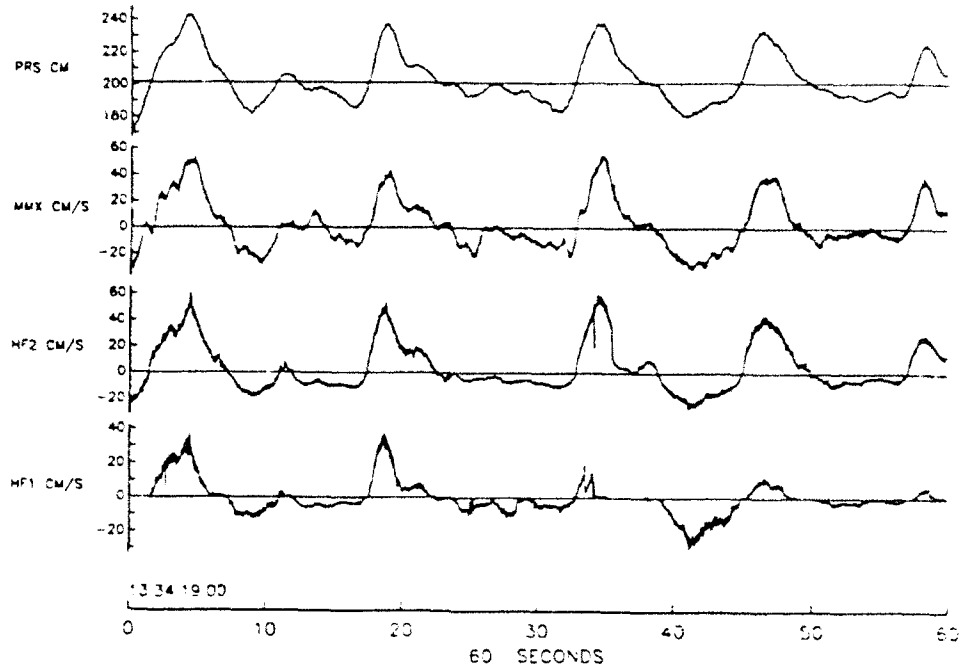

Fig. 2. Typical time series from June 5, 1989, experiment. Sensor outputs (top to bottom) are pressure, mid-depth cross shore velocity (em current meter), and bottom velocities (hot films). Hot film probes 1 and 2 were approximately 0.5 cm and 1.5 cm above the "at rest" bed.

the bed. The convention used designates onshore flow as positive.

The video camera was a Sony V9 8-mm video camera and was used in data runs of approximately 10 min. The video was synchronized with the data through the use of the time signal recorded on the video record. Pre- and postcalibrations indicated that the video and data were synchronized to within ± one frame (1/30 s).

Data from all the sensors were cabled from the surf spider up onto the pier and recorded at 128 Hz. A typical section of data is shown in Figure 2. The video and still photos were used to determine boundary layer development patterns, while the synchronized data records were used to determine onset conditions and to verify interpretations of the various patterns in the development of the fluid-granular boundary layer.

We shall rely primarily on the June 5, 1989, experiment, which provided the most comprehensive data set for most of the quantitative results presented here. During this experiment, incident waves had a spectral peak T of 12.8 s, a significant wave height H_{mo} of 70 cm, and mean water depth h of 190 cm. For significant waves, this corresponds to a $\hat{R}e$ of 1.2×10^6, a Shields number of 260 and a ratio of $(a_0 / k_s) = 5400$. Using the results of *Jensen et al.* [1989, Figure 3d], this corresponds to a boundary layer thickness of $\delta = 3.0$–3.1 cm. Six 512-s data runs were collected over a 2-hour period. The power spectra of cross-shore velocities for all runs are shown in Figure 3. Supplementary calculations have been made from underwater photographs taken during two experiments on August 8, 1985, and September 6, 1985, when $T = 6.4$, 9.4 s; $H_{mo} = 69$, 71 cm; and $h = 120$, 150 cm, respectively. These correspond to $\hat{R}e = 0.9 \times 10^6$, 1.1×10^6; $\theta = 420$, 360; $a_0/k_s = 3400$, 4500; and $\delta = 1.9$–2.0, 2.6–2.7 cm.

Data Analysis

Each of the six data runs for June 5, 1989, consisted of 512 s of data recorded at 128 Hz. Laboratory calibrations were applied to the em current meter and pressure sensor records. The hot films were calibrated following *Flick and George* [1990] in whose work the em current meter is used as a velocity standard in field calibrations. From calibration runs in which the hot film probes and current meter were at the same elevation in a plane parallel to the wave front, a nonlinear hot film calibration following King's law was calculated by comparing the hot film and current meter signals. Once calibrations were applied, the hot film records were derectified, rendering them of value for computing mean flows as well as instantaneous speeds. Spectra for each run were calculated by ensembling coefficients calculated from four data blocks of 128 s.

The videos were first observed in their entirety in order to develop impressions of boundary layer development patterns. When certain events or sequences were identified, the entire video record was systematically analyzed using stop action or frame stepping to identify the points of occurrence or to measure specific length scales. When times of occurrence were identified, cross reference could be made with the velocity and pressure signals. When events or phenomena were observed in the videos but could not be resolved with "freeze" frame, still photographs were employed. While still photography provides good quantitative information about length scales, event specific flow parameters could not be obtained, as there was no synchronization between the still camera and sensors.

The natural variability of wave amplitude and period resulted in

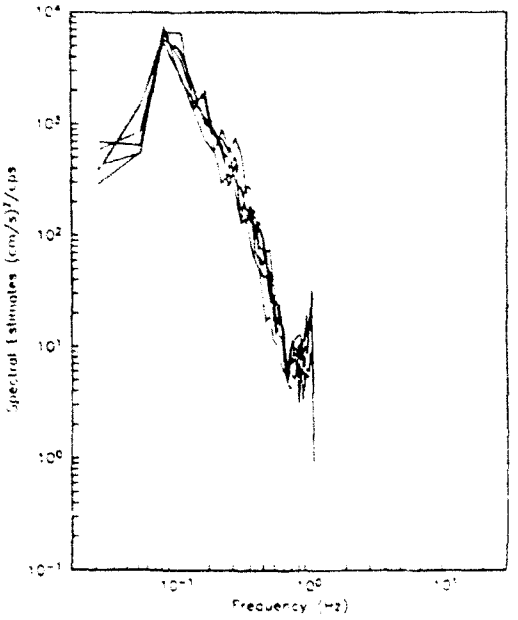

Fig. 3. Six power spectra with 8 DOF each of cross-shore velocities measured by em current meter on June 5, 1989.

widely varying conditions which significantly impacted the video records. The most dramatic effects occurred following the passage of groups of higher waves in which clouds of suspended sediment obscured the bottom for several wave half-cycles. Other cycles were rendered unusable by the presence of kelp or because the wave intensity barely exceeded the threshold of motion. The 3072 s of record from the June 5 experiment contained 197 individual waves of sufficient magnitude to set the top layer of sediment in motion at some point under the crest of the wave. The number of waves in which the bottom was clearly visible throughout all aspects of the fluid-granular boundary layer development was less.

BOUNDARY LAYER DEVELOPMENT UNDER THE WAVE CREST

Streaking

Beginning with the fluid at rest, the first visual indication of the *fluid-granular boundary layer* development is the initiation of motion where grains begin to roll along the bed and then rapidly develop into a series of sand streaks (Figure 4). Although occurring in apparently laminar oscillatory flow, the streak development resembled the sequence described by *Weedman and Slingerland* [1985] for the formation of streaks in fine and medium sand under conditions of weak friction velocity. The streaks here are visually manifested by the dark lines which result when quartz grains (large white) are separated from hornblende (small dark) along lateral shear lines by a sorting mechanism described by *Inman et al.* [1966]. These streaks initially appear as rather long $O(10$ cm) and regularly spaced lines which become more entwined, giving an echelon or lambda-like pattern. For the duration of this regime, the sediment is in a rolling grain or shooting flow where some portion of the immobilized bed is visible and the thickness of the layer of sediment in motion is never more than a few grain diameters. This entire regime is labeled "streaking."

Visual impressions of the particle paths of neutrally buoyant organic material and sediment grains remaining in the fluid column from previous events suggest that the flow, starting from rest after the reversal of motion, is laminar. As the flow accelerates, it attains the magnitude necessary for the onset of grain motion, u_*, and grains of sediment on the *surface of the bed* begin to roll in the streamwise direction. This is quickly followed by the appearance of sand streaks which can persist for the entire half-cycle of wave motion when the motion is weak.

Analysis of two photographs taken at times of "no motion" during the August 8 experiment gives a mean spacing for 151 remnant streaks as 4.8 mm with a standard deviation of 1.7 mm. The mean spacing for 69 streaks from a photograph taken during conditions of weak motion on the September 6 experiment was 3.9 mm with a standard deviation of 1.3 mm. Using the wave parameters for August 8 and the assumption that streaking occurs around $\sigma t = 15°$, the results of *Jensen et al.* [1989] give a friction velocity of 2 cm/s. This results in a normalized streak spacing s^+ of 89. For September 6, $u_* = 1.2$ cm and $s^+ = 43$. As these streaks occur during apparently laminar flow, it is unlikely that they are the turbulent low speed streaks observed by *Weedman and Slingerland* [1985]. This is supported by the fact that the observed streak spacing in our experiments is lower than that expected for turbulent streak spacing in unidirectional flow.

Roiling

The next regime begins with the abrupt transition of the fluid-granular boundary layer to a thicker carpet or sheet type flow (Figure 4). During this regime, the layer of sediment in motion resembles a carpet whose surface is composed of tufts of sediment laden fluid. The "tufts" seem to be regular in size with heights above the "at rest" bed of about 1.6 cm and spacing between the tufts of about 6 cm. The result is a layer of sediment in motion whose easily recognized surface is fully three-dimensional with variations in elevation in both the cross and streamwise directions (Figure 5). The entire video record from June 5 was analyzed in order to isolate examples of this regime. Of the 197 "significant" waves in the record, 109 half-cycles under the crest exhibited this carpet flow. Of these, 31 had an unobstructed view of the bottom at the time of transition. The abruptness and clarity of this transition is supported by the fact that repeat estimates of the onset of transition for 31 different events resulted in a mean variation of onset time of 3 video frames (0.1 s).

Under relatively low amplitude, long period swell as sometimes prevailed during the earlier deployments, this carpet flow can begin to exhibit streamwise periodicity much like the wales in corduroy (Figure 6). If the flow sequence terminates with this flow regime and the flow has developed streamwise periodicity, the bed exhibits transition ripples at the cessation of motion (Figure 7). If, as was the case throughout the June 5 experiment, the flow sequence terminates with this regime in the three-dimensional state (Figure 5), the bed deposited is flat. We have labeled this regime "roiling."

Jensen et al. [1989] defined a "temporal" friction factor $f_*^*(\sigma t)$. The expression for this friction factor contained a phase offset of $\pi/4$ as required by (2). However, as they showed in their paper, this phase lag is a function of $\tilde{R}e$ [*Jensen et al.*, 1989, Figure 11] so we propose a slightly modified temporal friction factor $f^*(\sigma t)$ defined by

$$f^*(\sigma t) = \frac{\tau_b(\sigma t)/\rho}{(1/2)u_*^2 \sin(\sigma t + \phi)} \qquad (7)$$

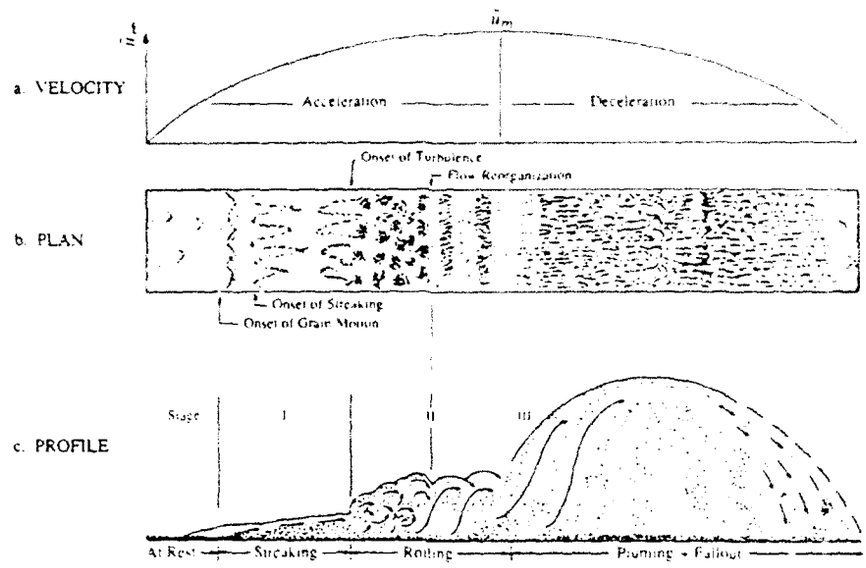

Fig. 4. Schematic illustration of the sequences in the development of the fluid-granular boundary layer for the case of "fully developed" plunging under the crest of a near-breaking wave (case C of Figure 12).

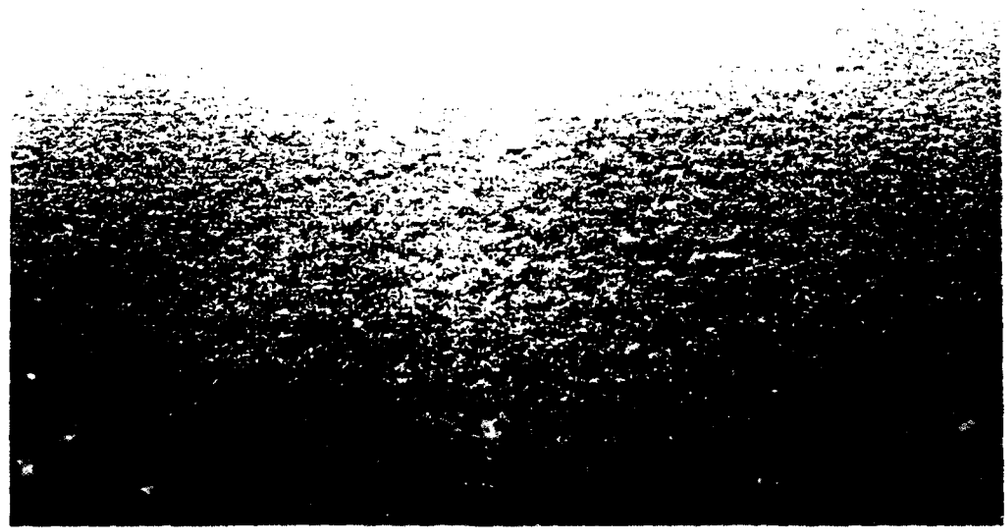

Fig. 5. Photograph of carpet flow under the crest of a wave. Spacing between "tufts" is $O(6$ cm).

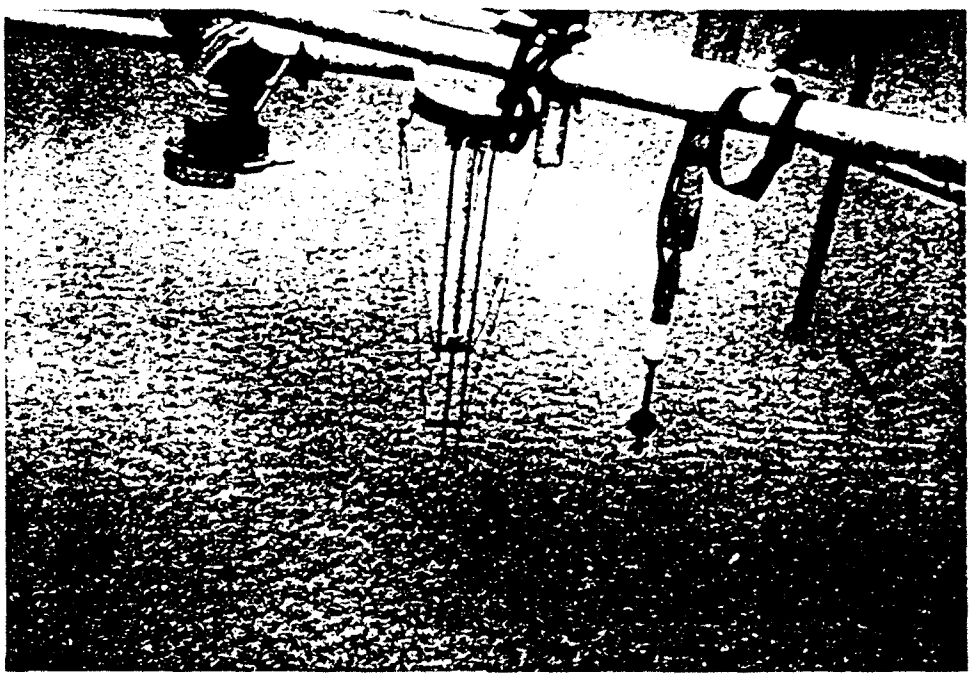

Fig. 6. Photograph of carpet flow under the crest of a wave. Rolled layer is beginning to compartmentalize and exhibit streamwise periodicity with cross-stream extension; leg of surf spider in upper right has a diameter of 1.5 mm.

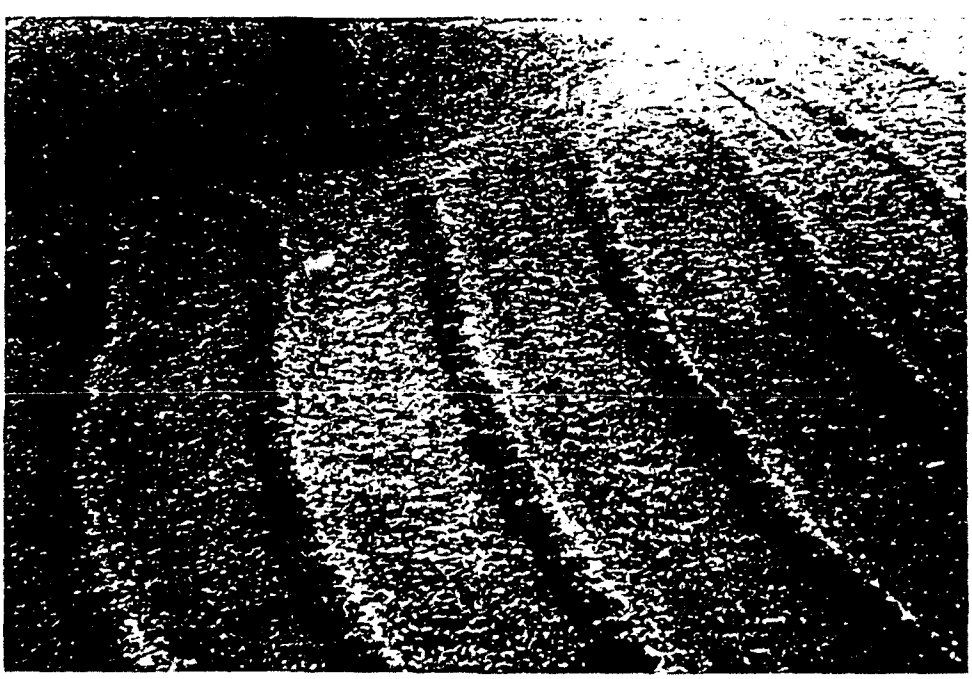

Fig. 7. Bed with transition ripples resulting from "reorganized" rolling in the absence of plunging. Ripple height is 5–7 mm, and wavelength is 3–4 cm.

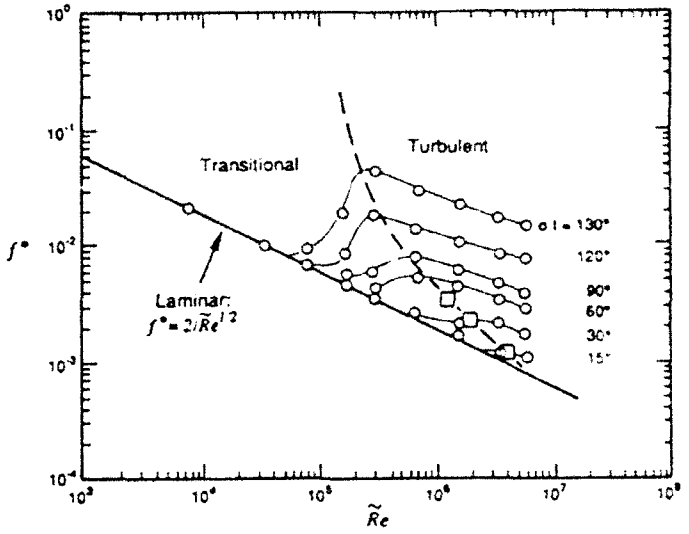

Fig. 8. Temporal friction factor f^* versus Reynolds number $\tilde{Re}$ for constant wave phase σt, where 90° corresponds to maximum orbital velocity. The heavy solid line represents laminar Stokes boundary layer, and the heavy dashed line is the limit for fully turbulent flow. Circles are data points. All are from *Jensen et al.* [1989, Figure 8]. Boxes are points reproduced in our Figure 9.

In the original expression, the phase lag ϕ was fixed at $\pi/4$ but here is dependent on $\tilde{Re}$ and equal to 45° for $\tilde{Re} \leq 4\times10^4$ and falls off to ≈8° for $\tilde{Re} = 10^7$. *Jensen et al.* constructed a plot of f_w^* versus $\tilde{Re}$ in which turbulent transition can be seen to be a function of both phase and Reynolds number. Using f^* from relation (7), we recreate this plot in Figure 8. The light solid lines indicate how the friction factor at different wave phase (σt) varies from the laminar case. Fully turbulent flow occurs to the right of the dashed line and transitional flow is assumed to occur in the region between the dashed and laminar line. The identified trend is for transition to occur at lower phase with larger Reynolds number.

We use these results to suggest that the transition from streaking to roiling is the fluid-granular oscillatory boundary layer expression of the transition to turbulence. This can be seen in Figure 9 which is a plot of the wave phase at which the onset of roiling occurs versus the $\tilde{Re}$ of the wave in which it occurred. In order to compute Reynolds numbers for this plot, u_m was defined as the peak velocity during the wave half-cycle in which roiling was observed. The half-cycle was defined by subsequent zero crossings in the velocity record, and d_0 was calculated by integrating velocity over the half-cycle. The wave phase was calculated as $\sigma t = \arcsin(u_r / u_m)$ where u_r was the free stream velocity at onset of roiling. As can be seen, the transition to roiling follows the trend of the transition to turbulence. That is, transition occurs at lower phase for higher Reynolds number. It should also be clear from this figure that streaking, which precedes roiling, occurs at a phase angle of 15° or less. It should be noted that Figure 8 corresponds to flows over a smooth and immobile bed. It is not surprising that transition in a flow over a loose sediment bed occurs at lower $\tilde{Re}$ than that expected under the above idealized conditions.

Of the 88 remaining waves, those with the most energetic half-cycles under the crest were isolated for analysis. The highest $\tilde{Re}$ calculated for such a flow was 2.6×10^5, and 29 of 33 half-cycles studied had Reynolds numbers below 2×10^5. The lowest $\tilde{Re}$ for a wave in which roiling was observed was 2.2×10^5. This suggests that waves in which roiling is not observed under the crest either experience transition late in the half-cycle when the wave is approaching deceleration or not at all.

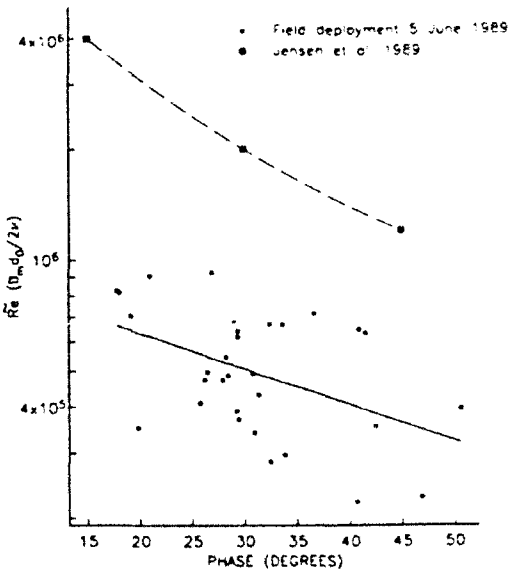

Fig. 9. Wave phase at the onset of roiling versus $\tilde{Re}$, where a phase of 90° corresponds to maximum orbital velocity. The dashed line represents transition to turbulence from Figure 8. The solid line is a least squares fit of an exponential curve to the values obtained at the onset of roiling.

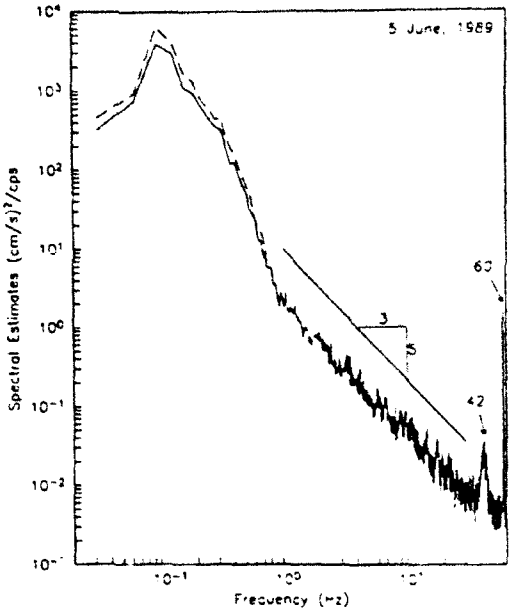

Fig. 10. Spectrum with 24 DOF of hot film velocities composed from an ensemble of three different 512-s runs. For reference, the dashed line is ensemble average (48 DOF) of six spectra of cross-shore velocities shown in Figure 3.

A power spectrum with 24 degrees of freedom (DOF) formed from an ensemble of three hot film spectra is shown in Figure 10. These spectra were computed from data runs which were entirely unaffected by kelp or other types of biofouling and were fully derectified prior to transforming. Inspection shows that the spectral roll-off below 1 Hz follows the Kolmogorov -5/3 power law, supporting the possibility of a turbulent inertial range. While the turbulence in these boundary layers is intermittent, this is not inconsistent with the -5/3 spectrum [*She and Orszag*, 1991]. In an earlier report [*Inman et al.*, 1986], it was reported that the hot film data roll-off had a -2 slope, but we now believe this to be an artifact resulting from rectification. The higher frequencies in Figure 10 are polluted by what is believed to be the natural frequency of the frame of the surf spider (42 Hz) and by noise from the 60-cycle power source.

Using the results of *Kim et al.* [1971], it can be shown [e.g., *Hinze*, 1975] that for steady turbulent flow, the turbulent burst period T_b scales as

$$\frac{T_b u_*}{\delta} = 5 \tag{8}$$

where δ is the boundary layer thickness. Now if a flow over a quasi-passive tracer is experiencing turbulent bursting such that fluid originating at the tracer interface is periodically being thrust into the free stream, one might expect a visual pattern of puffs of tracer with a streamwise spacing l_b, where

$$l_b = u_* T_b = 5\delta \tag{9}$$

Notice how similar this is to the earlier calculated wavelength for the most unstable T-S wave, $l_s = 7\delta$. Using the boundary layer thicknesses of 3 cm given earlier for the June 5, 1989, experiment, equation (9) would suggest a burst spacing of ≈15 cm. Another indication of the boundary layer thickness would be the thickness of the granular-fluid layer. The mean thickness of all 31 rolled layers as measured from the at rest bottom to the top of the tuft surface was found to be 1.6 cm with a standard deviation of 0.4 cm. Using this as the boundary layer thickness gives a burst spacing of 8 cm. While these estimates of the turbulent burst spacing in a steady, unidirectional flow do not match exactly with the measured tuft spacing of 5–7 cm, it is certain that the surface character of the rolled layer suggests a process dominated by ejection of granular laden fluid from somewhere inside the rolled layer.

The mechanism by which this apparently turbulent flow develops coherent cross-stream structures as evidenced by the wales in the granular-fluid mixture in Figure 6 is unknown. However, the appearance of coherent structures in turbulent flows is not a new phenomenon [e.g., *Winant and Browand*, 1974]. In visual studies of a turbulent oscillatory boundary layer, *Hayashi and Ohashi* [1982] observed coherent large-scale vortices with cross-stream axis occurring in the boundary layer just prior to the reversal of motion.

Pluming

The final regime, "pluming," also occurs under relatively low amplitude, long period waves where the rolled flow has developed a periodic structure (Figure 4). At or just after the passage of the wave crest when the flow begins to decelerate, the rolled layer explosively lifts off the bed, injecting sediment-laden fluid into the interior of the fluid as high as 5–10 times the rolled layer thickness (Figure 11). The sediment ejecta is then carried by the free stream until falling out at the cessation of motion, leaving once again a flat bed.

The mechanism involved in pluming is difficult to identify, not only because of its complexity but also because of the stringent conditions apparently required for its occurrence. In fact, no examples of pluming were observed in the June 5 experiment, so onset criteria had to be estimated from earlier experiments. Nonetheless, as pluming was generally observed on the same days as the coherent wale-like structures in rolling, it is likely that they are related. Most probably, pluming represents the violent breakup of vortices in the advent of an adverse pressure gradient associated with the passing of the wave crest. The longitudinal vortices with cross-stream axis generated during the reorganization of rolling appear to be pressure sensitive and experience breakdown following the advent of deceleration.

Relative Occurrence

The sequence, streaking, rolling, and pluming, represents an idealized sequence which can be seen under certain conditions but more commonly is present only in part. For example, under very low wave conditions or deeper water, the only portion which may exist would be streaking. Under more general conditions (as exemplified by the June 5 experiment) with intermediate-period waves or incident waves with a broad spectral distribution, the development generally only includes streaking and rolling where the bottom is flat at the reversal of motion. This "mild" sequence is schematized by case A in Figure 12. In relatively "clean" swell the development might be moderate including streaking and fully developed rolling resulting in a bed with transition ripples (case B, Figure 12). Under relatively low amplitude, long period swell where wale-like structures in rolling are well formed, the fully

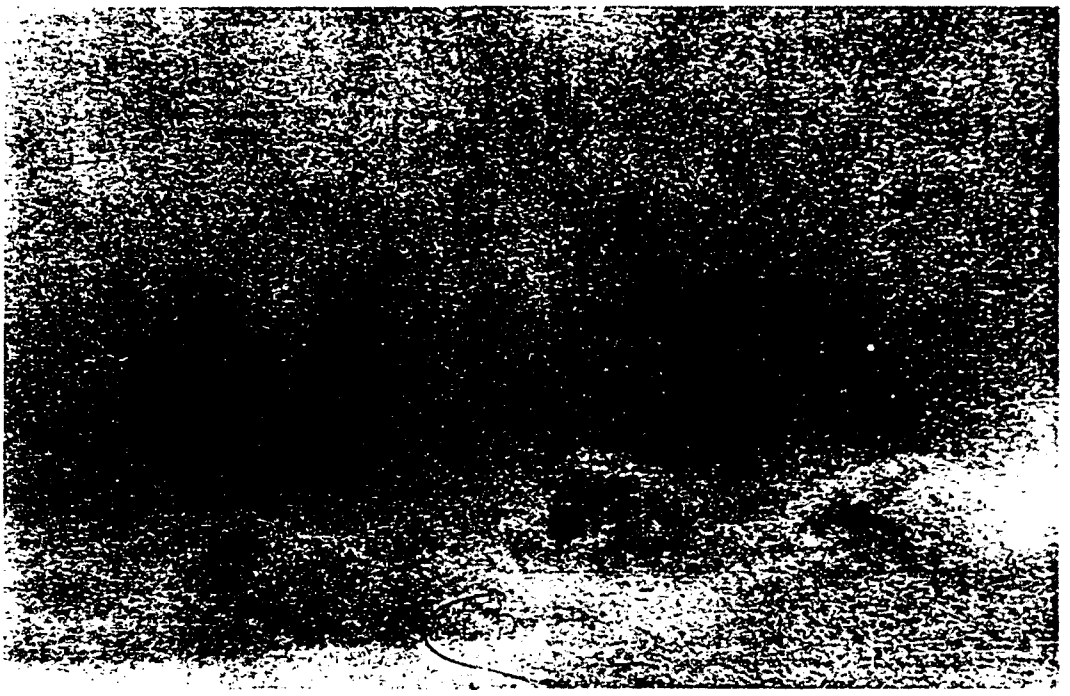

Fig. 11. Side view of beginning of pluming. Plume heights are 0.10 cm.

developed sequence, streaking-rolling-pluming, occurs resulting in a flat bed (case C, Figure 12). A final case under particularly intense flows characterized by a rapidly growing granular-fluid layer is shown as case D in Figure 12. This case may entail some portion of all the previous cases but occurs too rapidly to be dissected by the present methods.

Boundary Layer Development Under the Wave Trough

The observations of boundary layer development under the wave trough show a striking contrast to that under the crest. The initial stages of the boundary layer development under the trough appear to be qualitatively the same as those under the crest, starting with a laminar boundary layer which leads into the onset of motion followed by streaking. The subsequent regimes of rolling and pluming were never observed to develop under the wave trough. Indeed, development of the granular-fluid layer under the trough appears to consist instead of a steady thickening of a granular-fluid sheet without the abrupt transitions to rolling and pluming. The surface of this sheet flow exhibits random fluctuations in cross-stream elevation, but the elevation in the streamwise direction is more or less uniform. In contrast to the rolled layer, the surface of this sheet suggests the predominance of turbulent mixing. The thickness of the granular-fluid layer for similar free stream velocities appears to be smaller under the trough than under the crest. It is not implied that transition to turbulence does not occur under the trough. On the contrary, the visual impression is that the granular-fluid sheet under intense conditions is most clearly turbulent. However, there is no clear demarcation for the transition to turbulence, and it appears that the transition is a gradual process. While low steepness ripples have been observed under the trough of the wave, they are the result of waves with low Shields number and were never observed to form immediately following sheet flow. No pluming has been observed under the wave trough in the field.

Laboratory Observations

Following the field observations, an attempt was made to recreate these granular-fluid flow regimes in the laboratory. A bed of loose sand 5 cm deep and 225 cm long was placed in a 44.5 m long by 200 cm wide wave channel. The surf spider, complete with the same instrumentation as in the field studies minus the video camera, was mounted in the center of the bed. Shallow water waves of 5-s periods and 51-cm wave heights were generated in water with a depth of 132 cm. The bed was filmed with a movie camera viewing through a Plexiglas window while synchronized measurements were recorded as in the field experiments. The main observation from these tests was that no rolling or pluming occurred and that any asymmetry between crest and trough was not readily apparent or could be attributed to velocity and acceleration asymmetries inherent in the shallow water wave form. This is in contrast to our field experiments where waves with a similar Reynolds number ($Re = 3.5 \times 10^5$) clearly developed into rolling (Figure 9) and exhibited the associated crest-trough asymmetry.

Discussion

Other investigators [e.g., *Hanes and Huntley*, 1986] have observed crest-trough asymmetries in the sediment response and

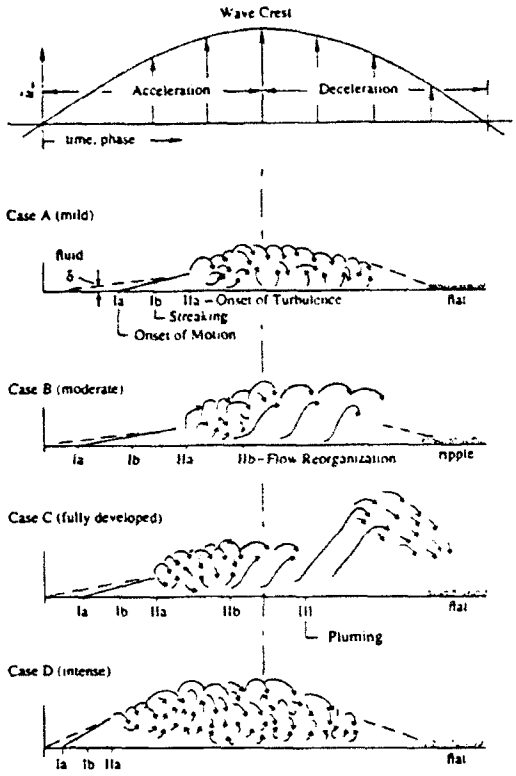

Fig. 12. Schematic drawing of four identifiable sequences in the development of the fluid-granular boundary layer under the crest of near-breaking waves, shown in the order of increasing intensity of motion at the interface. Details of case C are shown in Figure 4.

have attributed this behavior to asymmetries in the free stream velocity and/or acceleration. However, Figure 13 indicates that such an explanation cannot fully explain the asymmetry observed in our experiments. A histogram of the maximum onshore (crest) and offshore (trough) velocities observed during the June 5 experiment is shown in Figure 13*a* together with the observed range of free stream velocities at the onset of roiling. Clearly, the offshore flows are not velocity limited, yet roiling did not occur. In Figure 13*b* we have plotted the maximum onshore Eulerian accelerations as well as the observed range of accelerations at the onset of roiling. For the offshore motion, we have plotted the observed trough acceleration maxima for only the wave half-cycles which had free stream velocities within the observed range for the onset of roiling. Again it is clear that the trough flow, when compared to the crest, is not acceleration limited.

Many theoretical investigations [e.g., *Longuet-Higgins*, 1953; *Jacobs*, 1984] predict a steady mass transport in the boundary layer beneath progressive gravity waves. While observations of this phenomenon have been made in the laboratory, there was little mean boundary layer current observed in our near-breaker experiments. The three hot film runs used to compute the ensemble spectrum which appears in Figure 10 had probe heights of 1.5 cm, 4.2 cm, and 1.8 cm above the at-rest bed prior to the start of each run. The field calibrations for these three runs had standard deviations with respect to the em current meter of 0.9%, 1.2%, and 0.9% respectively, where the values are expressed as a percentage of the measured values. The mean current over each of the three data runs was 0.5, 2.5, and 1.9 cm/s respectively. It is clear from Figure 13 that mean currents of this magnitude are not sufficient to explain the asymmetry observed in our experiments.

Numerous theoretical investigations of progressive gravity waves propagating over a permeable bed [*Reid and Kajiura*, 1957; *Packwood and Peregrine*, 1980] indicate that an oscillating flow is induced in the bed and results in flow normal to the bed surface under the crest and trough of the wave. This flow is the result of the spatially varying pressured field imposed on the bed over an entire wavelength. This ventilation flow is out of the bed and into the fluid (injection) under the wave trough and into the bed (suction) under the crest. These studies also indicate that with typical natural beds, the induced velocities are several orders of magnitude smaller than the horizontal, free stream, wave-orbital velocities, and so any effect on the free stream velocities is small. On the other hand, the effect of small normal flows on the oscillatory boundary layer is not necessarily negligible.

It has long been known (see for example *Tewfik* [1963], *Mickley and Davis* [1957], *Schlichting* [1979]) that except for transitional processes, boundary suction with steady flow leads to enhanced bed stress and injection leads to reduced bed stress even for the small ratios of boundary normal to free stream velocity to be expected in an oscillatory boundary layer over a sand bed. It is also known that suction has the effect of stabilizing the flow, reducing the three-dimensionality of the turbulent boundary layer

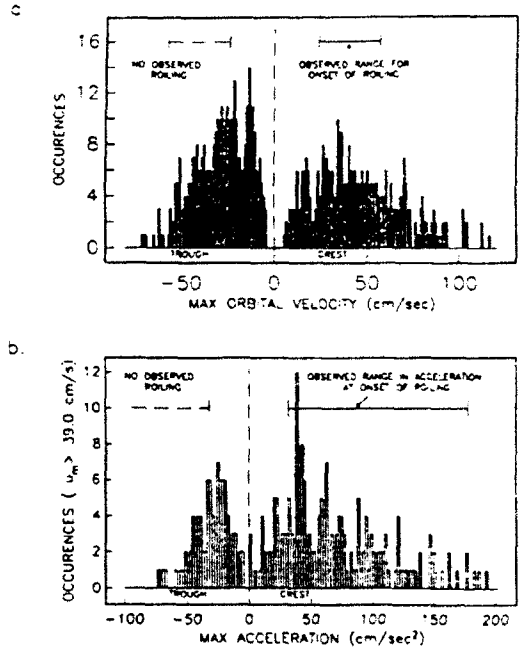

Fig. 13. Histograms of (a) orbital velocity and (b) acceleration maxima associated with onshore-offshore orbital motion for the field deployment of June 5, 1989. Solid brackets indicate ranges of observed roiling onset during onshore (crest) motion. Dashed brackets indicate same ranges for offshore (trough) motion.

and increasing the relative contribution of large-scale coherent structures [*Fulachier et al.*, 1982]. *Tewfik* [1963] reports that injection decreases the rate of growth of the turbulent boundary layer. Injection also moves the shear maxima away from the bed which, combined with a "law of the wall" type approximation, suggests that under the trough sediment suspending turbulent kinetic energy (TKE) is removed from the bed which is the source of sediment. The reverse is true of suction.

It is suggested from the above that an oscillatory boundary layer over a permeable sand bed, alternatingly experiencing suction and injection under the crest and trough of the wave respecively, would exhibit the following characteristics. The turbulent boundary layer under the trough would be expected to be slow developing and fully homogeneous with little structure. Any internal dynamics within the boundary layer under the trough would be obscured by strong turbulent mixing which would occur further from the bed, around the displaced TKE maxima. The sediment-mobilizing properties of the flow would be diminished (decreased bed stress with TKE removed from the bed) which would be reflected in thinner, less dense granular-fluid layers. Flow under the crest would be characterized by a more rapid and therefore distinct turbulent boundary layer development. The boundary layer would be expected to be less homogeneous, exhibiting more structure than under the trough. Sediment mobilization would be enhanced. Such a phenomenon would clearly have strong repercussions for any type of modeling which treats boundary layer development as a function of magnitude only. For example, the concept of friction factors in this type of situation would require a separate set of friction factors for flow under the crest and trough respectively.

It should be noted that turbulent transition under the crest which occurs at a phase greater than 90° would be experiencing the destabilizing affect of an adverse pressure gradient and would be expected to be qualitatively different than transition which occurs earlier, even though suction could still be playing a roll in boundary layer characteristics.

For permeable beds where the thickness of the bed is small relative to the wavelength, *Packwood and Peregrine* [1980] show that the ratio of vertical velocity to free stream velocity, w_{bed}/u_∞, under the crest of the wave is linearly proportional to the thickness of the permeable bed. Thus the crest-trough asymmetry observed in the field would not be expected to be seen in a laboratory setting which does not have a permeable bed which is either relatively deep and/or long enough to simultaneously "feel" an entire wavelength.

All our observations support this theory and a laboratory experiment utilizing a ventilated bed is under way in order to investigate this phenomenon more closely.

CONCLUSIONS

In situ field observations have been made of the development of the wave-induced fluid-granular boundary layer over permeable beds of loose sand. The visual record accompanied by synchronized measurement of physical parameters leads to the following conclusions:

1. The full fluid-granular boundary layer development under the crest of the wave can be divided into an identifiable three-part sequence composed of streaking, roiling, and pluming.

2. The streaking-roiling transition is the manifestation of a sudden laminar-turbulent transition.

3. A crest-trough asymmetry in the fluid-granular boundary layer development has been identified. This asymmetry is independent of asymmetries in the near-bed orbital velocity and acceleration and is thought to be related to effects of ventilation in the permeable bed.

Acknowledgments. This study was funded by the Office of Naval Research, Coastal Studies under grant N00014-89-J-1060 with the University of California, San Diego. We are especially indebted to Scott A. Jenkins for ideas and help in the field since the inception of the project. Useful insights into this complex problem were provided by D. Murray Hicks, Hyung Ki Kim, and A.W. Green. Aid in instrumentation, field measurements and data analysis was provided by Bill Boyd, David W. Skelly, Joseph Wasyl, and B. Walton Waldorf. Patricia M. Masters aided in the terminology of sequences in the development of the fluid granular boundary layer.

REFERENCES

Bagnold, R. A., Motion of waves in shallow water; Interaction between waves and sand bottoms, *Proc. R. Soc., London, Ser. A, 187*, 1–18, 1946.

Diegler, J. R., and D. L. Inman, Wave-formed ripples in nearshore sands, *Proc. Conf. Coastal Eng., 15th*, 2109–2126, 1976.

Fleck, R. E., and R. A. George, Turbulence scales in the surf and swash, *Proc. Conf. Coastal Eng., 22nd*, 557–569, 1990.

Fulachier, L., M. Elena, E. Verollet, and R. Dumas, Suction effects on the structure of turbulent boundary layer on a heated porous wall, *Structure of Turbulence in Heat and Mass Transfer*, edited by Z. P. Zoraic, pp. 193–220, Hemisphere, Washington, 1982.

Hanes, D. M., and D. A. Huntley, Continuous measurements of suspended sand concentration in a wave dominated nearshore environment, *Cont. Shelf Res.*, *6*(4), 585–596, 1986.

Hayashi, T., and M. Ohashi, A dynamical and visual study on the oscillatory turbulent boundary layer, in *Turbulent Shear Flows*, vol. 3, edited by L. J. S. Bradbury, pp. 18–33, Springer Verlag, New York, 1982.

Heathershaw, A. D., Bursting phenomena in the sea, *Nature*, *248*(5447), 394–395, 1974.

Herbert, T., Secondary instability of boundary layers, *Annu. Rev. Fluid Mech.*, *20*, 487–526, 1988.

Hino, M., M. Kashiwayanagi, A. Nakayama, and T. Hara, Experiments on the turbulence statistics and the structure of a reciprocating oscillatory flow, *J. Fluid Mech.*, *131*, 363–400, 1983.

Hinze, J. O., *Turbulence*, 2nd ed., 790 pp., McGraw-Hill, New York, 1975.

Inman, D. L., Wave generated ripples in nearshore sands, *Tech. Memo 100*, 65 pp., U.S. Army Corps of Eng., Beach Erosion Board, 1957.

Inman, D. L., and A. J. Bowen, Flume experiments on sand transport by waves and currents, *Proc. Conf. Coastal Eng., 8th*, 137–150, 1962.

Inman, D. L., and E. B. Tunstall, Phase dependent roughness control of sand movement, *Proc. Conf. Coastal Eng., 13th*(2), 1155–1171, 1972.

Inman, D. L., G. C. Ewing, and J. B. Corliss, Coastal sand dunes of Guerrero Negro, Baja California, Mexico, *Bull. Geol. Soc. Am.*, *77*(8), 787–802, 1966.

Inman, D. L., S. A. Jenkins, D. W. Hicks, and H. K. Kim, Oscillatory bursting over beds of fine sand, *SIO Ref. 86-13*, 46 pp. + appendix, Scripps Inst. of Oceanogr., Univ. of Calif., San Diego, La Jolla, 1986.

Jackson, R. G., Sedimentological and fluid-dynamic implications of the turbulent bursting phenomenon in geophysical flows, *J. Fluid Mech.*, *77*(3), 531–560, 1976.

Jacobs, S. A., Mass transport in a turbulent boundary layer under a progressive water wave, *J. Fluid Mech.*, *146*, 303–312, 1984.

Jensen, B. L., B. M. Sumer, and J. Fredsoe, Turbulent oscillatory boundary layers at high Reynolds numbers, *J. Fluid Mech.*, *206*, 265–297, 1989.

Jonsson, I. G., Measurements in the turbulent wave boundary layer, *Proc. Congr. IAHR, 10th*(1), 85–92, 1963.

Jonsson, I. G., Wave layers and friction factors, *Proc. Conf. Coastal Eng., 10th*(1), 127–148, 1966.

Jonsson, I. G., A new approach to oscillatory rough turbulent boundary layers, *Ocean Eng.*, *7*, 109–152, 1980.

Jordinson, R., The flat plate boundary layer, 1, Numerical integration of the Orr-Somerfeld equation, *J. Fluid Mech.*, *43*(4), 801–811, 1970.

Justesen, P., Turbulent wave boundary layers, *Ser. Pap. 43*, 226 pp., Inst. of Hydrodyn. and Hydraul. Eng., Tech. Univ. of Denmark, Lyngby, 1987.

Kamphuis, J. W., Friction factor under oscillatory waves, *J. Waterw., Harbors Coastal Eng.*, Am. Soc. Civ. Eng., *101*(WW2), 135–144, 1975.

Kim, H. T., S. J. Kline, and W. C. Reynolds, The production of turbulence near a smooth wall in a turbulent boundary layer, *J. Fluid Mech.*, *50*(7), 133–160, 1971.

Kline, S. J., W. C. Reynolds, F. A. Schraub, and P. W. Runstadler, The structure of turbulent boundary layers, *J. Fluid Mech.*, *30*(4), 741–773, 1967.

Lamb, H., *Hydrodynamics*, 738 pp., Dover, New York, 1945.

Landahl, M. T., and E. Mollo-Christensen, *Turbulence and Random Processes in Fluid Mechanics*, 154 pp., Cambridge University Press, New York, 1986.

Longuet-Higgins, M. S., Mass transport in water waves, *Proc. R. Soc. London, Ser. A*, *245*(903), 535–581, 1953.

Madsen, O. S., Stability of a sand bed under breaking waves, *Proc. Conf. Coastal Eng., 14th.*, 776–794, 1974.

Mercerat, F. J., An experimental study of wind velocity profiles over a wavy surface, *Tech Rep. 2*, 90 pp. + appendix, Coll. of Mar. Stud., Univ. of Del., Newark, 1972.

Mickley, H. S., and R. S. Davis, Momentum transfer for flow over a flat plate with blowing, *Tech. Note 4017*, 64 pp., Natl. Adv. Comm. Aeronaut., Washington, 1957.

Packwood, A. R., and D. H. Peregrine, The propagation of solitary waves and bores over a porous bed, *Coastal Eng.*, *3*, 221–242, 1980.

Putnam, J. A., and J. W. Johnson, The dissipation of wave energy by bottom friction, *EOS, Trans. AGU*, *30*, 67–74, 1949.

Reid, R. O., and K. Kajiura, On the damping of gravity waves over a permeable sea bed, *EOS, Trans. AGU*, *38*, 662–666, 1957.

Schlichting, H., *Boundary Layer Theory*, 7th ed., 817 pp., McGraw-Hill, New York, 1979.

She, Z.-S., and S. A. Orszag, Physical model of intermittency in turbulence: Inertial-range, non-Gaussian statistics, *Phys. Rev. Lett.*, *66*(13), 1701–1704, 1991.

Sleath, J. F. A., The effect of waves on the pressure in a bed of sand in a water channel and on the velocity distribution above it, *Ph.D. thesis*, Univ. of Cambridge, Cambridge, England, 1968.

Sleath, J. F. A., Wave induced pressures in beds of sand, *J. Hydraul. Div., Am. Soc. Civ. Eng.*, *96*, 367–379, 1970.

Tewfik, O. E., Some characteristics of the turbulent boundary layer with air injection, *AIAA J.*, *1*(6), 1306–1312, 1963.

Tunstall, E. B., and D. L. Inman, Vortex generation by oscillatory flow over rippled surfaces, *J. Geophys. Res.*, *80*(24), 3475–3484, 1975.

Weedman, S. D., and R. Slingerland, Experimental study of streaks formed in turbulent boundary layers, *Sedimentology*, *32*, 133–145, 1985.

Winant, C. D., and F. K. Browand, Vortex pairing: The mechanism of turbulent mixing-layer growth at moderate Reynolds number, *J. Fluid Mech.*, *63*(2), 237–255, 1974.

D. C. Conley and D. L. Inman, University of California, San Diego, Scripps Institution of Oceanography, Center for Coastal Studies, 0209, 9500 Gilman Drive, La Jolla, CA 92093-0209.

(Received June 6, 1991;
revised December 31, 1991;
accepted December 31, 1991.)

CHAPTER II

VENTILATED OSCILLATORY BOUNDARY LAYERS

1. INTRODUCTION

Laboratory studies of the boundary layer arising from oscillatory flow have always treated the problem as a cyclical process composed of two purely symmetrical half cycles [eg Jonsson, 1963; Sleath 1987]. Asymmetries occurring in the laboratory [Flick et al, 1981] or the field [Hanes & Huntley, 1986] have been explained by asymmetries in the fluid velocity or acceleration inherent in shoaling waves. In a paper reporting on field observations of wave driven oscillatory boundary layers over sand beds, Conley and Inman [1992] reported the observation of an asymmetry in the development of the boundary layer which could not be explained by velocity or acceleration asymmetries in the overlying fluid. As a possible mechanism for this asymmetry, they proposed a type of transpired boundary layer which is here called the ventilated oscillatory boundary layer. This work reports on laboratory experiments designed to investigate the effect of boundary ventilation on the velocities, bed stress and turbulent flow properties of the turbulent oscillatory boundary layer.

Transpired boundary layers have practical significance in many applications and have been the subject of studies for well over forty years [eg Libby et al, 1952; Antonia et al, 1990]. These are boundary layers which arise from a fluid flowing with velocity u parallel to a solid permeable boundary through which a secondary fluid is flowing with velocity w. The secondary flow through the boundary is generally referred to as transpiration. If the sense of transpiration is into the overlying fluid ($w > 0$), it is called injection or blowing. If the sense of transpiration is

from the fluid into the surface ($w < 0$) it is termed suction. In general the two fluids are identical and the transpired flow is smaller in magnitude than boundary parallel flow so that the transpiration parameter $V=w/u$ has a magnitude less than 1.

Ventilated oscillatory boundary layer is a term applied here to the boundary layer arising from an oscillating boundary parallel flow subject to oscillating transpiration of the same period and shape. In this work, the dominant flow is of the form $u(t) = u_m sin(\sigma t)$ and subject to transpiration of the form $w(t) = w_m sin(\sigma t+\phi)$. Here $\sigma = 2\pi/T$ is the radian frequency, T is the period and ϕ is an arbitrary constant phase. Analogous to the transpiration parameter V, a flow ventilation parameter $\tilde{V}$ shall be defined as $\tilde{V} = w_m/u_m$. The sign of $\tilde{V}$ indicates whether injection ($\tilde{V}>0$) or suction ($\tilde{V}<0$) occurs concurrently with positive flow. Additionally, an instantaneous ventilation parameter shall be defined as $\tilde{V}' = w(t)/u(t)$. Through most of this work, the phase ϕ will be 0 in which case $\tilde{V}'$ becomes a constant, identically equal to $\tilde{V}$.

In general boundary transpiration affects the boundary layer velocity profile. Suction tends to pull streamlines down closer to the bed shifting the velocity profile closer to the wall. This results in higher shear near the bed and therefore higher shear stress at the bed. This is demonstrated quite clearly in a comparison of the asymptotic suction profile, an exact solution to the Navier Stokes equations for flow over a flat plate with constant suction, and the Blasius profile [Schlichting, 1979]. In contrast, injection results in a spreading of the streamlines near the boundary which reduces the near bed shear and the resultant bed stress.

In a study of turbulent boundary layers in steady flow over flat plates with injection, Mickley & Davis [1957] show that the friction factor C_f is a strong function of V and Re_x where Re_x is the Reynolds number based on distance along the plate. However their results can be shown to indicate that the ratio C_f/C_{f_o} where C_{f_o} is the friction factor with out injection, is a strong function of V but exhibits almost no Re_x dependency. The results of Simpson et al [1969] show the same to be true for steady suction on a flat plate.

The asymptotic suction profile shows reduced curvature in the boundary layer velocity profile relative to the Blasius profile [Schlichting, 1979]. This suggests that suction tends to stabilize the flow. Analytical solutions for boundary layers with injection show an inflection point in the velocity profile suggesting that injection tends to destabilize the flow. Experiments have shown these findings to be true not only for laminar flow but turbulent flow as well. Tewfik [1963] demonstrated that turbulent boundary layers with injection were thicker than would be the case without injection. It was also shown that while injection reduces stress at the bed and through out the inner tenth of the boundary layer, it increased it elsewhere. Antonia et al [1988] reconfirmed that suction results in a significant reduction in turbulent velocity fluctuations u' and w'. While investigating the effect of suction on organized motion in turbulent boundary layers, they observed that low speed streaks in the near wall region were more persistent and that the frequency of dye injections into the outer layer was reduced. This is consistent with the results of Fulachier [1982] where the rate of turbulent production was found to decrease and the relative contribution of large scale structures was found to increase.

Kays [1972] shows that transpired turbulent boundary layers seem to respond to local conditions. That is a boundary layer experiencing a sudden change in injection will, following a short period of adjustment, behave as though it had always been subject to that level of injection. This appears to be less true for a reduction in injection than for an increase. It is also shown that transpired boundary layers are sensitive to acceleration, the sensitivity increasing with V. No studies have been reported on the effects of transpiration in oscillatory flow.

2. EXPERIMENTAL SETUP

The experiments have been performed using the oscillatory flow tunnel (OFT) at the Scripps Institution of Oceanography hydraulics laboratory (Figure 1). The OFT is composed of an acrylic working section 7.0 m long which terminates in painted steel cylindrical risers at each end. One riser acts as a reservoir and is open to the atmosphere, the other riser is sealed by a 62

cm diameter acrylic piston which drives the oscillating flow. The piston is controlled by a hydraulic ram which can be programmed to respond to any electrical input. Further details of the facility are described by King et al [1984]. For these experiments a false floor was placed in the working section giving a tunnel cross section 39 cm wide and 28 cm deep. The test section was created by placing a rigid, permeable floor in the center 4.25 m of the working section. This floor was composed of fourteen 30 x 30 x 2.5 cm bricks of fused Alundum. These bricks were composed of Alundum grains with a mean diameter of 250 microns which were fused under high temperature. Prior to fireing, the bricks were pressed at high pressure. As a result, the flat surfaces of the rather angular grains aligned to form a smooth surface on the bricks. Roughness elements are caused by pores in the surface, not by protuberant grains. The mean pore size of the internal pores is stated to be 180 microns. A secondary piston which was plumbed into the the cavity below the test section was used to drive the boundary layer ventilation.

Tests were performed using a period of oscillation, T = 7 s and an orbital displacement d_0 of 207 cm. This results in a flow with oscillatory Reynolds number, $\tilde{\mathrm{Re}}$, of 1.0×10^6 where $\tilde{\mathrm{Re}}$ is defined by

$$\tilde{\mathrm{Re}} = \frac{u_m d_o}{2\nu} \tag{1}$$

where u_m is the maximum mass averaged velocity. The results of Jensen et al [1989] have shown that oscillatory boundary layers of this $\tilde{\mathrm{Re}}$ will be fully turbulent for phases greater than 45^o and transitional for phases greater than 15^o. For the unventilated case, the boundary layer thickness δ_0 is 1.8 cm where δ_0 has been defined as the first level at which the vertical derivative of velocity vanishes at a phase of 90^o. The maximum friction velocity $u_{*m} = \sqrt{\tau_m/\rho}$ is 4.1 cm/s. The Nikuradse equivalent roughness parameter k_s as determined from boundary layer velocity profiles was found to be 0.003 cm giving a roughness Reynolds number $k_s^+ = u_{*m}k_s/\nu$ of 1.3. The ventilation parameter $\tilde{V}$ was zero in the control tests and ranged in magnitude from 2.5×10^{-4} to $4.\times10^{-3}$ in other tests. The amplitude of w was calculated by assuming uniform velocity over

the test bed and distributing the volumetric displacement of the secondary piston over the entire test bed. Calculations indicate that uniform velocity over the test bed is a good assumption given the manufacturers supplied permeability of 192 Darcys for the Alundum bricks. This assumption was tested through dye studies in which no systematic variations in the flow through the bricks could be detected.

Three main flow parameters are presented in this work. These include the bed stress $\tau(t)$, fluid velocity $u(z,t)$ and the vertical component of fluctuating velocity $w'(z,t)$. The bed shear stress was measured using a TSI model 1237W flush mounted hot film sensor as shown in Figure 2. The sensor was locked into an acrylic probe holder 9.5 mm in diameter which fit through an O-ring seal into a cylindrical acrylic sleeve of 1.8 mm wall thickness. The sleeve was permanently epoxied into the test bed with the top of the sleeve flush with the tops of the roughness elements forming the fixed surface of the Alundum bed. When inserted, the tops of the probe and holder were level with the top of the sleeve. This arrangement allowed the shear stress sensor to be calibrated in a separate facility and maintain the same relationship between probe and holder when transferred to the test facility.

The longitudinal component of velocity was measured using a TSI model 1210-20W cylindrical hot film sensor. The probe was mounted on a sting projecting through the lid of the OFT with the axis of the sensing element horizontal and transverse to the direction of flow. This probe was calibrated by placing it in the tunnel center and calibrating against the tunnel mass averaged velocity using a technique adopted from Flick & George [1990] While the hot film measures fluid speed, the time series was derectified using the mass averaged fluid velocity zero crossings as a reference. Turbulent velocity fluctuations were measured using a TSI model 1287W split film hot film. This sensor has a cylindrical sensing element composed of two halves which are electrically insulated. This design permits decomposition of the measurements into two components of velocity. Briefly, the magnitude of the cooling for both halves is dependent on the magnitude of the velocity vector and the ratio of the cooling is dependent on angle the vector

makes with the plain of the splits. Operation of the sensor is discussed in [Blinco & Sandborn, 1975]. The directional sensitivity was calibrated once before and after all tests while the velocity magnitude response was calibrated for every test as described for the cylindrical hot films above.

Depending on the test, data runs were of 500 or 700 seconds in duration. The time series collected over each run were ensemble averaged in order to determine the phase averaged quantities. In oscillatory flows, the turbulent decomposition of a flow property $\xi(t)$ has three components, the time mean $<\xi>$, the ensemble averaged mean $\bar{\xi}(\theta)$ and the ensemble averaged r.m.s. mean of the fluctuating quantity $\sqrt{\overline{\xi'^2}}(\theta)$. In a purely oscillatory flow, the traditionally defined time mean is identically zero. For a time series collected over N cycles of period T, the ensemble average mean is calculated as

$$\bar{\xi}(\sigma t) = \frac{1}{N}\sum_{i=1}^{N}\xi\left[\sigma t + (i-1)T\right] \tag{2}$$

where σ is the radian frequency $\frac{2\pi}{T}$ and the definition is valid for t=0 to t=T. Similarly the ensemble averaged r.m.s. mean of the fluctuating quantity is defined by

$$\overline{\xi'^2}(\sigma t) = \frac{1}{N-1}\sum_{i=1}^{N}\left[\xi\left[\sigma t + (i-1)T\right] - \bar{\xi}(\sigma t)\right]^2 \tag{3}$$

This decomposition is schematicized in Figure 3. Sleath [1987] and others have shown that there was no significant improvement in the consistency of the estimate of ensemble averaged mean quantities for averages of greater than 50 cycles. The 500 s tests in this work represent 71 cycles and the 700 s tests represent 100 cycles. When discussing the phase of the oscillatory flow θ, the convention will be used that θ=0 corresponds to the negative to positive velocity zero crossing.

3. EFFECTS OF VENTILATION

The ensemble averaged centerline velocity for the case of no flow through the bed is shown in Figure 4a. As can be seen from the plot, the velocity is relatively symmetric throughout the entire cycle. Each half cycle appears qualitatively similar to the other half cycle and the accelerating portions of each half cycle appear to be mirror images of the decelerating portion. Figure 4b. is a plot of ensemble averaged centerline acceleration. This plot reveals asymmetries in the flow which are not obvious in the velocity. In particular it is seen that acceleration tends towards a monotonical decrease through out the first half cycle as would be expected in an oscillatory flow. This is not true for the second half cycle where periods of decreasing acceleration are clearly present in what would be expected to be a time of monotonically increasing acceleration.

While these fluctuations don't appear to have a big affect on fluid velocity, it might be anticipated that these fluctuations in pressure gradient would have a larger affect in the boundary layer and on the bed stress. This seems to be born out by the results presented in Figure 4c. The solid line represents the ensemble averaged bed stress as derived from the shear stress sensor. The bed stress in the second half cycle is much peakier than would be expected in an oscillatory flow of this Reynolds number $\tilde{Re} = 10^6$ while the first half cycle is more typical [see Jensen et al, 1989].

Jensen et al [1989] have shown that the boundary layer velocity profiles in high Reynolds number flows do exhibit a logarithmic-layer from which the Nikuradse equivalent roughness length k_s and the bed stress can be determined. This was found to be especially true around the occurrence of peak free stream velocity. In order to test this in the present experiments, k_s was taken as the average value derived from the best fits to a logarithmic layer in the phase range $45^o \leq \theta \geq 135^o$ This value of k_s was then used to calculate the bed stress through out the wave cycle. These values are plotted as heavy dots in Figure 4c and as can be seen, they give a reasonable estimate of bed stress in the first half cycle. However when this same procedure is

performed using the roughness derived from profiles in the range $225^o \leq \theta \geq 315^o$, it results in a underestimation of bed stress as can be seen by the open dots in Figure 4c. In fact it appears that bed stress estimates based on k_s derived from the first half cycle are better than those based solely on second half cycle parameters. The logarithmic-layer is a consequence of the presence of a constant stress layer in the boundary layer. It is not surprising that the presence of a fluctuating pressure gradient would disturb this constant stress layer as evidently occurs in the second half cycle. As a consequence of this anomalous behavior, the following convention is adopted throughout the paper. When discussing bed stress, results from only the first half cycle shall be used and the sense of ventilation will be alternated to provide both suction and injection during that half cycle. The full cycle shall only be utilized when presenting velocity and turbulence profiles. While in general the bed stress results from the second wave half cycle differ quantitatively from the first, the conclusions arrived at in this work are qualitatively supported by the results from both half cycles.

Boundary Layer Velocity

As discussed earlier, the most direct way that suction is expected to affect the boundary layer is to draw the velocity profile down close to the bed. In the boundary layer this results in higher mean velocities near the bed and a greater shear at the bed. The affect of injection is expected to be just the reverse, namely streamlines pushed away from the bed leading to lower mean boundary layer velocities and a reduced bed shear. This pattern is exactly what is seen in Figure 5. This figure shows a series of boundary layer profiles at various phases throughout the entire cycle. At each phase there are two profiles. The solid line represents the velocity profile for the case of no ventilation and the dashed line represents the velocity profiles for $\tilde{V} = 5\times10^{-4}$. It is immediately obvious that even for such a small value of the ventilation parameter, the mean velocities in the boundary layer are affected. In particular it is seen that during the occurrence of suction ($0^o \leq \theta \leq 180^o$) the mean velocities throughout the boundary layer and well above it are

uniformly greater than the unventilated velocities. This fact necessitates that the shear at the bed is greater which is in fact clear in the figure. Once again, just the reverse is true for injection ($180^{o} \leq \theta \leq 360^{o}$). It is even more readily evident that the mean velocities throughout the boundary are lower with injection than the unventilated case and therefor the boundary shear is less than the unventilated case.

Considering the symmetric nature of unventilated oscillatory flow, it is clear that the above observations require an asymmetry in the mean boundary layer velocities for a ventilated oscillatory boundary layer. In fact this asymmetry must be realized as a net current in the boundary layer above the permeable bed. This current will be positively directed for negative $\tilde{V}$ and vise versa.

Turbulence

A contour plot of the development of $\sqrt{\overline{w'^2}}$ over phase and elevation is shown in Figure 6. This is for the case of no ventilation and the results are qualitatively similar to those reported by others [see Sleath 1987]. Sleath [1987] reported that $\sqrt{\overline{w'^2}}$ and $\sqrt{\overline{u'^2}}$ behave qualitatively the same, so for the following discussion, it shall be assumed that the behavior of $\sqrt{\overline{w'^2}}$ is indicative of turbulent intensities in general. In general the maximum in turbulence intensity is seen to occur near the bed just following the start of deceleration (90^{o} and 270^{o}). From this maxima the turbulence slowly diffuses upward over phase giving the impression of an inclined plume. For unventilated oscillatory flow, this pattern is relatively symmetrical with turbulence maxima occurring at about the same level in each half cycle and the size, shape and inclination of the turbulent plumes are the same in each case. It is also seen that the turbulence levels associated with each half cycle return to the background level prior to the arrival of the next plume.

The effects of ventilation on the turbulent properties of the flow are shown in Figure 7. This is a contour plot of the development of $\sqrt{\overline{w'^2}}$ over phase and elevation for the case of $\tilde{V}$ =

0.001. The figure shows three major effects of ventilation. The first effect is that near the bed, the turbulence levels are higher with suction ($0^o \leq \theta \leq 180^o$) than injection. This is observed in the figure where the contours of $\sqrt{\overline{w'^2}}$ are one level higher for the suction half cycle than for the injection half cycle. Second, with suction the turbulence maximum is drawn closer to the bed. Finally, due to the flow stabilizing tendency of suction and the destabilizing influence of injection, the turbulent plumes have become totally distorted. In particular, the turbulent plume originating in the half cycle with suction is very much diminished and is contained in a thin layer ($\approx$5mm) drawn near the bed. The turbulent plume from the injection half cycle is much enhanced, extending higher into the flow and, consequentially, much later in the flow. This tendency is so pronounced that it would appear that the majority of the turbulence that arises from the injection half cycle occurs during the subsequent half cycle. The net affect of this is that a "snapshot" of turbulence levels at constant phase would show the highest turbulence levels to occur during the half cycle with suction!

Using a logarithmic elevation scale, the contour plot of the time history of $\sqrt{\overline{w'^2}}$ (Figure 8) shows that the previously described qualitative picture is true for $\tilde{V}$ as low as -0.0005, the lowest ventilation parameter for which data of this type was collected. In short, the turbulence levels near the bed are enhanced for suction, the turbulent plume associated with suction is confined close to the bed and the turbulent plume associated with injection is enhanced and persists in time throughout most of the subsequent half cycle.

Bed Stress

The effect of boundary ventilation on bed stress is summarized in Figure 9. Plotted in this figure is the ensemble averaged bed stress from 500 second runs for various ratios of the ventilation parameter $\tilde{V}$. The heavy solid line is the bed stress for the case of no ventilation and serves as the baseline for the other tests. The peak value from this curve has been used to

normalize all the data. As can be seen in the figure, ventilation clearly affects the bed stress in oscillatory flow with suction ($\tilde{V}<0$) leading to increased bed stress and injection ($\tilde{V}>0$) causing reduced bed stress. This figure shows that there is a significant stress reduction or enhancement for ventilation parameters with magnitudes as low as 2.5×10^{-4}.

The data from Figure 9 has been used to construct Figure 10. For each value of $\tilde{V}$, the bed stress was integrated over all positive values and normalized by the integrated bed stress for no ventilation. These points are plotted as a function of ventilation parameter and are represented by the open points in Figure 10. The solid line is a composite of two functions which seem to give a good fit to the data points. Let R_i represent the ratio of integrated bed stress, then for $\tilde{V}\geq0$

$$R_i = e^{-a\tilde{V}} \tag{4}$$

where a was found to be 403. For $\tilde{V}>0$, R_i appeared to behave like

$$R_i = \frac{1}{b+c\ ln(\tilde{V})} \tag{5}$$

where b was found to be 1.506 and c = .1707. While this last relation performs well for the larger values of $\tilde{V}$, it is not defined for no ventilation and gives R_i=1 for a finite value of $\tilde{V}$. For the purposes of the figure, a straight line has been drawn between the point at $\tilde{V}$ = .00025 and $\tilde{V}$ = 0.

Even in a turbulent boundary layer, viscous stresses dominate within the viscous sub-layer. This means that the bed stress can be approximated as

$$\bar{\tau} = \mu\frac{\partial\bar{u}}{\partial z} \tag{6}$$

if $\bar{u}$ is measured sufficiently close to the bed. It is generally accepted that the viscous sublayer is present for $z^+\leq 5$ where z^+ is the dimensionless vertical coordinate defined by

$$z^+ = \frac{u_* z}{\nu} \tag{7}$$

and u_* is the friction velocity $\sqrt{\tau/\rho}$. The lowest elevation for which velocity was measured was at 0.01 cm which is within the viscous sublayer for all phases. It is therefore possible to calculate a second estimate of bed stress using (7). This process has been carried out using the velocity record at 0.01 cm and the results have been plotted on Figure 10 as filled boxes and show good agreement with the shear stress sensor data

4. PERSISTENCE OF VENTILATION EFFECT

$\tilde{\text{Re}}$ Dependence

In order to determine the $\tilde{\text{Re}}$ dependence of the effects of boundary ventilation, a series of tests were performed in which the flow $\tilde{\text{Re}}$ was varied. Using the linear relationship between d_0 and u_m, it can be shown that (1) is equivalent to

$$\tilde{\text{Re}} = d_0^2 \sigma / 4\nu. \tag{8}$$

As all tests were performed using the same frequency, reductions in $\tilde{\text{Re}}$ were achieved by reducing ${d_0}^2$ by the appropriate factor. The range over which $\tilde{\text{Re}}$ was varied was determined by limits of the physical apparatus. The largest $\tilde{\text{Re}}$ (1.0×10^6) represented the largest stroke which could be safely obtained from the hydraulic ram and the smallest (1.0×10^5) represented the lowest volume of water which could be accurately pumped through the permeable bed at the $\tilde{V}$ value of 1×10^{-3}.

Figure 11 shows the results of these tests. At each $\tilde{\text{Re}}$ the ensemble averaged mean stress with ventilation has been integrated over one oscillatory half cycle. These values were then normalized by the integrated bed stress for the unventilated case at the appropriate $\tilde{\text{Re}}$. These values have been plotted as the circles and squares in Figure 11. The bars on the plots represent 95% confidence intervals and the lines are linear least squares fits to the points. As can be seen in the figure any $\tilde{\text{Re}}$ dependence is weak as the fit to the data are essentially flat. Neither slope is

significantly different from 0 at the 95% confidence level although the slope for suction is significant at the 90% confidence level.

Phase Dependence

Since most of the results presented in this paper are for boundary ventilation which is in phase with the free stream flow, it was decided to test the sensitivity of the flow to variations in the phase relationship between the two flows. Zero phase in this section is defined as when the maximum magnitude of the boundary ventilation occurs simultaneously with the maximum in the free stream. Positive phase implies that that maximum ventilation occurs prior to the maximum free stream velocity and negative phase therefore implies maximum ventilation follows the free stream maximum. The range of phases has been restricted to $\pm 90^{o}$ with separate tests for suction and injection.

It should be noted that any phase difference between the two flows implies that each half cycle will experience periods of both suction and injection. For that reason, it was determined that presenting results in terms of bed stress integrated over a half cycle would not be useful and instead results are presented in terms of maximum bed stress normalized by maximum unventilated bed stress. These values are presented in Figure 12 where open circles represent the results for suction and the squares are the values for injection. The error bars represent 95% confidence limits calculated from the variance of the maximum stress measurements.

The simplest prediction for the effect of phase would indicate that flow history has no role in the effect of boundary ventilation. Such a formulation would state that the only parameter of importance is the instantaneous ventilation parameter $\tilde{V}'$. This parameter can be easily calculated as the cosine of the phase times the flow ventilation parameter $\tilde{V}$. Using these values of $\tilde{V}'$, the expected stress reduction or enhancement can be predicted from a plot similar to Figure 10 which is based on stress maxima rather than integrated stress. This procedure was used in

constructing the lines in Figure 12.

In a gross sense the results do appear to follow this trend. The effect of ventilation is a maximum around a phase of 0^o and drops off to no effect (ratio = 1) at $\pm 90^o$. The effects are seen not to be a critical function of phase, that is phase differences of $\pm 10^o$ do not radically change the effects of ventilation. In fact, the changes in bed stress over this range are not statistically different from each other. However for larger phase differences, the drop off rate is clearly different for each quadrant and therefore warrants inspection in all quadrants. The most straight forward behavior occurs for boundary suction with positive phase. Here the effects of ventilation appear to follow the simple cosine response. This indicates that with a stabilized boundary layer as exists with suction the stream lines equilibrate rapidly toward their undisturbed state as the level of applied suction is reduced. While not behaving as smoothly as suction with positive phase, injection with negative phase appears to also follow the cosine behavior. It is important to recall the sequence in the development of the boundary layer for this case. In particular the half cycle starts with suction occurring in the boundary which switches at some point to injection. We have already seen (above) that the boundary layer will quickly respond to the reduction of suction so the tendency for the bed stress to follow the cosine response implies that, when applied to a stable or unventilated boundary layer, the response time for shear reduction due to injection is small with respect to the time scales of the flow.

The behavior of injection with positive phase contrasts strongly with the above descriptions. In fact the only resemblance that the effect of boundary injection with positive phase has to cosine response is that the stress ratio does return to one at 90^o. Figure 12 illustrates that stress reduction due to injection grows at phases greater than 0^o even though the instantaneous ventilation parameter is decreasing. To understand this behavior it is important once again to consider the time history of the boundary layer. In this situation, the boundary layer has experienced boundary injection for the entire half cycle prior to the occurrence of maximum stress. The maximum injection rate occurs prior to the occurrence of maximum stress which occurs during a

time of decreasing injection. With this scenario in mind, it appears that the spreading of boundary layer streamlines induced by boundary injection is resistant to readjustment. In fact the slight tendency for increased stress reduction with phase suggest that once a level of spreading is developed, it can be maintained by smaller ventilation flows than originally present. In contrast to compressed boundary layer which appear to readjust immediately to changing conditions, boundary layer spreading appears to be resistant to readjustment. This result is fully consistent with results for steady flow subject to changing transpiration.

This interpretation seems to be validated by the results for boundary suction with negative phase. In this quadrant, the half cycle commences with boundary injection leading to boundary layer spreading. With the onset of suction, the stream lines are indeed drawn closer to the bed leading to greater bed stress for greater suction, but the level of bed stress enhancement never manages to attain the level it does working on a boundary layer which was not initially subject to injection.

Sensitivity to Velocity Asymmetry

In order to test how sensitive the effects of boundary ventilation are to the shape of the free stream velocity, a series of experiments were performed with an asymmetrical velocity waveform, a plot of which is shown in Figure 13. This waveform was taken from a time series of orbital velocities beneath near breaking waves in the ocean. This particular wave was chosen due to it's strong asymmetry, seven second period and the similarity of its flow parameters to the oscillatory wave forms generally employed in this study. The orbital displacement distance d_0 for this form was 182 cm. The maximum orbital velocity was 111 cm/s. Using (1) this give a $\tilde{\mathrm{Re}}$ of 1.0×10^6.

A series of runs were carried out to test the affects of boundary ventilation on this waveform. In these tests the exact same wave form was used to drive the ventilation velocity as

was used to drive free stream velocity and no phase difference was imposed. It should be understood that all suction results come from the peaked high velocity portion of the waveform (crest) and all injection results come from the flat low velocity portion of the waveform (trough). Once again, the integrated bed stress for each sub cycle, normalized by the unventilated integrated bed stress for the appropriate sub cycle is plotted as the open symbols in Figure 13. The solid curve is the same one plotted in Figure 10. It can be seen from this figure that in general shape has an insignificant affect on the effects of boundary suction. Shape does seem to have some affect on the effect of injection, particularly for larger values of $\tilde{V}$. This can be understood from the discussion in the previous section. It can be seen that the flat profile of the low velocity section leads to injection approaching its maximum value early in the sub cycle and then maintaining that value for a significant portion of the sub cycle. It seems likely that injection in this case would result in flow streamlines which exhibit a higher mean separation over the course of the longer duration sub cycle than would be expected with a more sinusoidal profile. This would result in greater bed stress reduction as is seen in the figure.

5. DISCUSSION

The results of these experiments show that the ventilated oscillatory boundary layer exhibits behavior which could have been qualitatively predicted from knowledge of the manner in which transpiration affects steady boundary layers. The importance of these effects can take on a larger significance in the oscillating case than they would appear to in the steady case. This can be demonstrated by considering the change in the boundary layer velocity profile. In an oscillatory boundary layer where the velocities in one half cycle are just the negative of the velocities in the second half cycle, the net velocity over one full cycle is identically zero. However in a ventilated oscillatory boundary layer where suction leads to higher velocities drawn nearer to the bed while injection causes a spreading of the velocity profile with lower velocities near the bed, a net velocity results in the boundary layer. The sense of this velocity is in the direction of the

oscillatory flow which is subject to suction.

A mean net boundary layer velocity has been determined for the values of $\tilde{V}$ for which velocity profiles where measured. This was done by integrating the mean velocity profiles over a height of 2 δ_0 (3.6 cm) where δ_0 was defined earlier. This vertically averaged mean velocity was then integrated over an entire cycle to arrive at the mean vertically averaged net velocity herein called the ventilation current $<v>_v$. These values have been plotted in Figure 14. The line in Figure 14 is a least squares fit for the relation $<u>_v/u_m = q\tilde{V}^n$. The best fit was found to be

$$<u>_v/u_m = 4.64\times|\tilde{V}|^{0.6}. \tag{9}$$

In this relation, the sign of $<u>_v$ is opposite the sign of $\tilde{V}$.

While the bed experiences no net stress in a purely oscillatory boundary layer, there is a net bed stress with ventilation. This net stress is a consequence of the bed stress reduction due to injection and the bed stress enhancement due to suction. When the two half cycles are averaged together they result in a net bed stress. Figure 15 shows the net bed stress due to a ventilated oscillatory boundary layer as a function of $\tilde{V}$. Here the results of Figure 9 have been used to construct this plot. The points in Figure 14 represent the integrated difference in the bed stress between the bed stress with suction and the bed stress with injection normalized by twice the integrated unventilated bed stress. These points therefor represent the mean net stress over an entire period as a percentage of the mean gross stress for the unventilated case. The solid line in the figure is straight line interpolation between the points. The dashed line is a linear fit to the first three values for ventilation which was forced to go through the origin. It appears that for small ventilation ($\tilde{V}\leq 0.001$), the net stress can be approximated by the linear relation

$$<\tau>_v/<|\tau_o|> = -420\times\tilde{V}. \tag{10}$$

Notice that this relation suggests that a 1% net stress is obtained with a ventilation parameter as small as 2.4×10^{-5}! It should again be observed that the direction of this net stress is in the

direction of the oscillating flow experiencing suction.

It is worthwhile to consider the importance these results may hold for geophysical situations. Reid & Kajiura [1957] as well as others have shown that a gravity wave traveling through a fluid medium over a permeable matrix will induce boundary ventilation. It can be shown that for geophysically reasonable permeabilities, the ventilation parameter $\tilde{V}$ will not exceed 1×10^{-3} and that phase differences between u and w will be $O(5^{o})$ or less. This means that in general wave driven ventilated boundary layers will produce a mean boundary current in the direction of wave advance and with a magnitude which can be determined through a knowledge of $\tilde{V}$. A net stress in the direction of wave advance will be induced, with a magnitude which can be predicted by (10). These phenomena will be $\tilde{\mathrm{Re}}$ independent over an order of magnitude of $\tilde{\mathrm{Re}}$ as shown in Figure 11. Over the expected range of phase separation between the wave potential flow and boundary ventilation, phase would not be expected to significantly alter these results. While gravity waves are not expected to exhibit a sinusoidal profile and will develop inherent asymmetries, the results of Figure 13 indicate that for low values of $\tilde{V}$ the flow will still exhibit the above discussed behavior.

This study shows that ventilated oscillatory boundary layers will develop net boundary velocity as well as net bed stress even in the absence of any other asymmetry. This result has obvious implications for studies of transport in such flows. The implications of the asymmetry in turbulence is not so obvious to predict. Figure 7 shows quite clearly that the majority of the turbulence throughout the cycle, originates from the injection half cycle. Yet how this would affect the transport of some quantity is far from clear. If transport is approximated by the product of suspension and local velocity and the level of suspension is proportional to the instantaneous turbulence levels, the argument can be made that transport would once again be in the direction of flow during suction. This can be understood by examining Figure 16. This figure gives a time history of the vertically averaged turbulence levels present in Figure 7. This figure which imparts no information about history clearly shows that the maximum vertically averaged turbulence

levels occur during the suction half cycle. By the above assumptions, transport due to turbulent suspension would be in the direction of flow during suction even in the absence of other asymmetries. As suspended transport under waves is a more complicated phenomenon than simple instantaneous averages the above scenario may be wholly inaccurate. However it does help to demonstrate the possible ramifications these findings have for suspended transport.

6. CONCLUSIONS

A laboratory experiment was performed to test the affect of boundary ventilation on the mean velocities, turbulent flow characteristics and bed stresses in an oscillatory boundary layer. The results of these experiments lead to the following conclusions:

1. Boundary suction causes flow streamlines to be pulled toward the bed, leading to higher velocities near the bed, while injection lead to streamline spreading and reduced near bed velocities. This effect results in a mean near bed flow in the direction of the flow experiencing suction.

2. The enhanced velocity shear near the bed during suction resulted in increased bed stress while the reduced shear during injection results in diminished bed stress.

3. The above affects are shown to be strong functions of the ventilation parameter $\tilde{V}$. The bed stress is shown to be independent of $\tilde{\mathrm{Re}}$ for the range of $\tilde{\mathrm{Re}}$ tested. It is also shown that phase dependence is small for small phase differences between u and w. The effects of suction were insensitive to waveform shape while the effects of injection increased with increasing length of the injection sub-cycle. This tendency was negligible for small values of $\tilde{V}$.

4. Boundary ventilation leads to a strong asymmetry in flow turbulence. Enhanced turbulent fluctuations are maintained in a thin layer near the bed with suction and turbulent diffusion

is reduced. Away from the bed turbulence levels are enhanced by injection leading to greater turbulent diffusion initiated during injection. The result of these effects is enhanced vertically averaged turbulence levels during suction.

Acknowledgements. This study was funded by the office of Naval Research, Coastal Sciences under grant N00014-89-J-1060 with the University of California, San Diego. We are deeply indebted to Robert Guza for his insightful comments and suggestions through out the experiments. Aid in instrumentation and facilities preparation was provided by Charles Coughran, John Powell, Mike Kirk and Domingo Goyena and others at the Scripps Institution of Oceanography hydraulics laboratory.

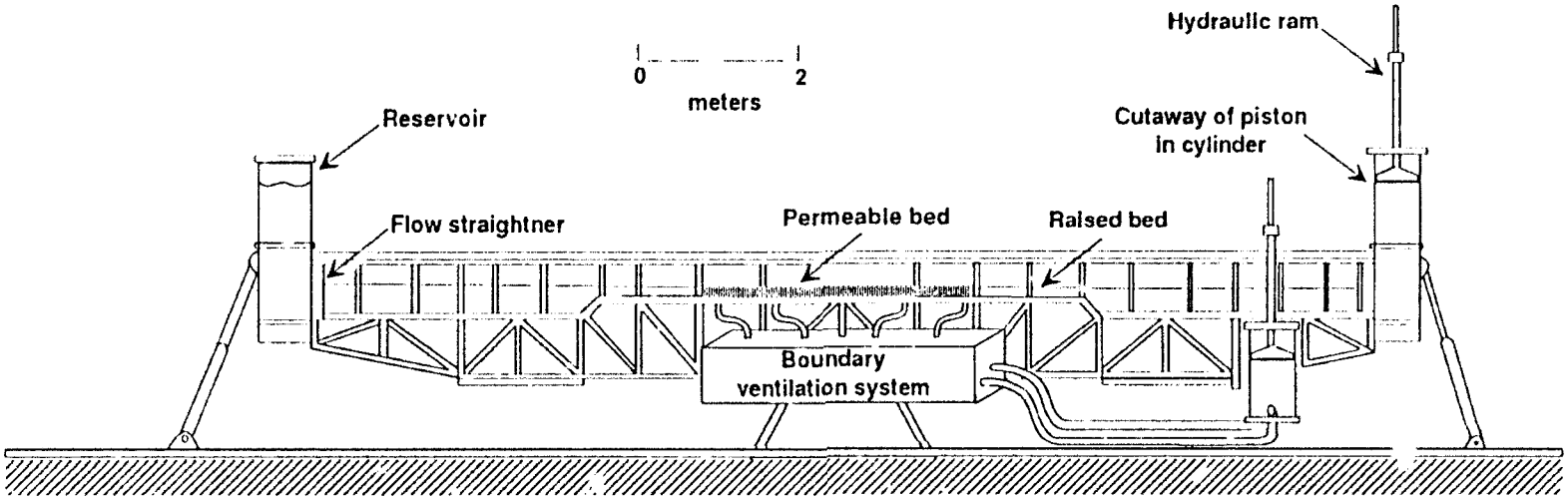

Figure 1: Schematic of the oscillatory flow tunnel showing permeable test bed and boundary ventilation pumping system.

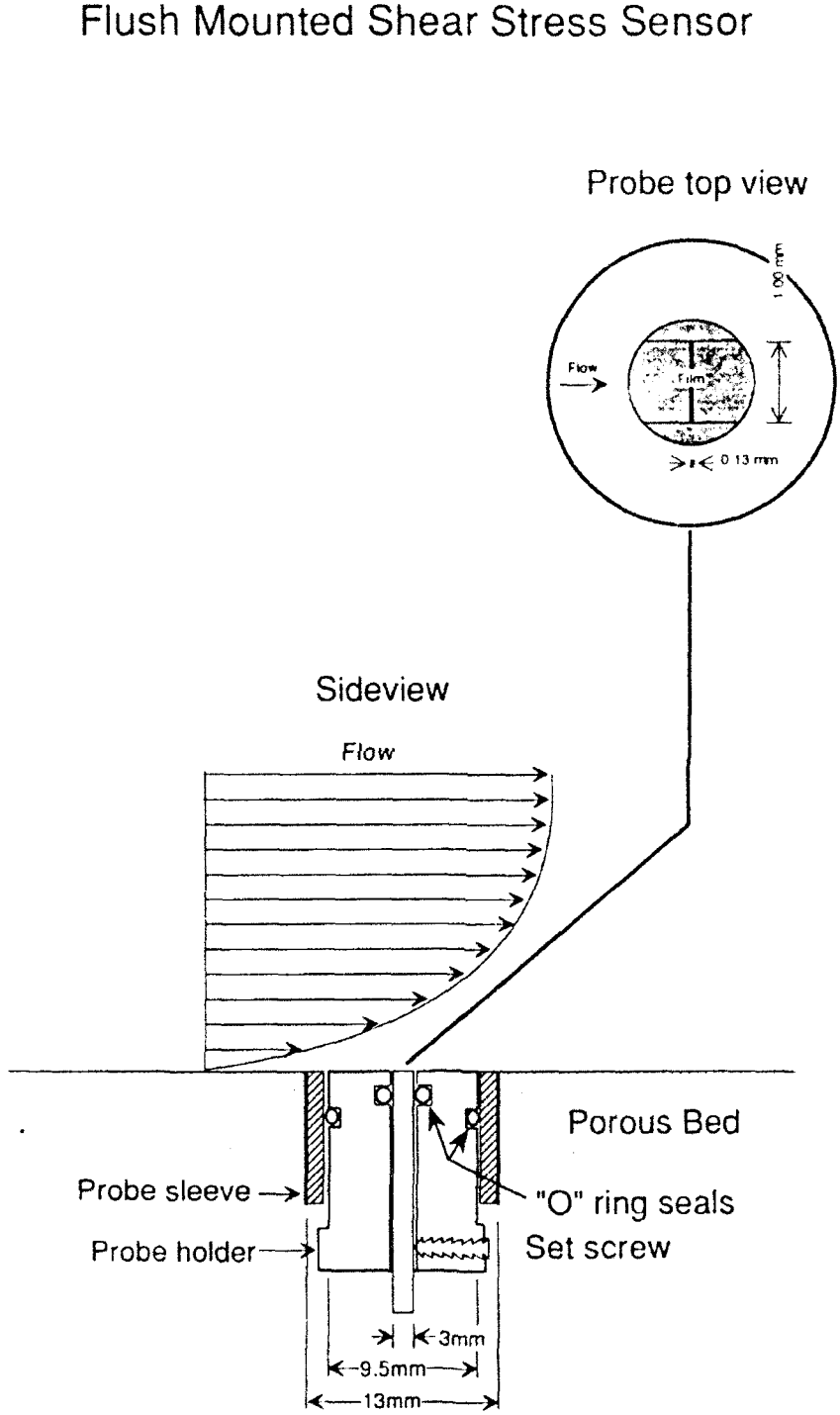

Figure 2: Schematic of the flush mounted hot film shear stress sensor showing emplacement technique. Insert shows face of probe.

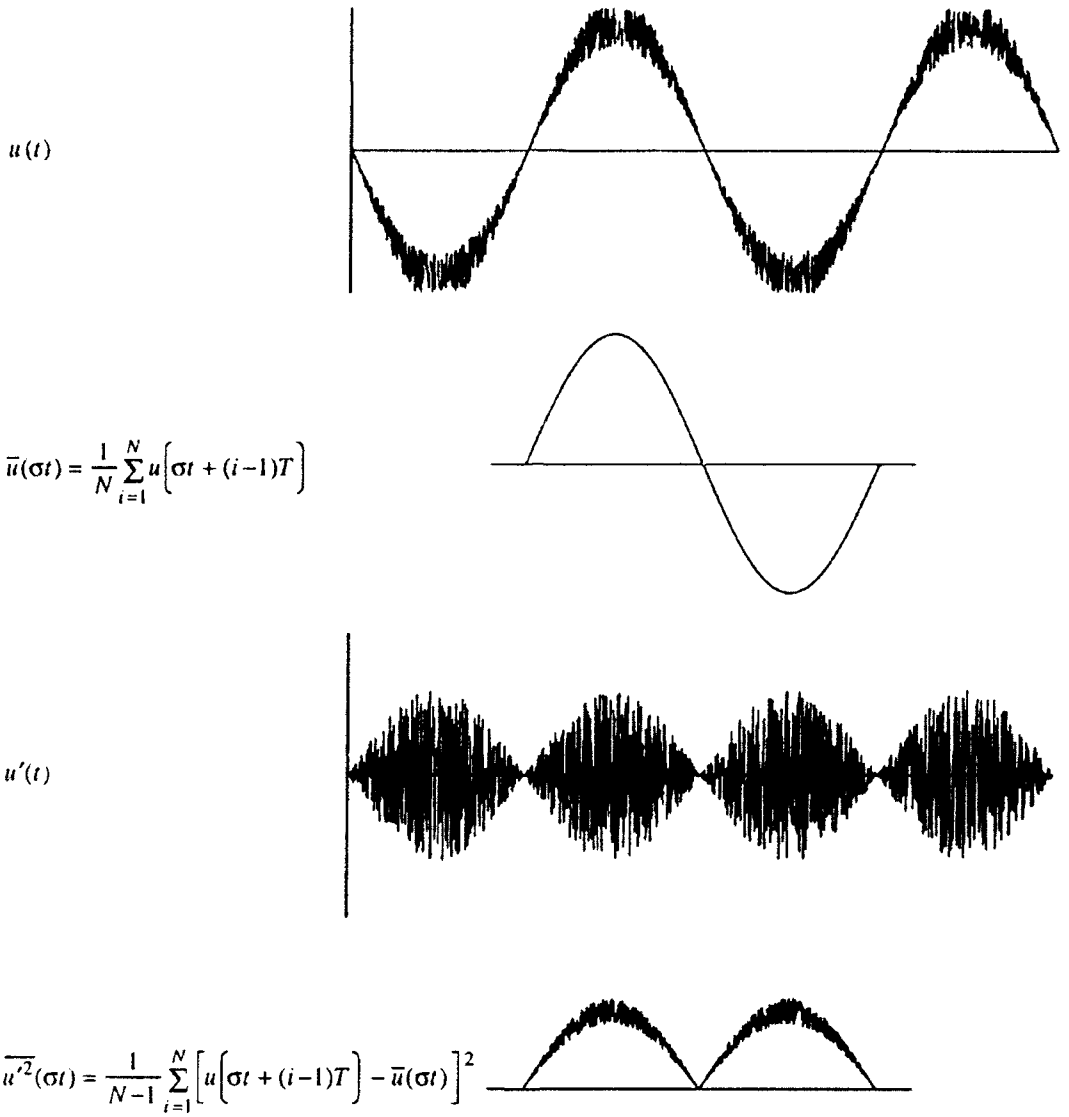

Figure 3: Schematic representation of the turbulent decomposition of an oscillating quantity.

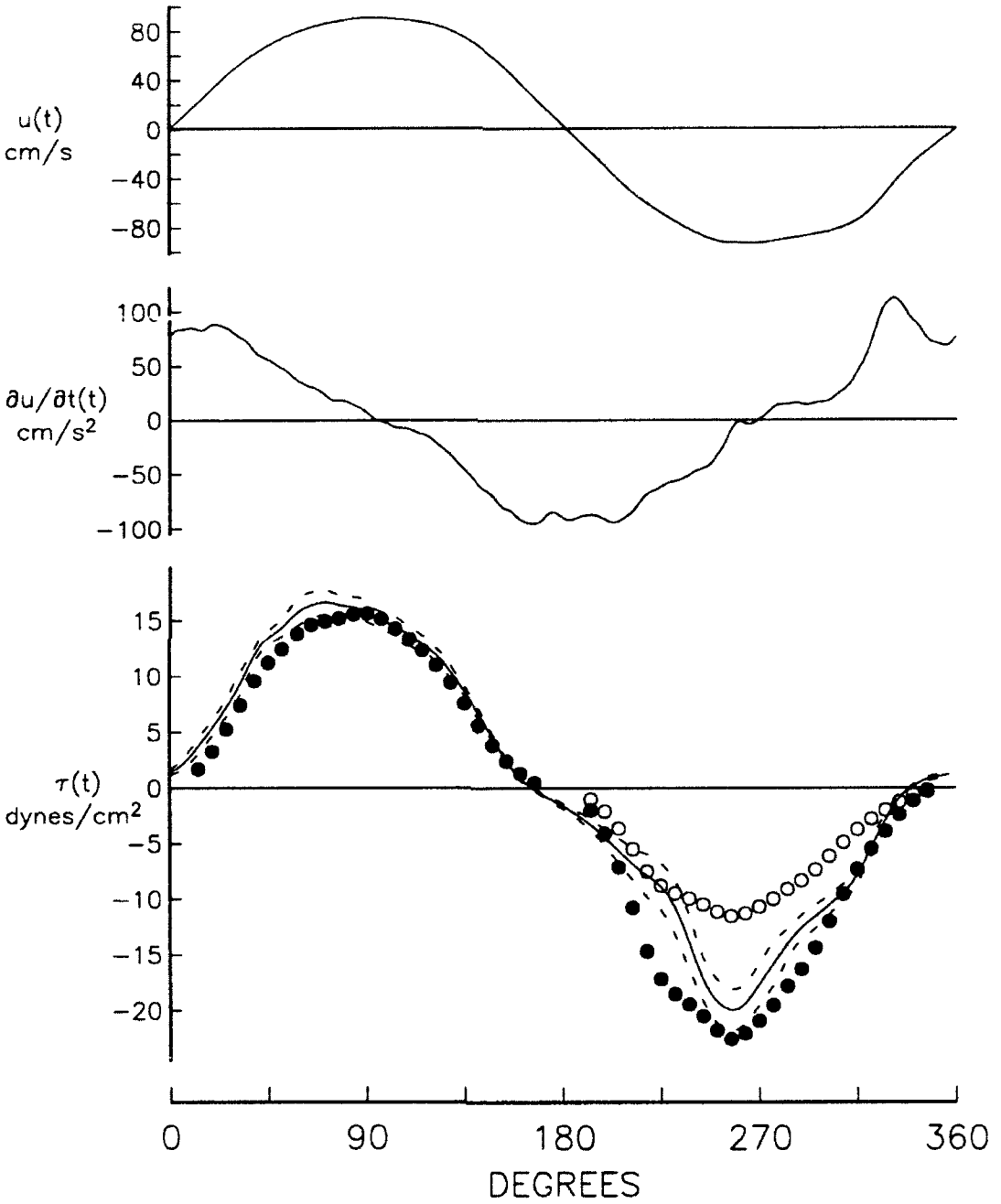

Figure 4: Ensemble averaged time series of (a) centerline velocity, (b) centerline acceleration, and (c) bed stress for the unventilated case. Dashed lines in (c) represent ± one standard deviation in absolute terms. Solid circles are bed stress estimates from log layer fit using k_s calculated from the first half cycle. Open circles represent bed stress estimates using k_s calculated from 2nd half cycle.

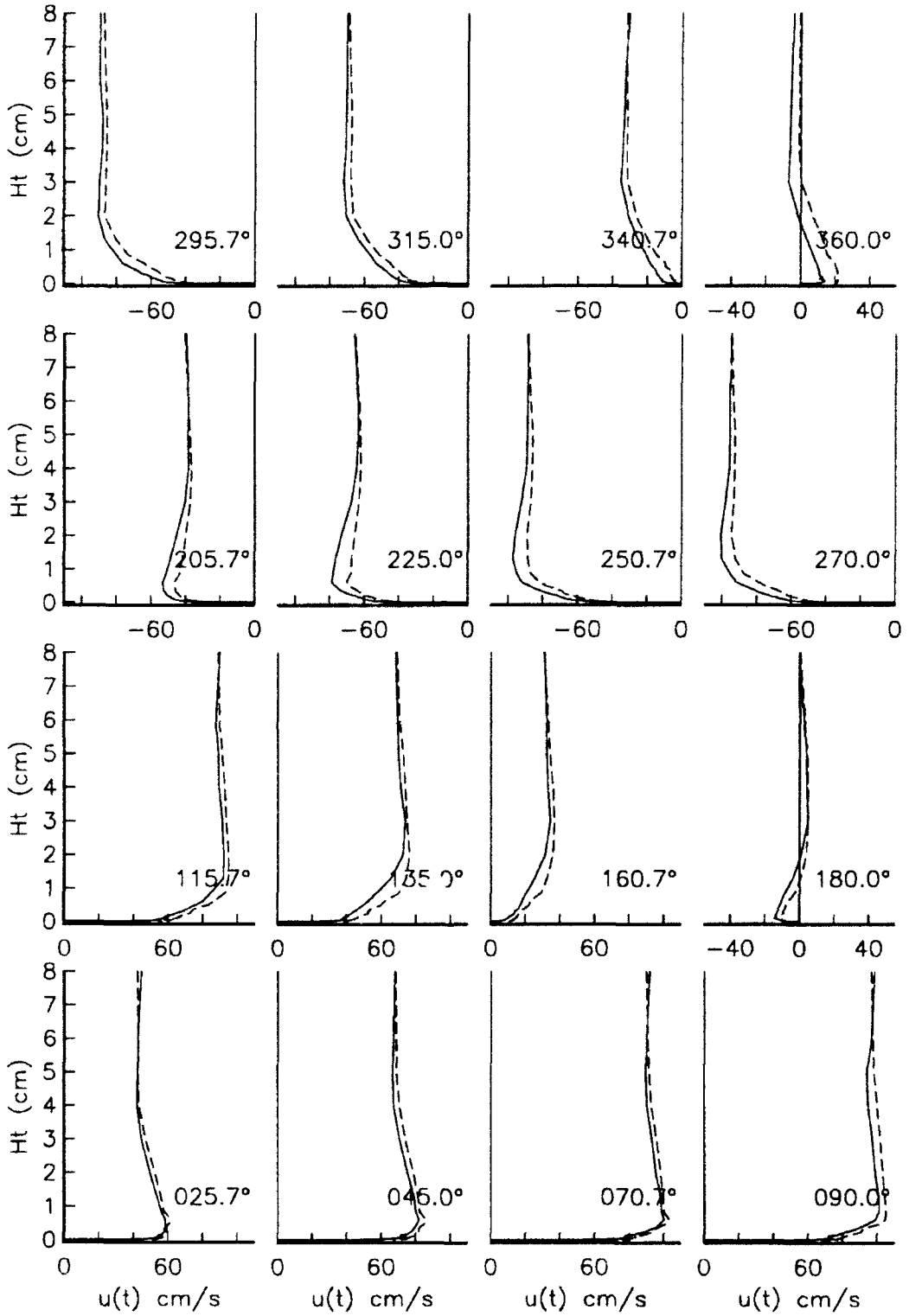

Figure 5: Boundary layer velocity profiles one cycle. Solid lines are for no ventilation and dashed are for $V = -5\times10^{-4}$ (suction occurs for $0<\theta<180$).

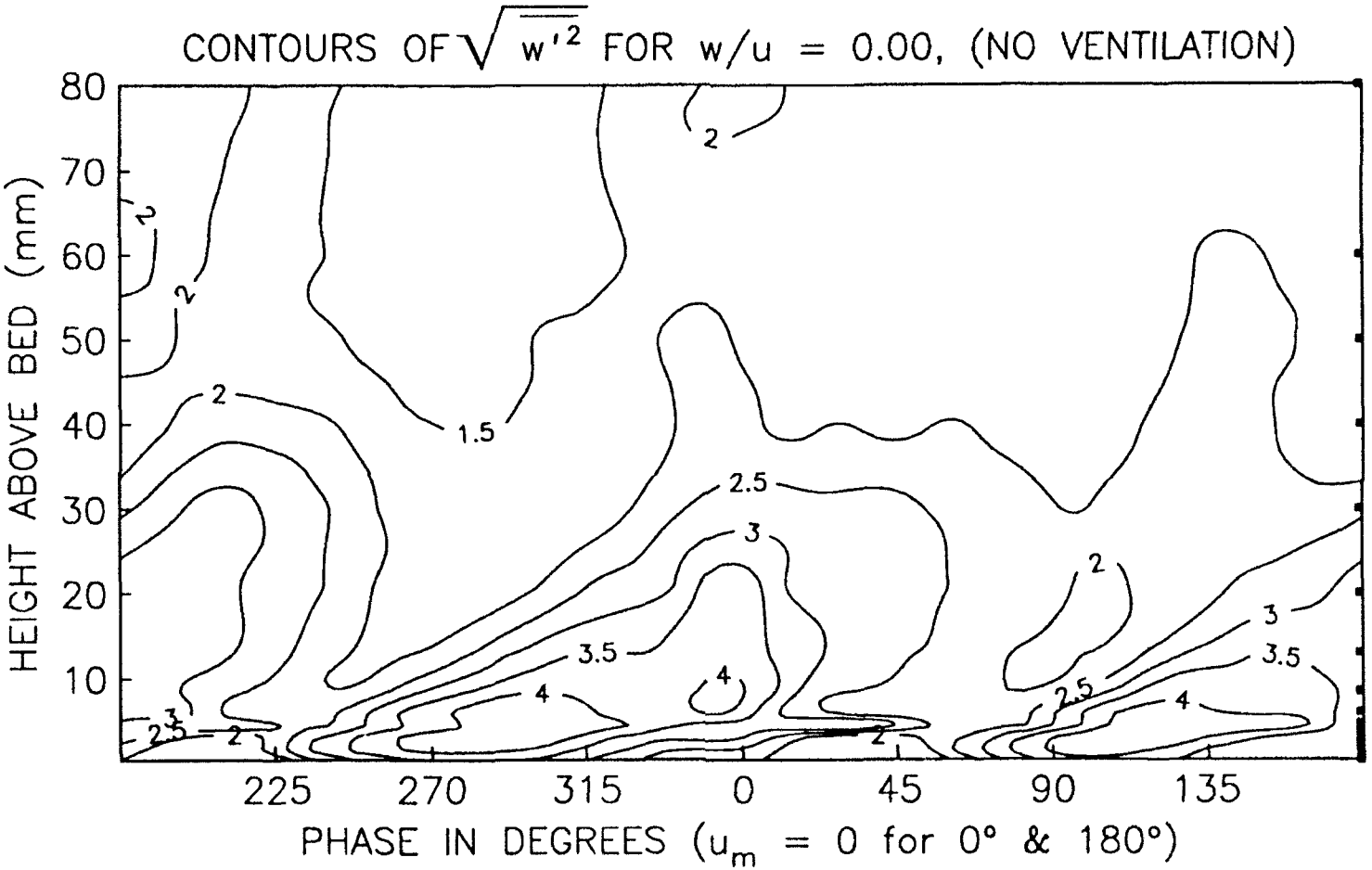

Figure 6: Contour plot showing development over height and phase of $\sqrt{\overline{w'^2}}$ for unventilated case. Contours are in units of $\%u_m$. Boxes on right correspond to measurement locations. Notice relative symmetry between half cycles.

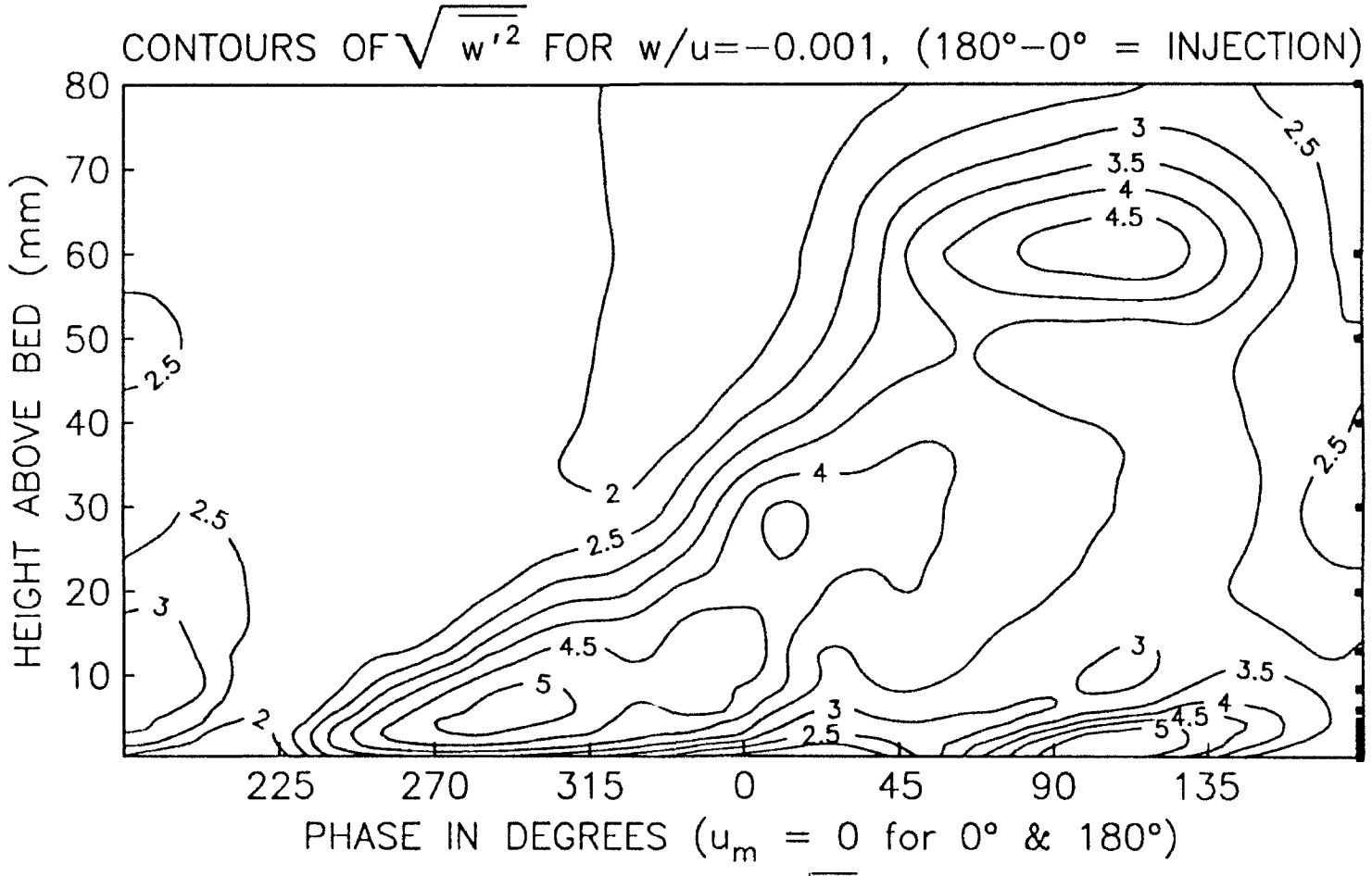

Figure 7: Contour plot showing development over height and phase of $\sqrt{\overline{w'^2}}$ for $\tilde{V} = -1\times10^{-3}$. Contours are in units of $\%u_m$. Boxes on right correspond to measurement locations.

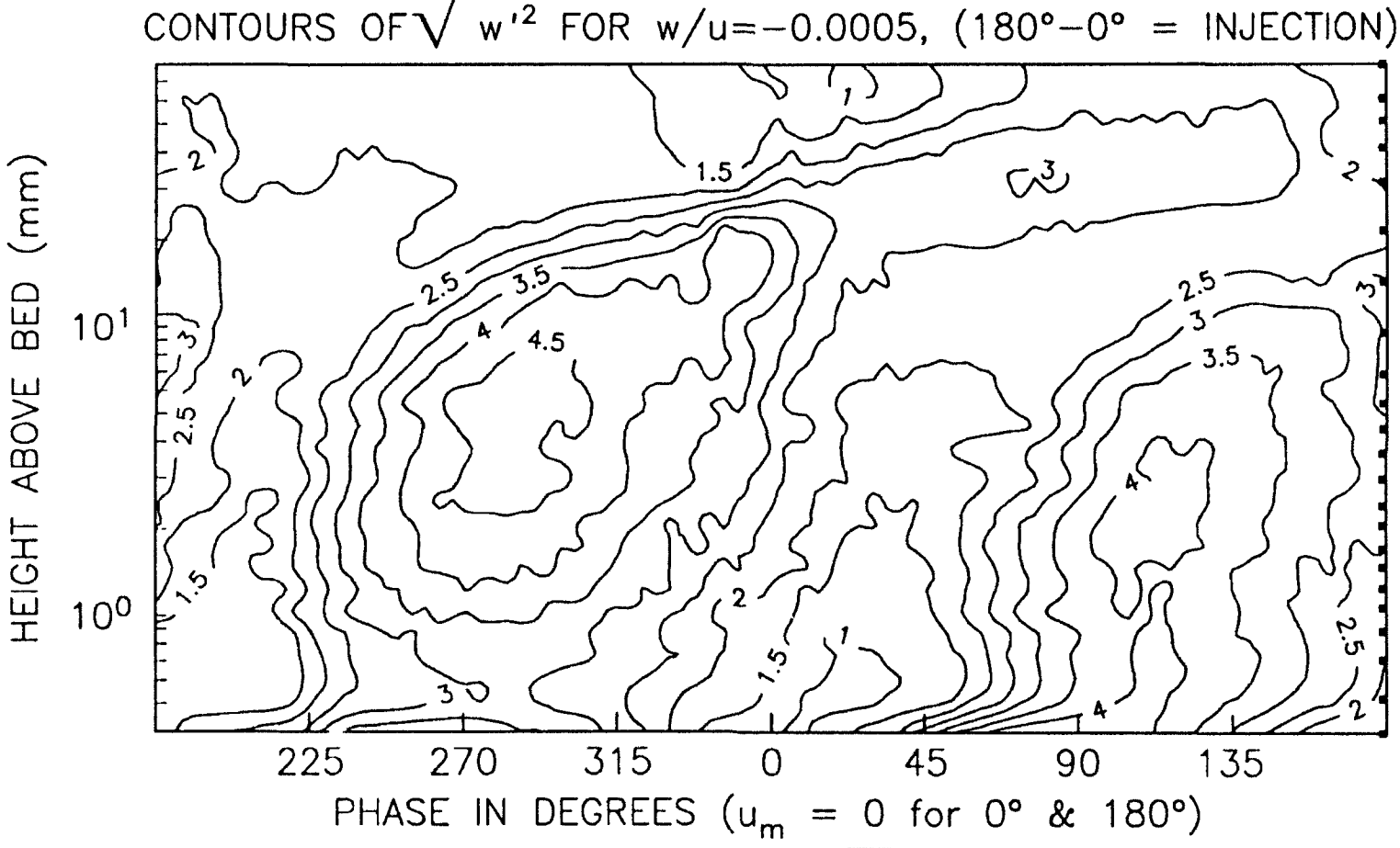

Figure 8: Contour plot showing development over height and phase of $\sqrt{\overline{w'^2}}$ for $\tilde{V} = -5\times10^{-4}$. Contours are in units of $\%u_m$ and height scale is logarithmic. Boxes on right correspond to measurement locations.

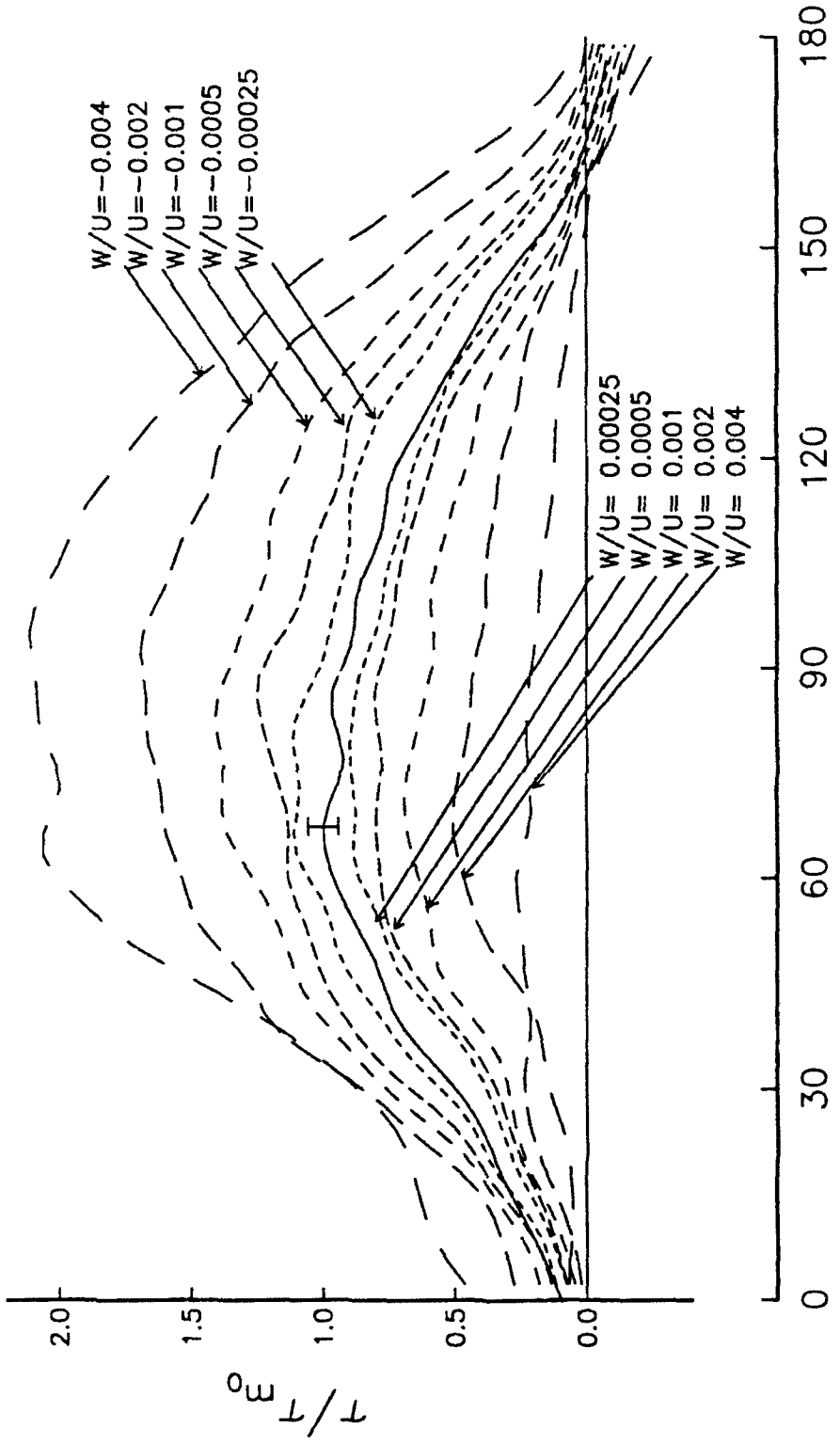

Figure 9: Ensemble averaged bed stress for various values of $\tilde{V}$. Solid line is bed stress for unventilated case. Brackets represent 95% confidence level of peak stress.

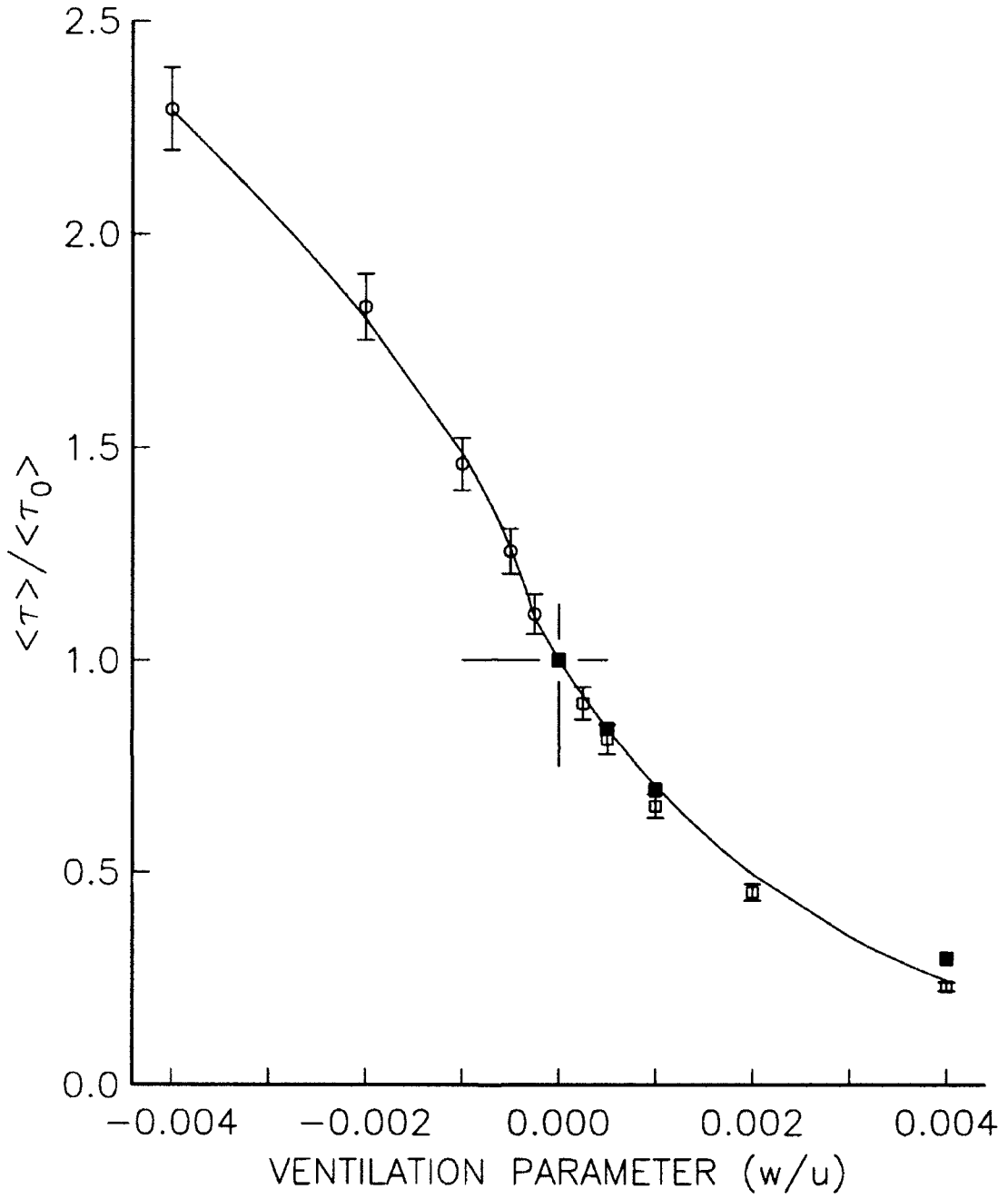

Figure 10: Time averaged ventilated bed stress vs injection parameter $\tilde{V}$. Values are normalized by time averaged unventilated bed stress. Averages are for first half cycle. Brackets represent 95% confidence interval based on repeated estimates of ensemble averaged quantity. Variance is assumed to be a constant fraction of measurement. Circles are for $\tilde{V}<0$ and boxes are for $\tilde{V}\geq 0$. Solid boxes represent estimates based on $\partial u/\partial z$ over the bottom 0.01 cm. Solid line is from equation (4) and equation (5).

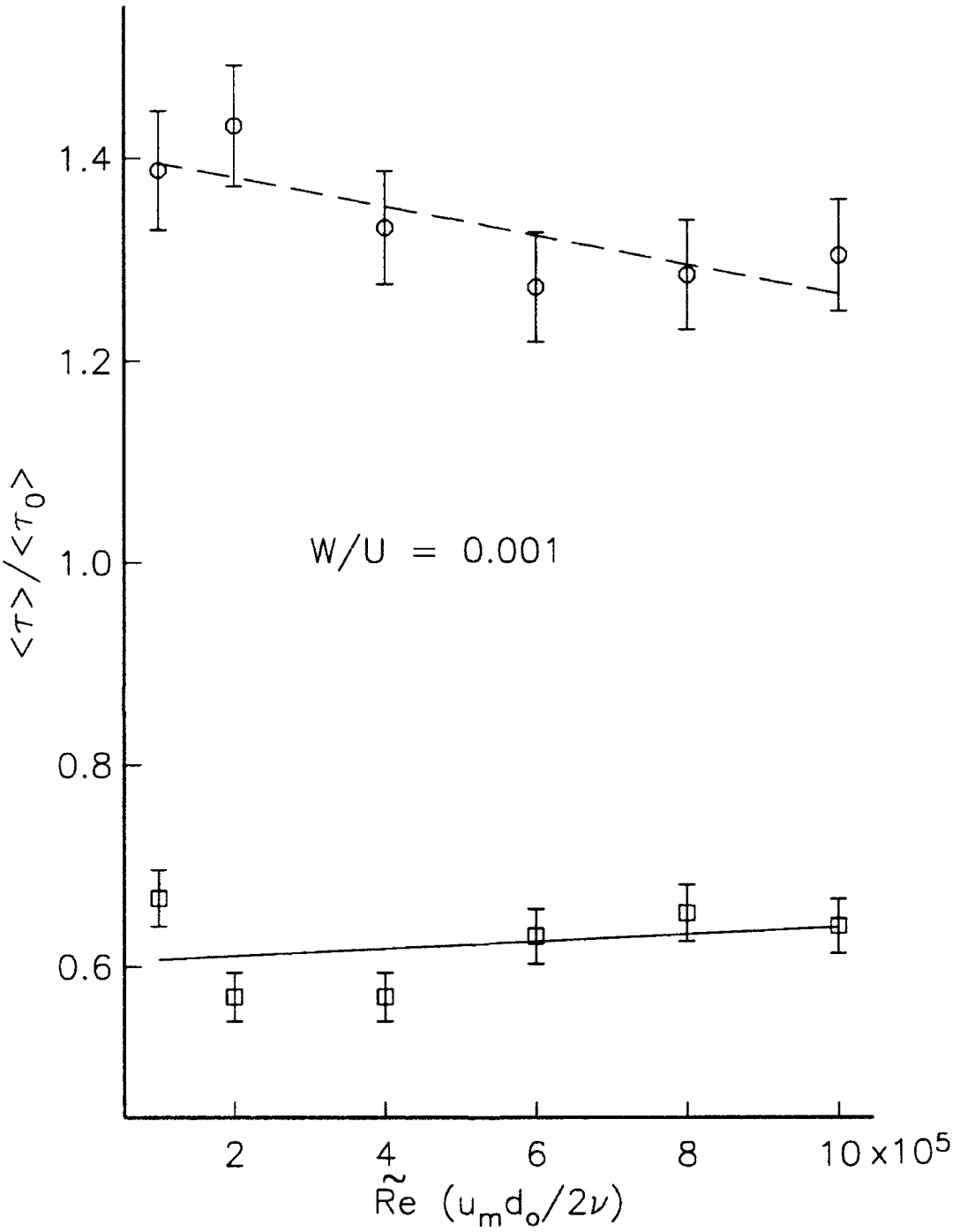

Figure 11: Time averaged ventilated bed stress vs $\tilde{Re}$. Values are normalized by time averaged unventilated bed stress. Averages are for one half cycle. Lines represent least squares fit to points. Brackets are 95% confidence interval (See Figure 10 for discussion of computation).

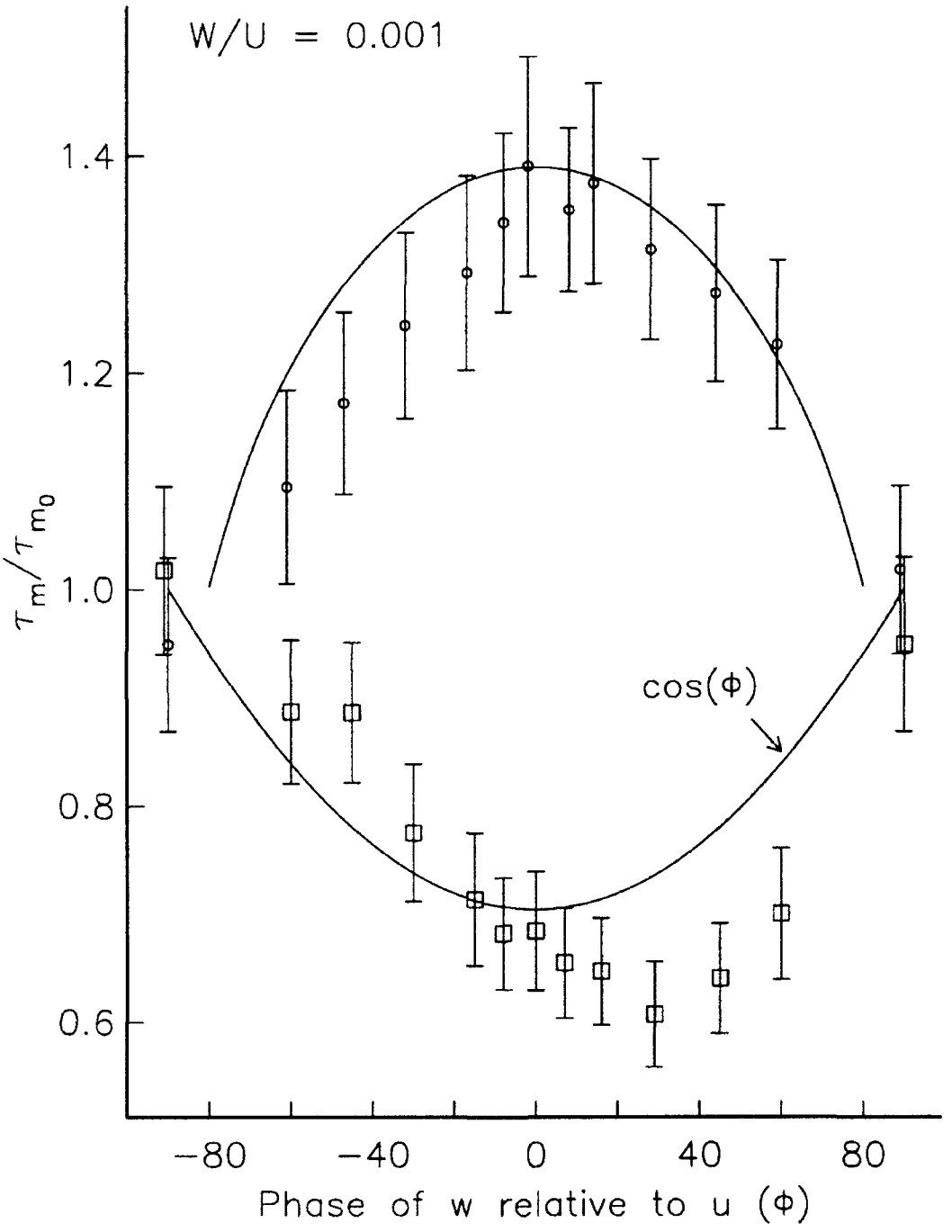

Figure 12: Maximum ventilated bed stress values normalized by maximum unventilated bed stress as a function of ventilation phase ϕ. Open circles are for suction, open boxes are for injection. Solid lines are expected response assuming instantaneous response. Brackets represent 95% confidence interval based on variance of ensemble averaged estimate.

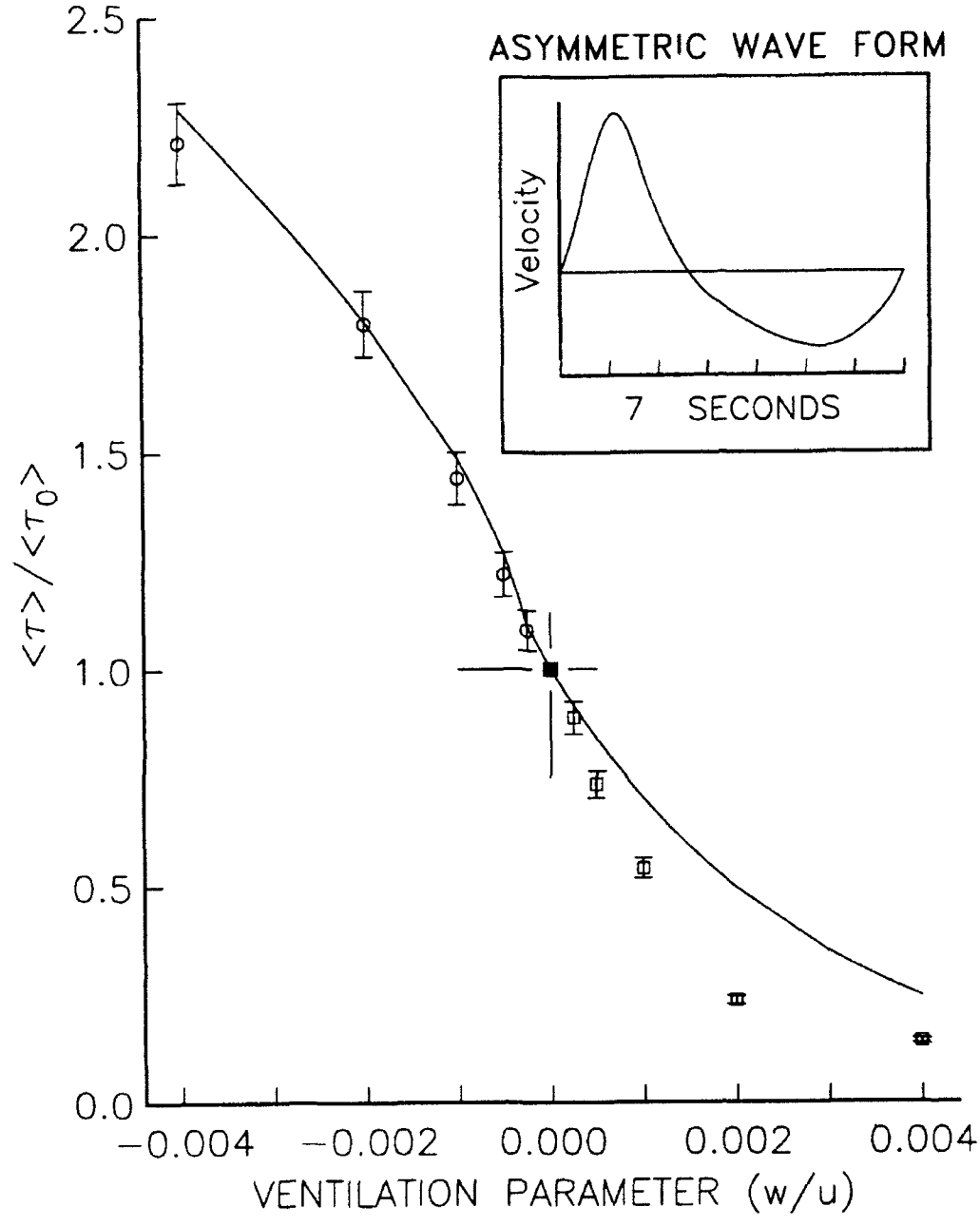

Figure 13: Time averaged ventilated bed stress vs injection parameter $\tilde{V}$ for asymmetric wave form (symbols). The line represents results for a symmetrical wave form (from Figure 10). Values are normalized by time averaged unventilated bed stress. Averages are over one half cycle. The peaked half cycle for $\tilde{V}<0$ and flat half cycle for $\tilde{V}>0$. Brackets represent 95% confidence interval based on repeated estimates of ensemble averaged quantity. Variance is assumed to be a constant fraction of measurement.

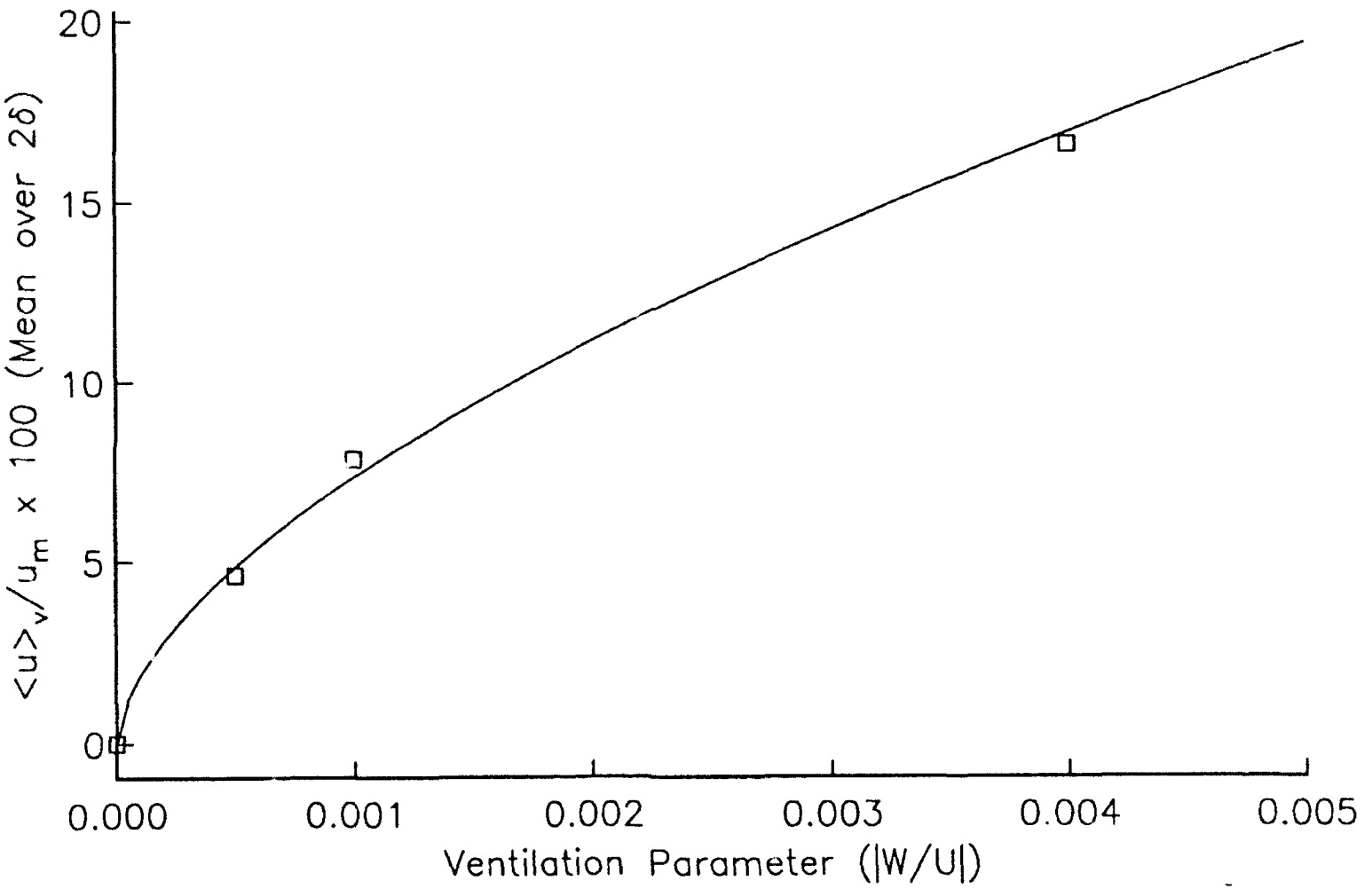

Figure 14: Net boundary layer velocity averaged over a distance $2\delta_0$ (ventilation current) vs absolute value of $\bar{V}$. Net velocity is presented as a percentage of u_m. Line is equation (9). Sign of net velocity is opposite the sign of $\bar{V}$.

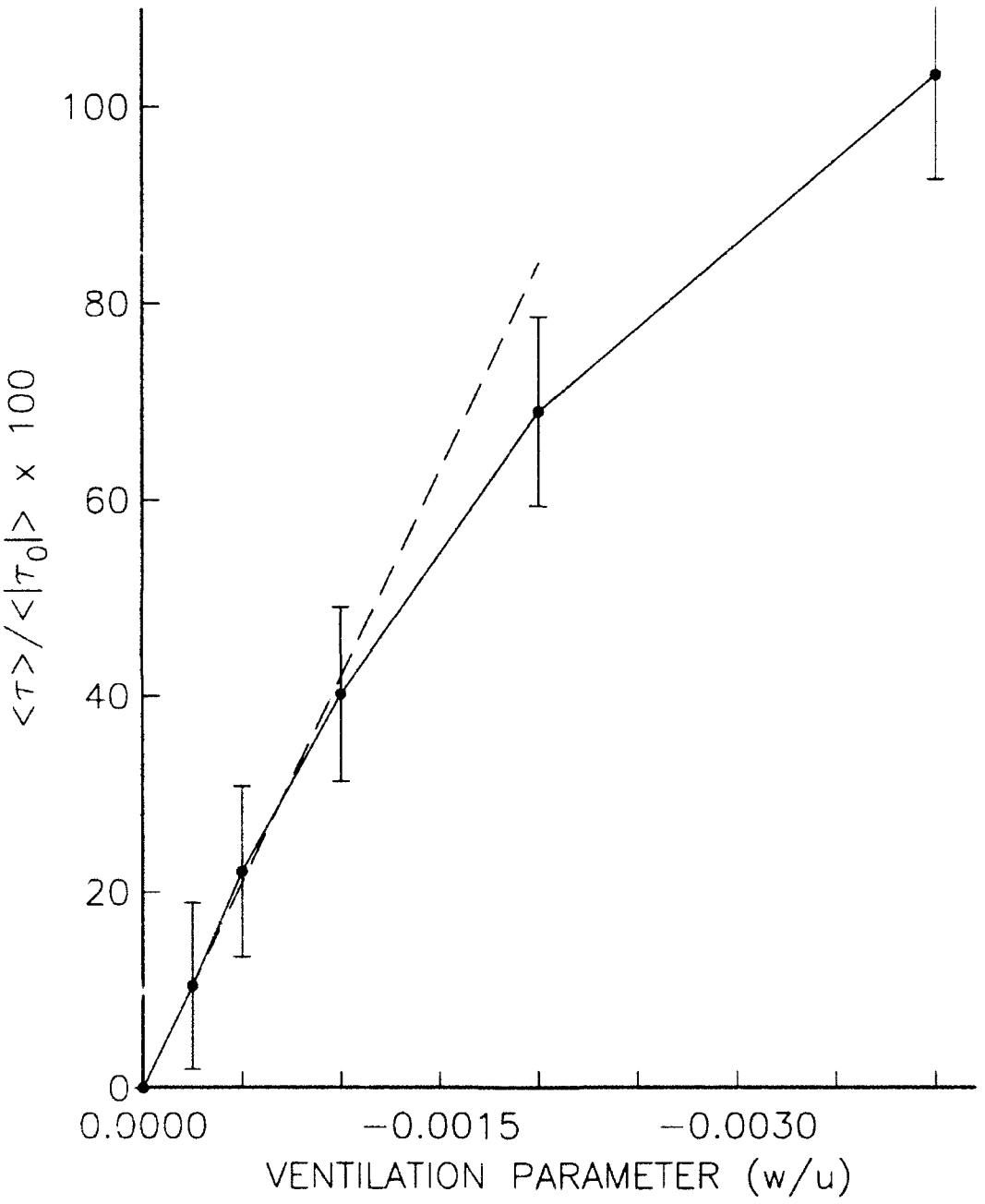

Figure 15: Average net ventilated bed stress as a percentage of average gross unventilated bed stress vs V. Dashed line is linear fit to points for $V \leq 1 \times 10^{-3}$. Brackets are 95% confidence interval.

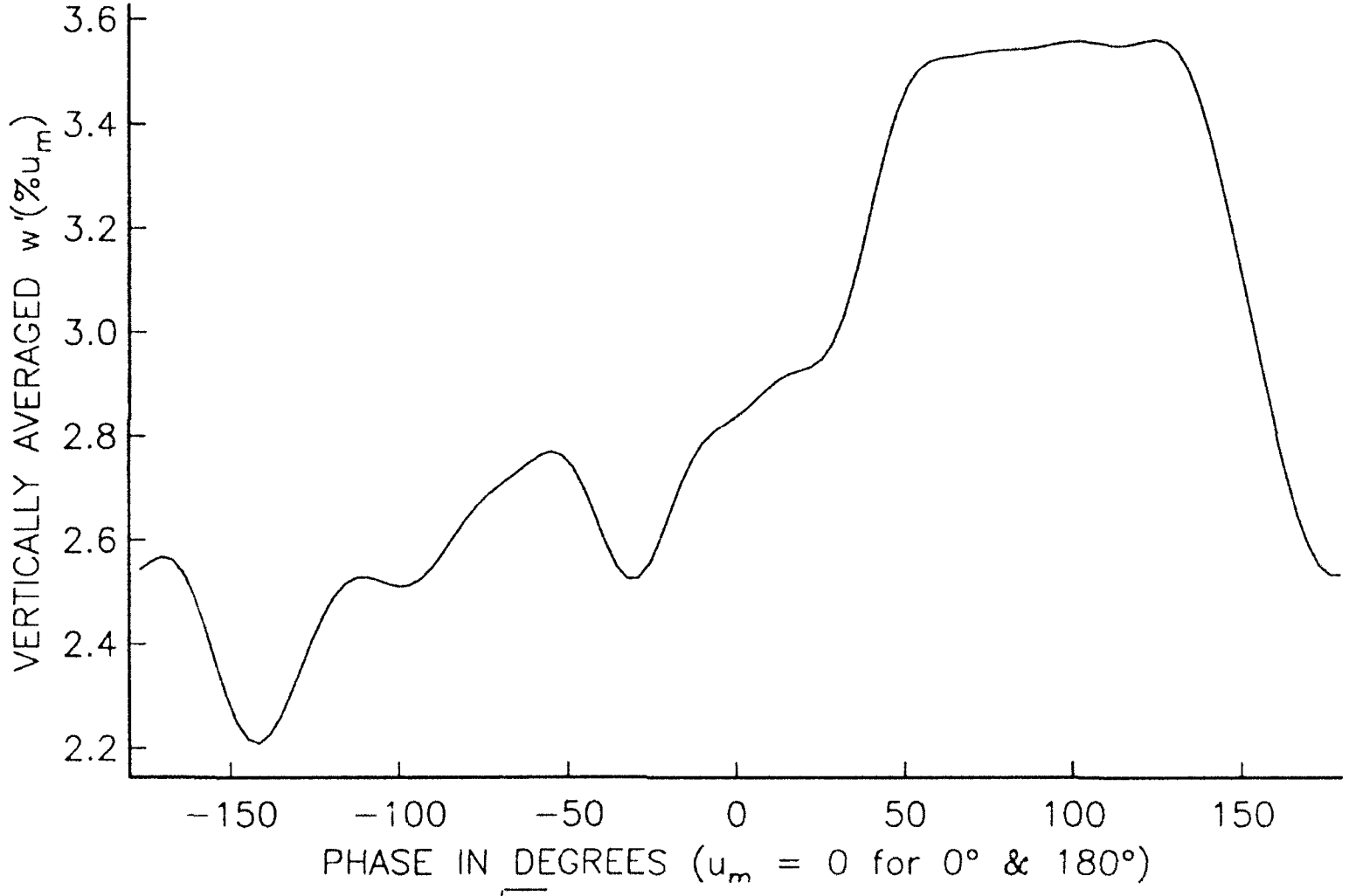

Figure 16: Vertically averaged turbulence ($\sqrt{\overline{w'^2}}$) level as a function of wave phase θ. Average is over 8 cm and $\tilde{V}=1\times10^{-3}$.

REFERENCES

Antonia, R.A., D. K. Bisset, L. Fulachier, and F. Anselmet, "Effect of wall suction on bursting in a turbulent boundary layer", *Phys. Fluids, A"*, 2(7), 1241-1247.

Antonia, R.A., L. Fulachier, L. V. Krishnamoorthy, T. Benabid, and F. Anselmet, "Influence of wall suction on the organized motion in a turbulent boundary layer," *J. Fluid Mech.*, 190, 217-240, 1988.

Blinco, P. H. and V. A. Sandborn, "Use of the split-film sensor to measure turbulence in water near a wall", *Turbulence in Liquids*, edited by G. K. Patterson and J. L. Zakin, pp 403-413, Dept. Chemical Engineering, University of Missouri-Rolla, 1975.

Conley, D. C., and D. L. Inman, "Field observations of the fluid-granular boundary layer under near-breaking waves," *J. Geophys. Res.*, 97(C6), 9631-9643, 1992.

Flick, R. E., and R. A. George, "Turbulence scales in the surf and swash", *Proc. Conf. on Coastal Eng., 22nd*, 557-569, 1990.

Flick, R. E., R. T. Guza, and D. L. Inman, "Elevation and velocity measurements of laboratory shoaling waves", *J. Geophys. Res.*, 86(c5), 4149-4160.

Fulachier, L., M. Elena, E. Verollet, and R. Dumas, "Suction effects on the structure of turbulent boundary layer on a heated porous wall", *Structure of Turbulence in Heat and Mass Transfer, edited by Z. P. Zorac, pp. 193-220*. Hemisphere, Washington, 1982.

Hanes, D. M., and D. A. Huntley, "Continuous measurements of suspended sand concentration in a wave dominated nearshore environment", *Cont. Shelf Res.*, 6(4), 585-596, 1986.

Jensen, B. L., B. M. Sumer, and J. Fredsoe, "Turbulent oscillatory boundary layers at high Reynolds numbers," *J. Fluid Mech.*, 206, 265-297, 1989.

Jonsson, I. G., "Measurements in the turbulent wave boundary layer", *Proc. Congr. IAHR, 10th(1)*, 85-92, 1963.

Justesen, P., "Turbulent wave boundary layers", *Series Paper 43*, 226 pp., Inst. Hydrodyn. and

Hydraul. Eng., Tech. Univ. of Denmark, Lyngby, 1987.

Kays, W. M., "Heat transfer to the transpired turbulent boundary layer," *Intl. J. Heat Mass Transfer*, 15, 1023-1044, 1972.

King, D. B., J. D. Powell, and R. J. Seymour, "A new oscillatory flow tunnel for use in sediment transport experiments", *Proc. Conf. Coastal Eng., 19th.*, 1559-1570, 1984.

Libby, P.A., L. Kaufman, and R. P. Harrington, "An experimental investigation of the isothermal laminar boundary layer on a porous flat plate", *J. Aero. Science*, X, 127-134, 1952.

Mickley, H. S., and R. S. Davis, "Momentum transfer for flow over a flat plate with blowing", *Tech. Note 4017*, 64 pp., Natl. Adv. Comm. Aeronaut., Washington, 1957.

Reid, R. O. & K. Kajiura, "On the damping of gavity waves over a permeable sea bed," *EOS, Trans. AGU*, 38, 662-666, 1957.

Schlichting, H., *Boundary Layer Theory*, 7th ed., 817 pp., McGraw-Hill, New York, 1979.

Simpson, R. L., R. J. Moffat, and W. M. Kays, "The turbulent boundary layer on a porous plate: Experimental skin friction with variable injection and suction," *Intl. J. Heat Mass Transfer*, 12, 771-789, 1969.

Sleath, J. F. A., "Turbulent oscillatory flow over rough beds", *J. Fluid Mech.*, 182, 369-409, 1987.

Tewfik, O. E., "Some Characteristics of the turbulent boundary layer with air injection," *AIAA J.*, 1(6), 1306-1312, 1963.

CHAPTER III

WAVE DRIVEN VENTILATION IN SAND BEDS

1. INTRODUCTION

Any beach which is composed of sediments of a non local origin stands as an incontrovertible proof of the existence of a shoreward directed force opposing the constant down slope and hence seaward pull of gravity. The source of this forcing has long been recognized to be the waves which shoal and dissipate on these beaches but the mechanism through which these waves generate this forcing is the subject of much discussion. The role that wave driven ventilation may play in this process is investigated in this study.

A surface gravity wave traveling in a fluid overlying a permeable bed has been predicted to induce an oscillating flow in that bed [Putnam, 1949; Reid & Kajiura, 1957]. This phenomenon was originally of interest to coastal engineers and scientists because it was proposed as a mechanism for the dissipation of wave energy prior to breaking. More recently Conley and Inman [1992] labeled this type of phase locked oscillatory flow in the bed "ventilation", and suggested that boundary layer phenomenon associated with ventilation could explain an asymmetry which they observed in the development of fluid granular boundary layer under waves. This work reports on field observations of wave driven ventilation, compares the observations to theory and discusses the importance of ventilation in nearshore processes.

2. VENTILATION THEORY

In the most basic treatment of this problem we consider a fluid of depth h overlying a bed of thickness b (Figure 1) [e.g. Putnam, 1949]. The bed is assumed to be homogeneous with permeability K and to overlay an impermeable substrata. Flow within the bed is assumed to follow Darcy's law so that

$$u_b = \frac{-K}{\mu}\frac{\partial p_b}{\partial x}, \quad w_b = \frac{-K}{\mu}\frac{\partial p_b}{\partial z} \tag{1}$$

where u_b and w_b are the vertical and horizontal flow in the bed respectively, p_b is pressure in the bed and μ is the viscosity of the pore fluid. Now substituting equation (1) into the continuity relation gives

$$\frac{\partial^2 p_b}{\partial x^2} + \frac{\partial^2 p_b}{\partial z^2} = 0 \tag{2}$$

Equation 2 must be solved subject to the following boundary conditions

$$p_b = p \ @ \ z = 0 \tag{3}$$

and

$$w_b = 0 \ @ \ z = -b. \tag{4}$$

Here p is the pressure in the fluid. From linear wave theory it is known that

$$p = \rho a g \frac{\cosh(kz)}{\cosh(kh)} \cos(\sigma t - kx) \tag{5}$$

where a is the wave amplitude, $k = 2\pi/L$ is the wave number, $\sigma = 2\pi/T$ is the wave radian frequency and L and T are the wavelength and period respectively. The solution for (2) which satisfies (3) and (4) is

$$p_b = \frac{\rho a g}{\cosh(kh)} \frac{\cosh[k(z+b)]}{\cosh(kb)} \cos(\sigma t - kx). \tag{6}$$

From (1) and (6) we can see that flow is induced in the bed by the pressure field associated with

the wave and that the vertical ventilation will be of the form

$$w_b = \frac{-K}{\nu}\frac{agk}{cosh(kh)}\frac{sinh[k(z+b)]}{cosh(kb)}cos(\sigma t - kx). \tag{7}$$

This flow is an oscillating flow into and out of the bed and is phase locked to the wave pressure such that maximum flow into the bed ($w_b<0$) occurs under the crest of the wave and maximum flow out of the bed occurs under the trough of the wave (Figure 2). A similar relationship exists between vertical ventilation w_b, and the horizontal wave orbital motion in the fluid u, where

$$u = ag\frac{k}{\sigma}\frac{cosh(kz)}{cosh(kh)}cos(\sigma t - kx). \tag{8}$$

Comparison of (7) and (8) shows that for linear progressive waves maximum ventilation into the bed occurs simultaneously with maximum horizontal orbital motion under the crest (onshore orbital motion) and maximum ventilation out of the bed occurs simultaneously with maximum offshore directed orbital motion. Because orbital velocities and ventilation are in phase, the ratio w_b/u is a constant. At the fluid bed boundary ($z=0$), this ratio is

$$\frac{w_b}{u} = -\frac{K}{\nu}\sigma\, tanh(kb). \tag{9}$$

Here $\nu = \mu/\rho$ is the kinematic viscosity. Inspection of (9) suggests the relative magnitudes of w_b and u. In particular, for common wave frequencies in the nearshore, $\sigma tanh(kb)$ will be assumed to be about 1. Darcys law is generally assumed valid where the grain Reynolds number, $Re_g = w_b D/\nu$, is $O(1)$ or less where D is the grain diameter. It is reasonable to make $u=10^2$ cm/s, then with $\nu = .01 cm^2/s$, (9) gives $w_b \approx 10^4 \times K$. Using this in the Re_g limit gives $KD_{max} \approx 10^{-6} cm^3$. Krumbein and Monk [1942] have shown that the permeability in sands is proportional to the square of the mean grain diameter. Explicitly,

$$K = 7.6\times10^{-4} D^2 e^{(-1.31\sigma_\phi)} \tag{10}$$

where D is in cm and σ_ϕ is the deviation measure in phi units. The result is permeability in cm^2.

Approximating this relation as $K = 10^{-4}D^2$ the Re_g limit is now $D^3_{max} \simeq 10^{-2}\mathrm{cm}^3$. In order to determine the largest value (9) could take, we shall let $D^2_{max} \simeq 10^{-1}\mathrm{cm}^2$ which when combined with (10) and (9) tells us that w_b/u is $O(10^{-3})$ or less. Notice that the above discussion indicates that (1) will be valid for grain sizes on the order of mm and smaller. This is consistent with the findings of Gu and Wang [1991] and others.

3. EXPERIMENTAL PROCEDURE AND RESULTS

Using the order of magnitude arguments mentioned above for K and ν, it can be seen from (1) that the vertical pressure gradient in the bed is expected to be $O(10^3)$ times the ventilation. It was therefore decided that ventilation in field conditions could best be determined from measurements of the vertical pressure gradient in the bed. The procedure was to bury a differential pressure sensor in a sand bed with the pressure ports separated in the vertical direction (Figure 3). Such an arrangement results in a steady pressure differential equal to the hydrostatic head between the two ports as well as a fluctuating component which is directly proportional to the ventilation. Pressure gradients due to the slope of the wave are effectively filtered out as there is no separation of the ports in the crosshore direction.

The experiment was performed on 20 and 21 August 1992 near the Scripps Institution of Oceanography pier. A Setra model 228-1 differential pressure sensor with a port separation of 10 cm was buried in the sand bed. The top port was placed 6 cm below the sand water interface. A Marsh-Mcbirney model 512 two component electromagnetic (em) current meter and a Setra model 280 absolute pressure sensor were placed in the water column directly above the buried sensor. Data was collected at 8 Hz over a two and one half hour run. Five runs were made spanning an entire tidal cycle with mean water depth ranging from 290 to 340 cm. The local significant wave height ranged from 50 - 66 cm at a peak wave period of 6.5 s. Sand in the top of the bed had a mean grain diameter of 180 microns with a σ_ϕ of 0.55. This gives a permeability of 12 Darcys ($10\times10^{-8}\mathrm{cm}^2$) using (10). Cores were taken at the instrument burial site during the

experiment and were later subject to a hydrostatic head in order to determine the permeability by direct measurement. This technique gave a permeability of 11 Darcys which is the value used in this work.

Figure 4 shows a typical section of time series. The top trace represents sea surface elevation as measured by the absolute pressure sensor, the middle trace is crosshore orbital motion (u) 46 cm above the bed as measured by the em current meter and the bottom trace is ventilation as calculated from the differential pressure sensor measurements. It is seen that ventilation is present and behaves qualitatively as predicted by (7). In particular maximum ventilation into the bed occurs under the crest of the wave concurrently with maximum onshore orbital motion. Likewise maximum flow out of the bed occurs under the trough of the wave concurrently with maximum offshore orbital motion. It can also be seen that the ratio of $|w_b/u|$ is $O(10^{-5})$.

If equation (7) is correct then it should be possible to use (5) to predict the ventilation at a depth $-z_b$ from knowledge of the pressure at a height above the bed equal to z_p. The relation would be

$$w_b(z_b) = -\frac{K}{\mu} k \frac{sinh\,[k\,(b-z_b)]}{cosh\,(kz_p)cosh\,(kb)} p\,(z_p). \tag{11}$$

As the processes discussed are linear, it should be possible to construct the power spectrum for w_b from p using (11). The only parameters in (11) which are not fixed by either the wave frequency or fluid properties are the bed permeability K and the bed thickness b. However as K is used in our determination of w_b, the only previously unspecified parameter in this problem is b.

Figure 5 gives the results of such a construction. The solid line in this figure is the spectra of w_b as calculated from the differential pressure sensor response. The dotted line is the predicted spectra for w_b as calculated from the absolute pressure spectra and a bed thickness of 250 cm. This thickness represents the minimum average sand bed thickness known to occur in this area. It can be seen from the figure that using this depth results in a significant under

prediction of ventilation. It was found that to best match the peak of the ventilation spectra, a bed thickness of 580 cm was required. The predicted spectra using a bed thickness of 580 cm is shown in the figure as the dashed line and it can be seen that (7) predicts the behavior of ventilation at least over the energetic part of the spectrum. This thickness (580 cm) worked equally as well for all five runs.

Knowledge of the local sediment cover indicates that 580 cm is an unrealistic estimate of the sand bed thickness but consideration of the local beach stratigraphy may give an explanation of where this value comes from. It is know that the sand in this bed overlies a cobble layer about 50 cm thick (Figure 6). If we assume that the sand bed in this region was at its thickest summer time configuration, a sand thickness of 350 cm is not unreasonable. Add 50 cm of cobble and we have a permeable bed of 400 cm. This is still short of the required 580 cm but it is suggested that this can be accounted for by considering that the permeability in the cobble layer is much higher than that in the sand layer. The derivation of (7) assumed a homogeneous permeable bed of constant permeability K. It is proposed that 580 cm represents an effective bed thickness b_e. That is that the two layer bed of sand and cobble "effectively" acts likes a homogeneous sand bed of permeability K with a thickness of about 580 cm.

4. DISCUSSION

It has been shown that ventilation is present in permeable beds beneath waves and that it's behavior can be well predicted by simple linear theory given that the local effective bed depth is known. It would now be useful to examine what significance this holds for sediment transport and other nearshore processes.

Conley and Inman [submitted] have shown that, similarly to steady flow, small boundary normal velocities can strongly affect the bed stress and turbulent boundary layer characteristics of an oscillating flow. They defined a ventilated oscillatory boundary layer as the boundary

layer arising from a purely sinusoidal bed parallel flow subject to a much smaller bed normal flow which was also varying sinusoidally with the same period and phase as the larger flow. This is just the situation suggested by (7). It was shown that the bed stress arising from such a flow when integrated over a full cycle would result in a net bed stress in the direction of the flow during the half cycle experiencing flow into the bed. This concept can be better understood by examining the schematic of wave driven ventilation in Figure 7. Flow into the bed under the crest of the wave leads to an enhancement of the bed stress while flow out of the bed leads to a reduction in the bed stress. The effect of this enhancement and reduction averaged over one wave cycle is to produce a net bed stress in the direction of wave advance or an onshore directed net stress. Conley and Inman [submitted] also demonstrated that the magnitude of the normalized net stress was a function of w/u and that for small values of w/u $(w/u \leq 10^{-3})$ this relationship could be approximated by the empirical linear relationship

$$\frac{<\tau>_v}{<|\tau_0|>} = -420 \times \frac{w}{u} \tag{12}$$

where τ is bed stress, τ_0 is the bed stress without ventilation, $< >$ implies the time average over one cycle and the subscript v indicates a ventilation related process. Notice that $<\tau>_v$ is the net bed stress. Using (9) and (12) we have

$$<\tau>_v = 420 \frac{K}{\nu} \sigma \, tanh(kb) <|\tau_0|> \tag{13}$$

A kinematic discussion of sediment transport requires knowledge of the time history of stress and velocity. This is clear when one considers that even the most basic sediment transport models assume that transport is proportional to the product of velocity and stress. However from a force balance point of view, net stresses are very important in nearshore processes. As discussed earlier, the argument here states that in a situation where a sloping bed of sediment is constantly agitated, a steady force must be exerted in the up-slope direction to counter balance the down-slope force due to gravity. The net stress due to boundary ventilation is one possible

source for just such a force.

Several other mechanisms have been proposed as sources for such a force and it is of interest here to make a comparison of the importance of some of these mechanisms relative to the boundary ventilation mechanism. The focus of this discussion will be on the two most commonly mentioned mechanisms; namely the net stress arising from velocity asymmetries in the nonlinear shoaling wave form [e.g. Grant, 1943; Inman and Bagnold, 1963] and the net stress arising from a sinusoidal oscillatory flow which has a steady boundary current imposed on it as would be predicted by bottom wind theory [Longuett-Higgins, 1953].

In order to arrive at a net stress, a quadratic stress relation is assumed where the coefficient of friction c_f is assumed constant through out the entire cycle. This is represented as

$$\tau(t) = \rho \frac{c_f}{2} u(t) | u(t) | . \tag{14}$$

From this, the net bed stress is seen to be

$$<\tau> = \frac{\rho}{T} \frac{c_f}{2} \left\{ \int_{-t_p}^{t_p} u^2 dt - \int_{t_p}^{T-t_p} u^2 dt \right\} \tag{15}$$

where the period $-t_p < t < t_p$ represents the portion of the wave period T over which velocity u is positive.

To represent a shoaling gravity wave, we use the third order Stokes wave as expressed in Koh and Le Mehaute [1966]. The wave orbital velocity at the bed is

$$u(t) = \frac{\sigma}{k} \sum_{n=1}^{3} n s_n \cos [n (kx - \sigma t)] \tag{16}$$

where s_n are constants determined from a, k and h and listed in Koh and Le Mehaute [1966]. It should be remembered that the ratio of s_n / s_{n-1} is $O(\varepsilon)$ where $\varepsilon = ak \ll 1$. The technique used to determine t_p was to set (16) equal to 0 and solve to order ε^2. This gives

$$t_p = \frac{1}{\sigma}\cos^{-1}\left\{\sqrt{\frac{\sinh^6 kh}{9\varepsilon^2}+\frac{1}{2}} - \frac{\sinh^3 kh}{3\varepsilon}\right\} \tag{17}$$

Substituting (16) into (15) results in

$$<\tau>_s = \frac{\rho}{2}\frac{c_f}{2T}\frac{\sigma^2}{k^2}\left\{\xi_0(4t_p - T) + 4\sum_{n=1}^{6}\frac{\xi_n}{n\sigma}\sin(n\sigma t_p)\right\} \tag{18}$$

$$\begin{aligned} &\xi_0 = s_1^2 + 4s_2^2 + 9s_3^2 \\ &\xi_1 = 4s_1 s_2 + 12 s_2 s_3 \\ &\xi_2 = s_1^2 + 6 s_1 s_3 \\ \textit{where}: \quad &\xi_3 = 4 s_1 s_2 \\ &\xi_4 = 4s_2^2 + 6 s_1 s_3 \\ &\xi_5 = 12 s_2 s_3 \\ &\xi_6 = 9 s_3^2 \end{aligned}$$

Here t_p is calculated as described above.

For the net bed stress due to bottom wind, we model the near bed velocity as

$$u(t) = u_m \cos(kx - \sigma t) + <u>_b. \tag{19}$$

The first term on the right is the near bed velocity from linear wave theory (8) where $u_m = a\sigma/\sinh(kh)$ is the maximum near bed orbital velocity. The second term, $<u>_b$, is the steady streaming velocity just outside the boundary layer, the "bottom wind" and is known to consist of a Eularian and a Lagrangian component [Batchelor, 1985]. As we are discussing a force balance at a fixed point, the component of interest is the Eularian term which is $(3/4)a^2 k\sigma/\sinh^2(kh)$. This result comes from calculations for a laminar boundary layer and laboratory experiments indicate that the value for turbulent boundary layers is less. Bijker et al [1974] report that $<u>_b$ for turbulent flows is about 0.4 times the prediction from laminar theory. Therefore, for this work the value used will be

$$<u>_b = 0.3\frac{a^2 k\sigma}{\sinh^2(kh)} \tag{20}$$

The equation for net stress due to bottom wind can be derived using (20), (19) and (15) as well as the fact that $t_p = (1/\sigma)\cos^{-1}(-<u>_b/u_m)$, giving

$$<\tau>_b = c_f \frac{\rho}{2} \frac{u_m^2}{\pi} \left[\left[1.+0.18\zeta^2 \right] \sin^{-1}(0.3\zeta)+0.9\zeta\sqrt{1.-0.9\zeta^2} \right] \qquad (21)$$

$$where: \quad \zeta = \frac{ak}{sinh(kh).}$$

The final calculation involves deriving an expression for the net stress due to ventilation. Once again we assume a quadratic stress relationship as in (14) and near bed velocity as in (8). Evaluating the mean gross stress ($<|\tau_0|>$) term in (13), we obtain the expression

$$<\tau>_v = 420\frac{K}{\nu} tanh(kb) \frac{\rho}{4} c_f u_m^2 \sigma \qquad (22)$$

It is helpful to normalize (22) in order to separate the effects directly related to wave intensity and those related to the ventilation process. This is accomplished by normalizing by the peak stress expected without ventilation τ_{max}. Inspection of (8) and (14) show that $\tau_{max} = c_f \rho u_m^2/2$. The normalized version of (22) becomes

$$\frac{<\tau>_v}{\tau_{max}} = 420\frac{K}{2\nu}\sigma\, tanh(kb) \qquad (23)$$

As can be seen from (23) the net stress due to ventilation is approximately a linear function of frequency and permeability.

Figure 8 shows a comparison of the net stress due to these three generating mechanisms as a function of grain size for a 60 cm high wave traveling in 300 cm deep water. The net stress due to the ventilation is calculated from (23) and (10) directly while the net stress due to the Stokes wave asymmetry and bottom wind are calculated from similarly normalized forms of (20) and (21) respectively. Figure 8a shows the relative strengths of net stress mechanisms for wave parameters similar to those present during the data run used to construct Figure 5. It is clear from this figure that the effects of ventilation are strongly grain size dependent. For fine sand the net

bed stress due to the ventilation mechanism appears to be negligible relative to the other two mechanisms. For medium grain sands around 500 microns, the net stress due to each of the three mechanisms is significant and for coarse grain sands and pebbles 1 mm in diameter or greater, net stress due to ventilation clearly dominates. The affect of increasing period is shown in Figures 8b and 8c. It is seen that ventilation decreases for increasing period but is still a significant factor for coarse grain sediments.

It is illuminating to consider what is happening when the grain size or wave frequency are altered. Comparing (23) and (9), we see that changes in $<\tau>_v$ come from changes in w/u. While linear theory indicates that changing the grain size (permeability) and frequency are the only means to change w/u, any other process which increases this ratio will result in increased importance of this phenomenon. One such mechanism could be the stressing of the sediment bed by the wave orbital motion. The bed dilates as it is stressed by the orbital motion, and this dilation leads to increased pore size. This increased pore size results in increased permeability and therefore increased ventilation. Maximum stressing of the bed occurs simultaneously with maximum ventilation. Any experiment such as this one where permeability is measured independently, would not detect this effect.

This limited study indicates that for fine sand the net stress due to ventilation is less significant than that due to bottom wind and wave form. However, this does not mean that the affects of ventilation are negligible in crosshore transport. Conley and Inman [submitted] have shown that another of the effects of ventilation is a disruption in the development of turbulence in the oscillatory boundary layer. Their results indicate that during suction (flow into the bed), turbulence is drawn closer to the bed and maintained in a compact layer near the bed. During injection (flow out of the bed) turbulence extends much higher into the fluid but is pushed away from the bed so that the near bed turbulence levels are reduced. Clearly such a difference in the development of turbulent characteristics of the boundary layer would be reflected in the sediment mobilizing and transporting capabilities of the flow. Such a difference may be significant even

for fine grained sands. It is also important to note that the results presented in Conley and Inman [submitted] were for a smooth and rigid permeable bed. It is not clear how the separate phenomena identified in this work would interact and reinforce each other in the presence of an moveable bed. The observation of an asymmetry in the development of fluid-granular boundary layers discussed in Conley and Inman [1992] occurred in fine grained sediments. It was shown that this asymmetry was not due to asymmetries in fluid velocity or acceleration which suggests that the combined effects of ventilation are indeed significant, even in fine grained sands.

The analysis in this paper of the relative importance of the net stresses due to wave asymmetry, bottom wind and ventilation assumes that their affects are mutually independent of each other. This assumption is questionable as all affects are mutually present in nature and may well interact in ways which can not be predicted. As an example of a likely interaction, consider that Longuet-Higgins [1958] points out that the bottom wind results from alternate boundary layer thinning under the crest of the wave and thickening under the trough of the wave. The phase between the vertical velocity associated with this thickening and thinning and the horizontal velocity in the boundary layer gives rise to the bottom wind. Conley and Inman [submitted] have shown that ventilation gives rise to a similar thinning and thickening under the crest and trough respectively and it is likely that the two affects may be mutually reinforcing.

5. CONCLUSIONS

A field experiment designed to detect the presence of wave driven ventilation in permeable beds was performed. Wave driven ventilation was tested as a possible mechanism for the maintenance of beach slope and this mechanism was compared against other mechanisms.

1. Utilizing Darcys law, ventilation which is driven by progressive surface gravity waves is observed in the permeable beds underneath the fluid on which the waves propagate.

1. Progressive surface gravity wave driven ventilation in the permeable bed beneath the fluid on which the waves propogate is observed through the utilization of Darcys law.

2. The magnitude of this flow is well predicted by linear theory given that the local effective bed thickness is known. The effective bed thickness is assumed to relate a homogeneous bed of constant permeability to the the true local stratigraphy.

3. The net stress arising from ventilation is found to be an important phenomena for short period waves and medium to coarse grain beds. This net stress can dominate the stresses arising from velocity asymmetries in shoaling waves or steady streaming velocities in the bottom boundary layer.

Acknowledgements. This study was funded by the office of Naval Research, Coastal Sciences under grant N00014-89-J-1060 with the University of California, San Diego. The manuscript was improved by spirited discussion with Bradley Werner.

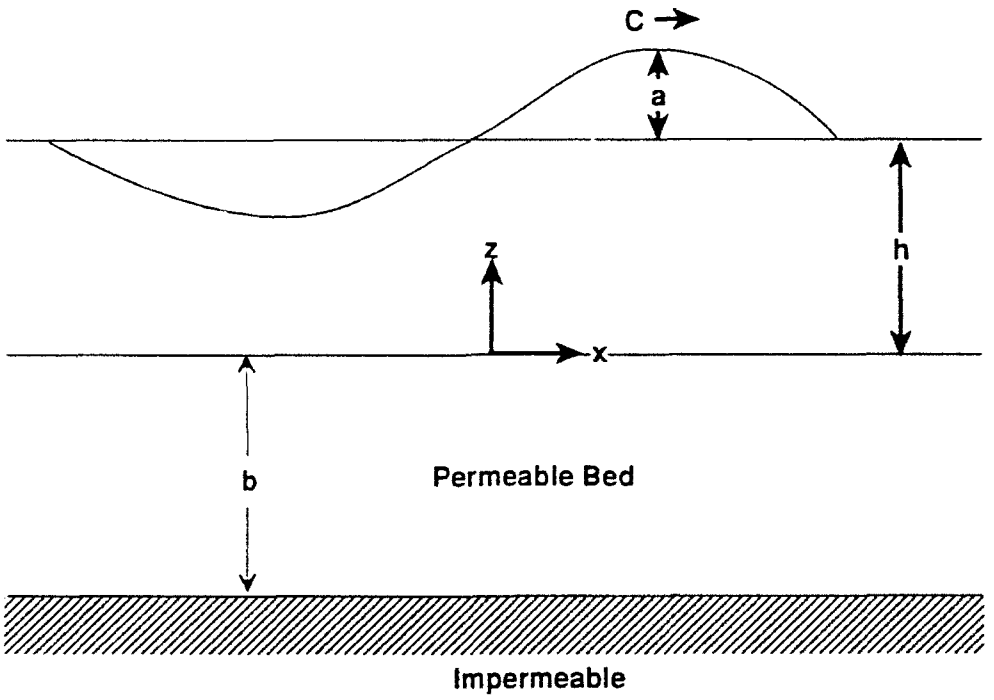

Figure 1: Schematic showing a wave of amplitude *a* on a layer of fluid of depth h. Fluid overlies a permeable bed of thickness b.

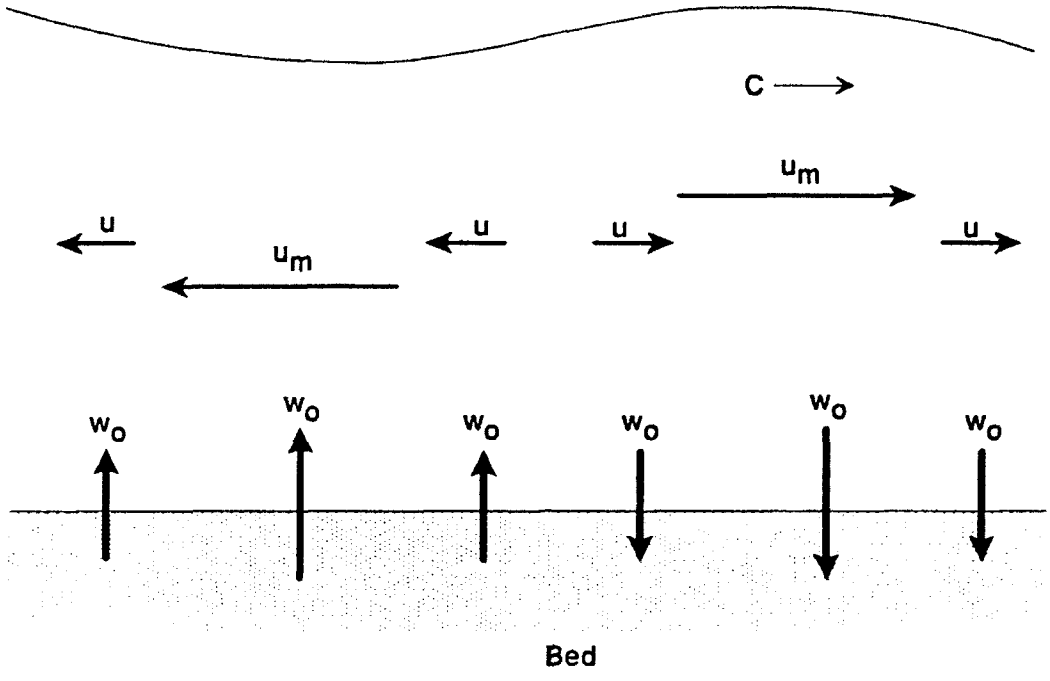

Figure 2· Schematic of bed ventilation predicted by (7). Flow is maximum into the bed under crest of the wave and maximum out of the bed under the trough of the wave.

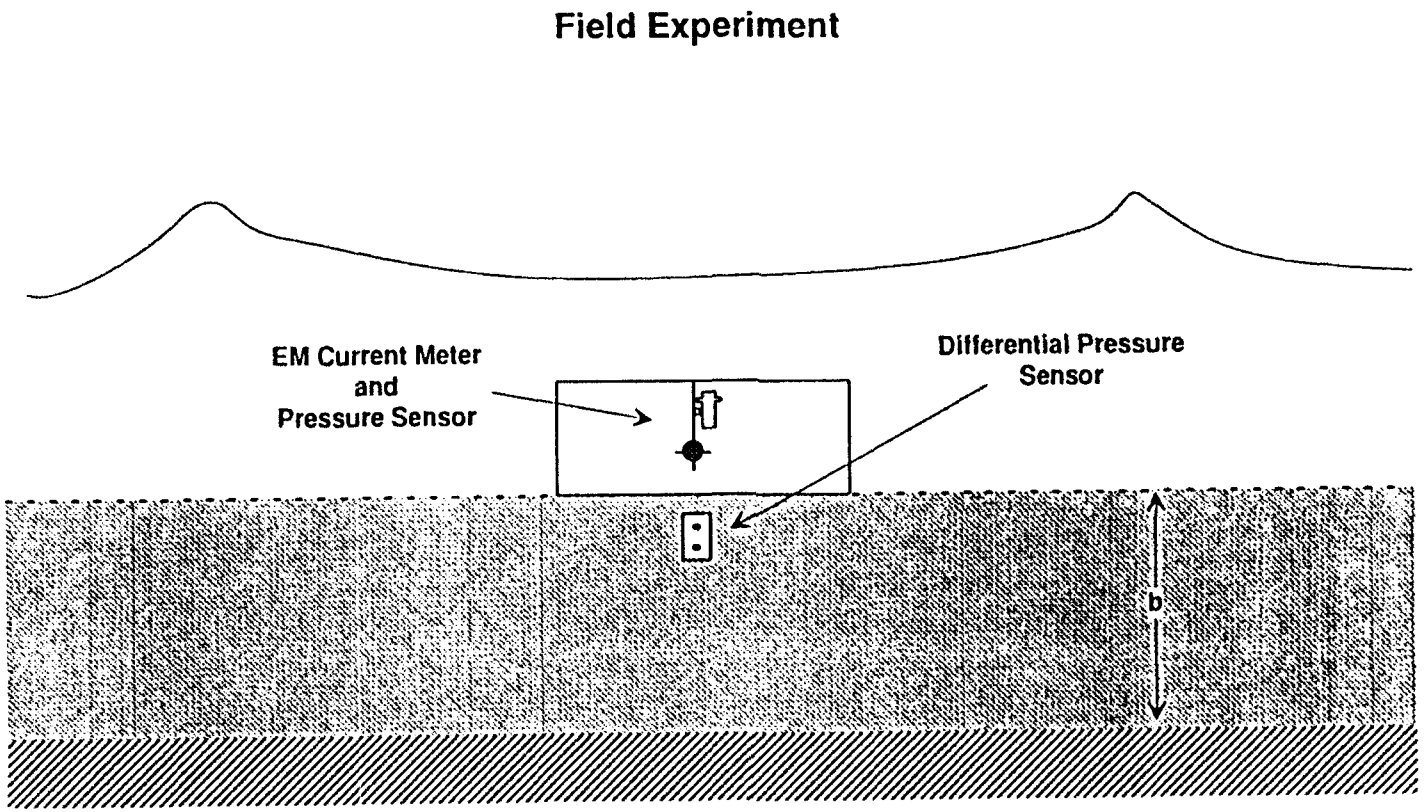

Figure 3: Schematic of the experimental layout. Differential pressure sensor is buried in the sand with pressure port separated in the vertical only. Absolute pressure sensor and em current meter are placed in the water column directly above the differential pressure sensor.

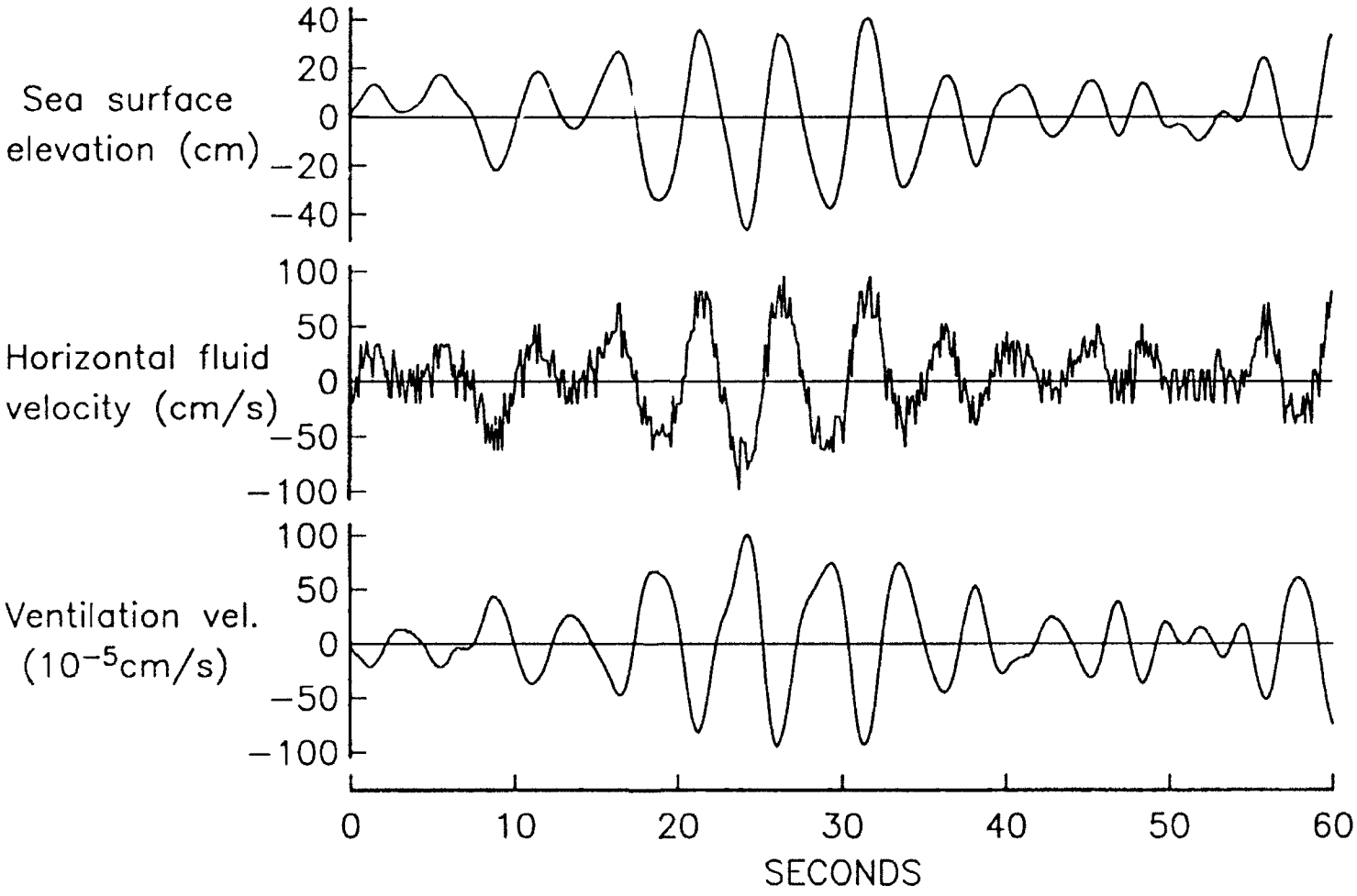

Figure 4: Typical section of time series from the experiment. Top trace shows sea surface elevation, middle trace is crosshore orbital velocity and bottom trace is vertical ventilation calculated from (1). The high frequency component in the orbital motion is noise from the current meter.

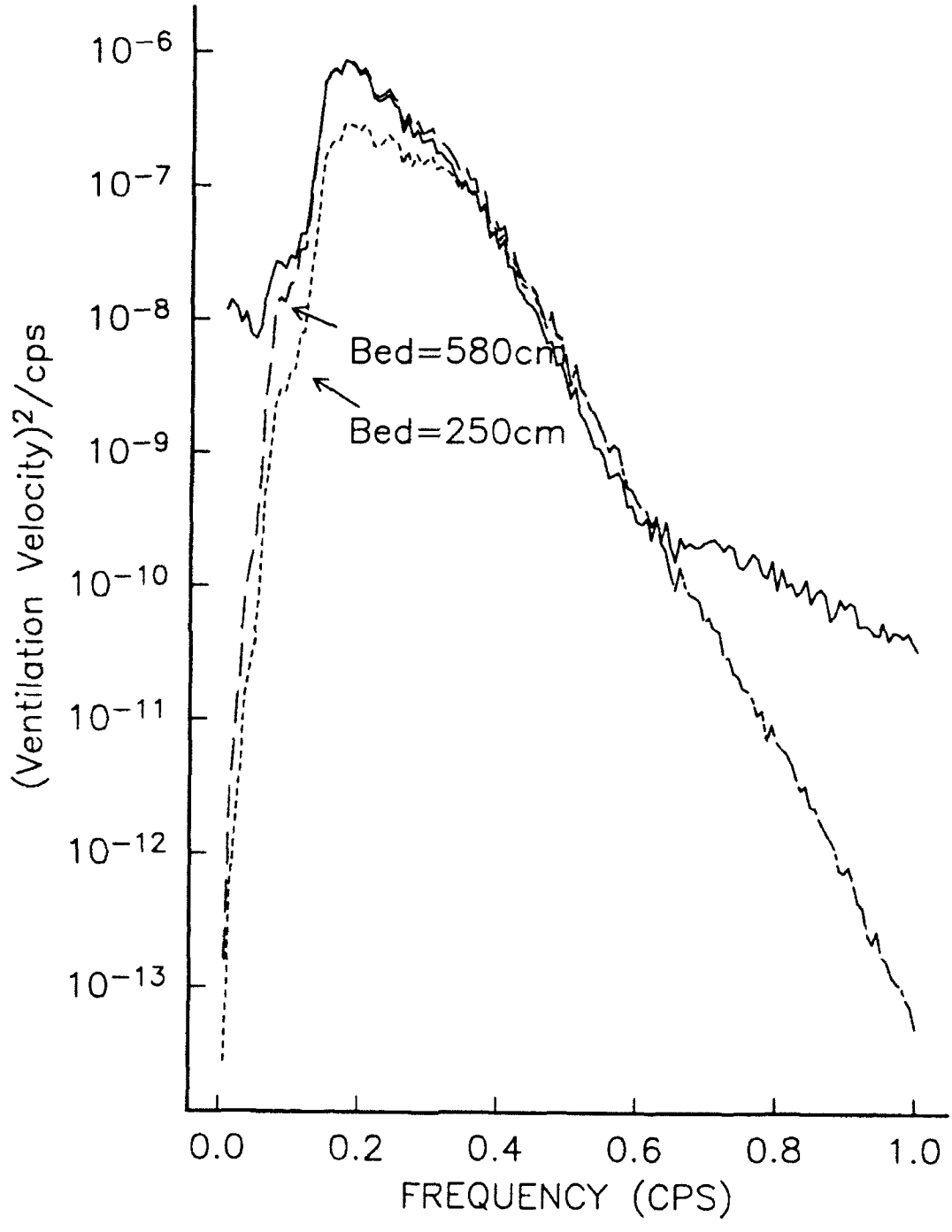

Figure 5: Solid line is ventilation spectra as calculated from differential pressure sensor. Dotted and dashed lines represent ventilation spectra predicted from (11). Dotted line assumes bed thickness of 250 cm and dashed assumes thickness of 580 cm. Units are in $(cm/s)^2/cps$.

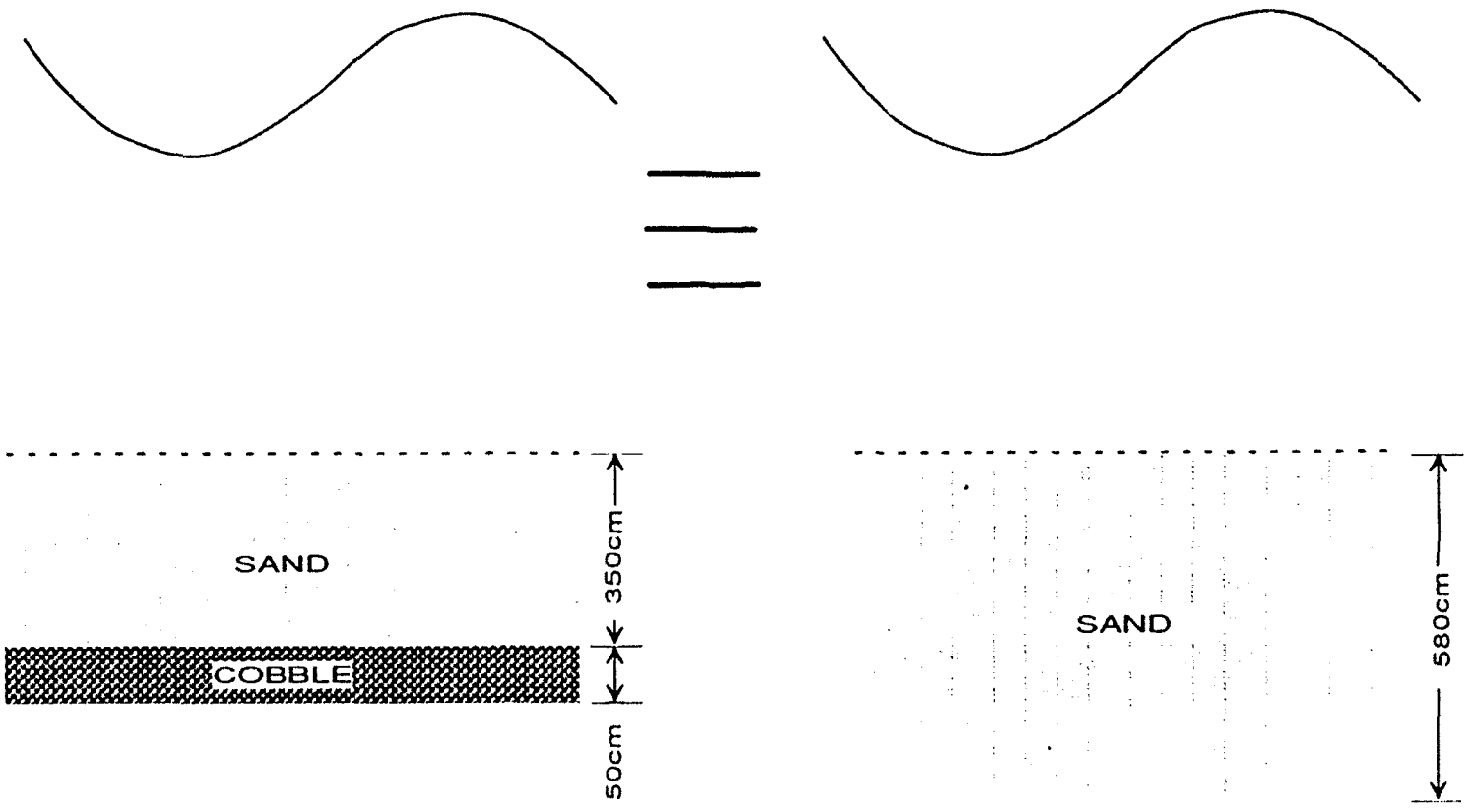

Figure 6: Schematic illustrating the concept of effective thickness. Shallow inhomogeneous bed of sand and cobble on left can be modeled as homogeneous bed of sand on right with effective thickness greater than the true thickness.

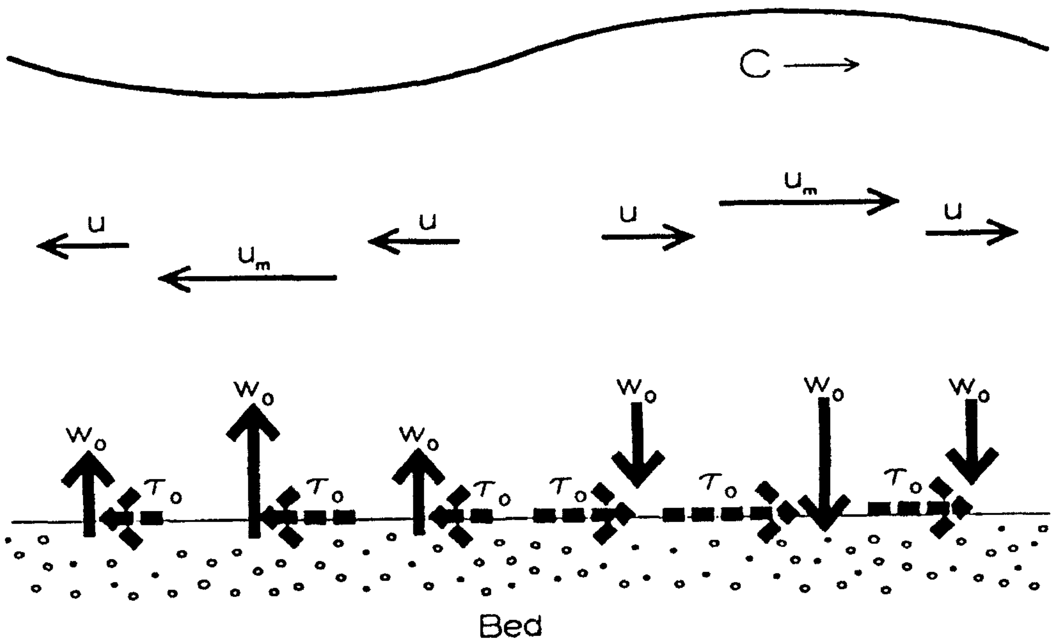

Figure 7: Schematic showing the effect of ventilation on oscillatory boundary layers. Flow into the bed enhances bed stress while flow out of the bed decreases bed stress. In an otherwise symmetrical oscillatory flow the result is a bed stress asymmetry which leads to a net stress. The direction of this stress is in the direction of the orbital velocities experiencing flow into the bed.

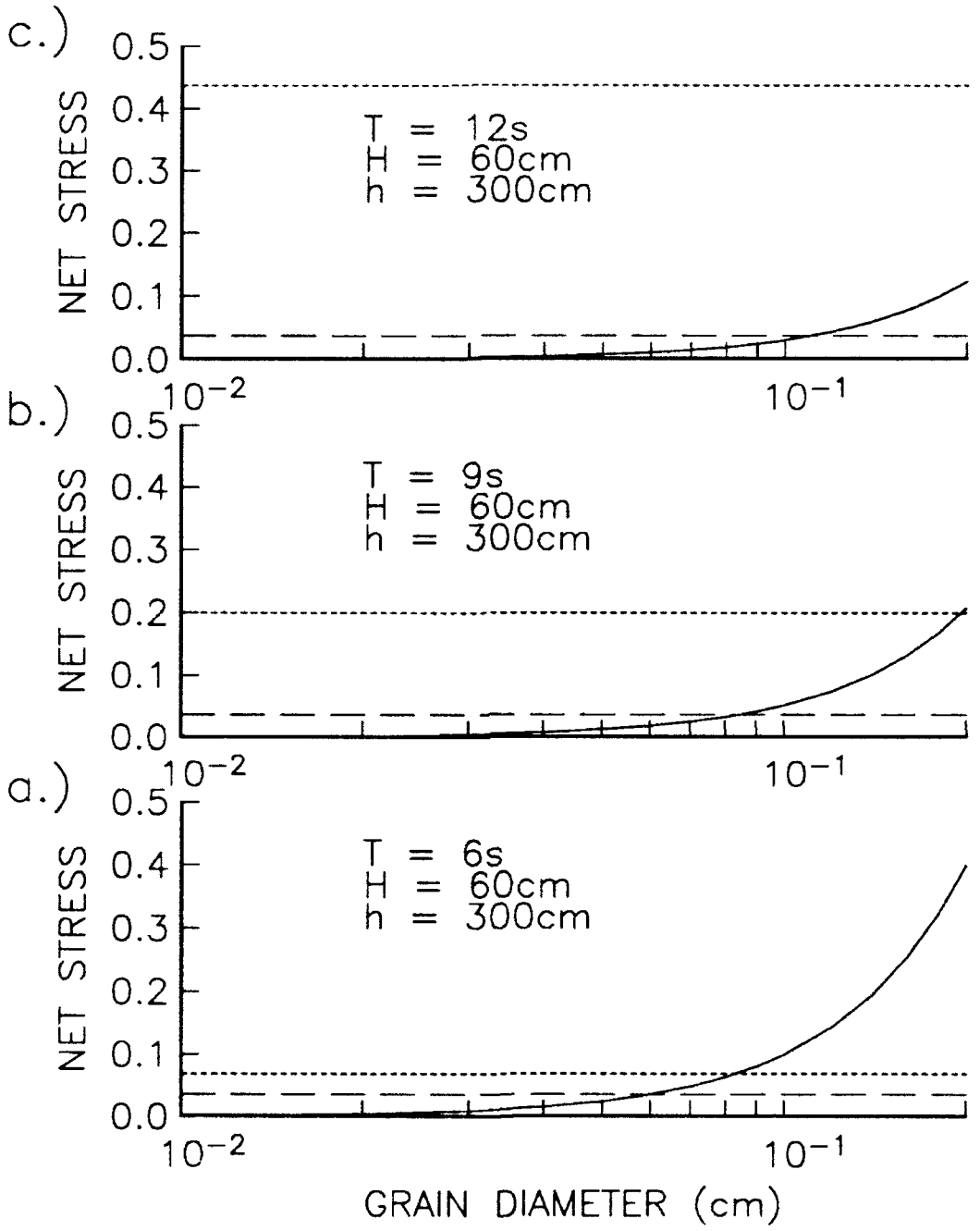

Figure 8: Comparisons of net stress arising from various mechanisms as a function of mean grain diameter. Solid line is net stress due to ventilation calculated from (23). Dashed line is stress due to bottom wind (21) and the dotted line is stress from a third order stokes wave (18). All values are normalized by $(\rho c_f a^2 \sigma^2 / [2 sinh^2(kh)])$. 8a uses wave parameters representative of field experiment while b. and c. show the effect of longer period waves.

REFERENCES

Batchelor, G. K.,*An Introduction to Fluid Mechanics*, 615 pp., University Press, Cambridge, 1985.

Bijker, E. W., J. P. Th. Kalkwijk, and T. Pieters, "Mass transport in gravity waves on a sloping bottom", *Proc. Conf. Coastal Eng., 14th(1)*, 447-465, 1974.

Conley, D. C., and D. L. Inman, "Ventilated oscillatory boundary layers", *J. Fluid Mech.*, submitted.

Conley, D. C., and D. L. Inman, "Field observations of the fluid-granular boundary layer under near-breaking waves," *J. Geophys. Res.*, 97(C6), 9631-9643, 1992.

Grant, U. S., "Waves as a sand - transporting agent", *Amer. J. Science*, 241(2), 117-123, 1943.

Gu, Z., and H. Wang, "Gravity waves over porous bottoms", *Coastal Engin.*, 15, 497-524, 1991.

Inman, D. L., and R. A. Bagnold, "Littoral processes", *The Earth Beneath the Sea, The Sea*, vol 3, edited by M. N. Hill, pp 529-553, Interscience, John Wilet & Sons, New York, 1963.

Koh, R. C. Y. and B. Le Mehaute, "Wave shoaling," *J. Geophys. Res,*. 71(8), 2005-2012, 1966.

Krumbein, W. C., and G. D. Monk, "Permeablility as a function of the size parameters of sedimentary particles", *Am. Inst. Min. and Met. Engin. Tech Pub 1492*, 153-163, 1943.

Longuet-Higgins, M. S., "The mechanics of the boundary-layer near the bottom in a progressive wave", *Proc. Conf. Coastal Eng., 6th*, 184-193, 1958.

Longuet-Higgins, M. S., "Mass transport in water waves", *Phil. Trans. Royal Soc. London, A*, 245, 535-581, 1953.

Putnam, J. A., "Loss of wave energy due to percolation in a permeable sea bottom", *EOS, Trans. AGU*, 30, 349-356, 1949.

Reid, R. O. and K. Kajiura, "On the damping of gavity waves over a permeable sea bed," *EOS, Trans. AGU*, 38, 662-666, 1957.